UC San Diego

UC San Diego Electronic Theses and Dissertations

Title

Tectonic signatures on active margins

Permalink

https://escholarship.org/uc/item/3kp6t2sc

Author

Hogarth, Leah Jolynn

Publication Date

2010

Peer reviewed|Thesis/dissertation

eScholarship.org Powered by the California Digital Library
University of California

UNIVERSITY OF CALIFORNIA, SAN DIEGO

Tectonic Signatures on Active Margins

A dissertation submitted in partial satisfaction of the requirements for the degree

Doctor of Philosophy

in

Earth Sciences

by

Leah Jolynn Hogarth

Committee in charge:

Neal W. Driscoll, Chair
Jeffrey M. Babcock
Steven C. Cande
Alistair J. Harding
Douglas L. Inman
Falko Kuester

2010

Copyright

Leah Jolynn Hogarth, 2010

All rights reserved.

The Dissertation of Leah Jolynn Hogarth is approved, and it is acceptable in quality and form for publication on microfilm:

_____

_____

_____

_____

_____

_____

Chair

University of California, San Diego

2010

For their constant encouragement and support,
I dedicate this dissertation to my parents and my sister.
Thank you for being so generous.

The finest workers in stone are not copper or steel tools,
but the gentle touches of air and water at their leisure
with a liberal allowance of time.

Henry David Thoreau

Table of Contents

Signature Page iii

Dedication iv

Epigraph v

Table of Contents vi

List of Figures ix

Acknowledgements xi

Vita xiv

Abstract xv

1 Introduction 1

1.1 Background and Rationale 2

1.2 Overview of Study 3

1.3 Outline of the Dissertation 4

1.4 References 5

2 Long-term Tectonic Control on Holocene Shelf Sedimentation Offshore La Jolla, California 6

3 Tectonic Controls on Nearshore Sediment Accumulation and Submarine Canyon Morphology Offshore La Jolla, Southern California 12

4 New Seismic Evidence for Active Deformation and its Control on Long-term Sediment Accumulation on the Eel Margin, Northern California 27

4.1 Abstract 28

4.2 Introduction 29

4.3 Regional Setting 34

4.3.1 Geology 34

4.3.2 Modern Hydrodynamics and Sediment Dispersal 37

4.4 Methods....38
4.5 Results....39
4.5.1 Major Structures and Features....39
4.5.2 Sequence I....40
4.5.3 Sequence II....42
4.6 Discussion....44
4.6.1 Evolution of the Transgressive Sequence....44
4.6.2 Tectonic Controls on Sedimentation....49
4.6.3 Sediment Source and Hydrodynamic Control on Sediment Distribution....51
4.7 Conclusions....53
4.8 Acknowledgements....53
4.9 References....70
5 New Insight into Lowstand Subaerial Accommodation: Implications for Fluvial Processes in a Sequence Stratigraphic Framework....77
5.1 Abstract....78
5.2 Introduction....79
5.3 Regional Setting....81
5.4 Methods....82
5.5 Results....82
5.6 Discussion....84
5.6.1 Fluvial Accommodation During Sea-level Lowstand....84
5.6.2 Implications for Fluvial Morphodynamics and Global Sediment Budget....87
5.7 Conclusions....91
5.8 Acknowledgements....92

5.9 References 110

A Appendix 115

A.1 Introduction 116

A.2 Heave Correction 116

A.3 Fish Depth Correction 116

A.4 Full Sioseis Code 118

List of Figures

Figure 4.1 Location Map and Local Tectonic Features 56

Figure 4.2 Uplift and Subsidence Rates Along the Margin 57

Figure 4.3 Survey Ship Tracks 58

Figure 4.4 Dip Lines T and 4p 60

Figure 4.5 Strike Lines 10, 15, and 17 61

Figure 4.6 Strike Line 15 Detail of Fault Offset 62

Figure 4.7 Structure Contour Maps 63

Figure 4.8 Core Q45 64

Figure 4.9 Perspective View 66

Figure 4.10 Isopach Maps 67

Figure 4.11 Strike Line 10 Detail of Diverging Reflectors 68

Figure 4.12 Predicted Stratigraphy and Cores 69

Figure 5.1 Sequence Stratigraphic Prediction During Sea-level Fall 93

Figure 5.2 Physiographic Model of Fluvial Response to Sea-level Fall 94

Figure 5.3 Dependence on Depth of Shelf-slope Break 95

Figure 5.4 Location Map and Local Tectonic Features 97

Figure 5.5 Survey Ship Tracks 98

Figure 5.6 Strike Line T 99

Figure 5.7 Dip Line 8 100

Figure 5.8 Offshore Strike Line with Channel 101

Figure 5.9 Dip Line 1S with Nested Channel 102

Figure 5.10 Perspective View of Lowstand Wedge 103

Figure 5.11 Structure Map of Sequence Boundary and Isopach Map of Lowstand Wedge 104

Figure 5.12 Sea-level Curve for the Last Glacial Cycle 105

Figure 5.13 Model of Lowstand Aggradation 107
Figure 5.14 Papua New Guinea Rivers Example 108
Figure 5.15 Global Sediment Flux to the Oceans and Major Submarine Fans 109
Figure A.1 Uncorrected and Corrected Seismic Lines.....120
Figure A.2 Fish Depth Change Schematic 121

Acknowledgements

First and foremost, I want to thank my advisor, Neal Driscoll, for all the guidance and inspiration he provided over the course of my studies. His genuine interest in my success and his excitement for the work inspired me countless times. I appreciate the field opportunities he provided and the encouragement to get this work published. Through this process he has helped me develop my skills as a scientist.

Doug Inman and Pat Masters deserve special thanks as they encouraged me to attend Scripps, and they provided me with several interesting projects to work on as I started my studies. I am grateful for Doug's active interest in my work and his guidance. Peter Adams, a visiting professor to the group also provided a positive collaborative experience and valuable career advice.

I would like to thank the other members of my dissertation committee. Jeff Babcock has been a great resource and supporter of my work, not to mention a main contributor to data collection. Steve Cande was very thoughtful, available whenever I needed him, and generously facilitated use of his computers and software. Alistair Harding was very genuine, giving meaningful insight into my work. I would like to thank Falko Keuster for coming to the rescue when my original main campus committee member moved to another university.

I feel very fortunate to have been a part of such a great lab, where everyone was always willing to lend a hand and treat each other as friends as well as colleagues. Thus thanks to my fellow lab mates: Jenna, Kurt, Nicolas, Becca, Christie, Liz, Danny, Jillian, Justin, Jessica, Pat, and John. I want to especially thank Nicolas for all of his hard work and thoughtful contribution to our studies in La Jolla. I am grateful for the educational and enjoyable interactions we shared.

In addition, I greatly appreciate the many professors who shared their knowledge

and time with me. The importance of teaching is perhaps not emphasized enough and I thankful to those of you who have undertaken the task with enthusiasm.

I would like to acknowledge all of the staff in the Graduate Office: especially, Josh Reeves, Becky Burrola, Dawn Huffman, Alice Zheng, and Denise Darling. In addition, I am grateful to the staff in the Geology Research Division. Edwina Riblet and Lawrance Baily from the Development Office have also been wonderful in their help with my ARCS Fellowship.

My family and close friends deserve a special thanks. Their presence and support has made my graduate school experience extremely enriching. I appreciate all the times they have been there to listen, advise, and distract!

In addition, I would like to acknowledge my funding sources. Four years of support from the Los Angeles chapter of the Achievement Rewards for College Scientists (ARCS) foundation has been invaluable. Their support helped me to pursue a new research focus when my original plans fell through. Their genuine interest in my success fostered a sense of relevance, which encouraged me over the years. In addition, the Kavli Institute and the Office of Naval Research provided funding for this work.

Chapter 2, in full, is a reprint of the material as it appears in Geology 2007. Hogarth, Leah J., Babcock, Jeffrey; Driscoll, Neal W.; Le Dantec, Nicolas; Haas, Jennifer K.; Inman, Douglas L.; Masters, Patricia M. The dissertation author was the primary investigator and author of this paper.

Chapter 3, in full, is a reprint of the material as it appears in Marine Geology 2009. Le Dantec, Nicolas; Hogarth, Leah J.; Driscoll, Neal W.; Babcock, Jeffrey M. The dissertation author was a primary investigator and co-author of this paper.

Chapter 4, in part is currently being prepared for submission for publication of the material. Hogarth, Leah J.; Driscoll, Neal W.; Babcock, Jeffrey M. The dissertation

author was the primary investigator and author of this material.

Chapter 5, in part is currently being prepared for submission for publication of the material. Hogarth, Leah J.; Driscoll, Neal W.; Babcock, Jeffrey M. The dissertation author was the primary investigator and author of this material.

Vita

2003	Bachelor of Science, Geological Sciences Michigan State University
2003-2010	Research Assistant University of California, San Diego
2010	Doctor of Philosophy, Earth Sciences Scripps Institution of Oceanography University of California, San Diego

Publications

Hogarth, L.J., Babcock, J., Driscoll, N.W., Le Dantec, N., Haas, J.K., Inman, D.L., and Masters, P.M. 2007. Long-term tectonic control on Holocene shelf sedimentation offshore La Jolla, California. Geology, 35 (3), p. 257-278.

Le Dantec, N., Hogarth, L.J., Driscoll, N.W., Babcock, J.M., Barnhardt, W.A., and Schwab, W.C. 2009. Tectonic controls on nearshore sediment accumulation and submarine canyon morphology offshore La Jolla, southern California. Marine Geology, 268 (1-4), p. 115-128.

Abstract of the Dissertation

Tectonic Signatures on Active Margins

by

Leah Jolynn Hogarth

Doctor of Philosophy in Earth Sciences

University of California, San Diego, 2010

Neal W. Driscoll, Chair

High-resolution Compressed High-Intensity Radar Pulse (CHIRP) surveys offshore of La Jolla in southern California and the Eel River in northern California provide the opportunity to investigate the role of tectonics in the formation of stratigraphic architecture and margin morphology. Both study sites are characterized by shore-parallel tectonic deformation, which is largely observed in the structure of the prominent angular unconformity interpreted as the transgressive surface.

Based on stratal geometry and acoustic character, we identify three sedimentary sequences offshore of La Jolla: an acoustically laminated estuarine unit deposited during early transgression, an infilling or "healing-phase" unit formed during the transgression, and an upper transparent unit. The estuarine unit is confined to the canyon edges in

what may have been embayments during the last sea-level rise. The healing-phase unit appears to infill rough areas on the transgressive surface that may be related to relict fault structures. The upper transparent unit is largely controlled by long-wavelength tectonic deformation due to the Rose Canyon Fault. This unit is also characterized by a mid-shelf (~40 m water depth) thickness high, which is likely a result of hydrodynamic forces and sediment grain size.

On the Eel margin, we observe three distinct facies: a seaward-thinning unit truncated by the transgressive surface, a healing-phase unit confined to the edges of a broad structural high, and a highly laminated upper unit. The seaward-thinning wedge of sediment below the transgressive surface is marked by a number of channels that we interpret as distributary channels based on their morphology. Regional divergence of the sequence boundary and transgressive surface with up to ~8 m of sediment preserved across the interfluves suggests the formation of subaerial accommodation during the lowstand. The healing-phase, much like that in southern California, appears to infill rough areas in the transgressive surface. Reflectors within the laminated upper unit exhibit divergence towards the Eel River Syncline, which suggests that deposition in the syncline is syntectonic. The transgressive surface is offset across the Eureka Anticline indicating deformation has occurred since ~10 ka. The relief observed along the transgressive surface is consistent with deformation rates measured onshore.

1

Introduction

1.1 BACKGROUND AND RATIONALE

Sequence stratigraphy is a relatively new concept, dating back perhaps half a century, but really growing in use starting ~30 years ago with the advent of seismic stratigraphy. Beginning in the mid-70's Vail and others (1977) used sequence stratigraphy to develop charts of regional sea-level changes, which they attempted to extrapolate to charts of global sea-level cycles. Attention has shifted away from using sequence stratigraphy to derive a sea-level curve and towards using sequence stratigraphy to investigate the geologic evolution of local and regional environments, as well as to predict the location of petroleum resources.

Sequence stratigraphy is a tool, which aims to determine how sedimentary layers are assembled through time. It is often the geometric nature of surfaces between these layers that provides the most insight into their formation. These geometric relationships are largely controlled by accommodation, which is the space available for sediments to fill. Accommodation is created by increasing water depth and by tectonic subsidence. Contrary to many of the first models, sequence stratigraphy does not require any assumptions about eustasy, and its concepts are now being used to investigate a large variety of marine, lacustrine, fluvial, and even subaerial environments.

The first models of sequence stratigraphy were built from observations in passive margin settings, but recently it has become clear that it is important to recognize the variability inherent in different settings. For example, tectonic deformation is a major factor creating and destroying accommodation, and this thesis focuses on how tectonic deformation influences sediment architecture.

CHIRP seismic reflection profiles allow unprecedented high-resolution imaging of sediment architecture in sediments up to ~50 m below the sea floor. These sediments often include products of the last sea-level cycle (~120 ka – present), but can be older sediment and rock. Early seismic methods provided deeper seismic sections, but lower

resolution. Through high-resolution investigation of the uppermost sediments and structures on the seafloor, CHIRP allows us to better link sedimentary successions observed in the rock record with modern, short time scale processes.

In addition to seismic reflection methods, this work utilized coring and bathymetric surveys to ground-truth CHIRP profiles. Highly detailed assessments of the dominant processes generating the observed architectures were made by assembling the data into three-dimensional maps and visualizations. The results have implications for not only sequence stratigraphy, but also submarine canyon morphology and formation, nearshore sediment dynamics, sand resources for beach replenishment, and fluvial geomorphology.

1.2 OVERVIEW OF STUDY

This thesis examines the question of how tectonics influences stratigraphic architecture by examining seismic profiles, high-resolution bathymetry, and core data in two distinct tectonic settings. The first focus site, the La Jolla margin, is located in the California Borderlands, an area marked by strike-slip faulting. The major tectonic feature is the Rose Canyon Fault Zone, a right-lateral, strike-slip fault creating deformation on and offshore. Horizontal motion on the fault within the Holocene is estimated at 1-2 mm/yr. Sediment supply to the region, consisting mostly of fine sands, is low. Episodic input from rivers to the north is transported south via longshore drift within the Oceanside littoral cell, and sea cliff erosion augments this source. The Eel margin, located in northern California, is a forearc basin setting overprinted by the influence of northward migration of the Mendocino Triple Junction. This imparts a highly complex pattern of active thrust faults, anticlines, and synclines oriented perpendicular to the shoreline. Horizontal motion on faults reaches ~6 mm/yr, and uplift and subsidence of these structures reaches a maximum of ~3 mm/yr. Sediment supply to the shelf is large, with

steep, mountainous rivers wearing down relatively easily eroded rock. Normalized to its basin area, the sediment supply of the Eel River is larger than that of any other river in the contiguous United States. Furthermore, several similarly sediment rich rivers yield additional discharge to the Eel shelf.

Both settings have an ideal geometry to separate the effects of eustatic sea-level fluctuations from those of tectonic deformation: structural variability is predominantly along shore, that is orthogonal to the variations due to eustasy. In southern California, the low sediment supply with very little organic matter results in very little internal structure in sediment units, making it necessary to draw conclusions from larger geometric relationships. In northern California, however, the huge influx of sediment leads to greater resolution within the seismic packages and more geometric clues to interpret their evolution.

1.3 OUTLINE OF THE DISSERTATION

The second and third chapters of this thesis present results from southern California, and the fourth and fifth chapters focus on northern California. Chapter 2 presents new seismic data used to identify structural deformation and sediment distribution on the shelf offshore of La Jolla. Chapter 3 looks in greater detail at the seismic data from La Jolla, detailing the succession of stratigraphic facies and their associated environments during the last sea-level rise. This chapter also examines structural and hydrodynamic controls on bathymetry. Chapter 4 provides a broad overview of the transgressive sequence development on the northern California shelf offshore of the Eel River. Chapter 5 presents new findings of lowstand sediment deposition and subsequent preservation on the shelf. This chapter includes new insight into the variability of river system sediment discharge to the ocean throughout the sea-level cycle, which has important implications for sequence stratigraphy.

1.4 REFERENCES

Vail, P.R., R.M. Mitchum, and S. Thompson, 1977, Seismic stratigraphy and global changes of sea level, part 4: Global cycles of relative changes of sea level, in C.E. Clayton, ed., Seismic stratigraphy - applications to hydrocarbon exploration: Tulsa, Oklahoma, American Association of Petroleum Geologists Memoir 26, p. 83-97.

2

Long-term Tectonic Control on Holocene Shelf Sedimentation Offshore La Jolla, California

Long-term tectonic control on Holocene shelf sedimentation offshore La Jolla, California

Leah J. Hogarth*
Jeffrey Babcock
Neal W. Driscoll
Nicolas Le Dantec
Jennifer K. Haas
Douglas L. Inman
Patricia M. Masters
Scripps Institution of Oceanography, University of California–San Diego, La Jolla, California 92093, USA

ABSTRACT

A high-resolution Compressed High-Intensity Radar Pulse (CHIRP) survey reveals shore-parallel variations in the Holocene sediment thickness offshore La Jolla, California. Sediment thicknesses decrease from >20 m in the south near Scripps Canyon to zero in the north approaching Torrey Pines. In addition to the south-to-north variation in sediment thickness, the transgressive surface observed in seismic lines shoals from Scripps Canyon to the north. Despite these dramatic shore-parallel subsurface changes, the nearshore bathymetry exhibits little to no change along strike. A left jog (i.e., a constraining bend) along the Rose Canyon fault causes local uplift in the region and appears to explain the northward shoaling of the transgressive surface, the decrease in relief on the transgressive surface away from the left jog, and the Holocene sediment thickness variation. This tectonic deformation is shore parallel, and thus the accommodation can be separated into its tectonic and eustatic components.

Keywords: tectonic deformation, accommodation, transgressive surface, transpression.

INTRODUCTION

Many investigators have recognized the important role of tectonics in the preservation of sediments on active margin shelves (e.g., Orange, 1999; Driscoll and Hogg, 1995). In most locations, tectonic uplift or subsidence offsets the coastline vertically and causes base-level changes that are difficult to distinguish from sea-level changes; a common manifestation of tectonic uplift is subaerial terraces parallel to the coastline. Eustatic sea level has risen ~125 m in the past 20 k.y. (e.g., Fairbanks, 1989). Consequently, in seismic images and in outcrop, it is often difficult to separate sea-level changes from tectonic changes acting in the same plane during this time period. In the San Diego, California, area, regional uplift and sea-level change have created terraces (e.g., Bay Point Formation), but due to the geometry of the Rose Canyon fault zone, much tectonic deformation occurs shore parallel or orthogonal to eustatic sea-level changes and regional tectonic uplift (Kennedy, 1975). Thus, we can use the stratigraphic variability parallel to shore to discern the tectonic signal associated with the Rose Canyon fault from glacial-eustatic fluctuations or regional tectonic uplift. Furthermore, this will aid us in understanding how tectonic processes govern the preservation of sediments on the shelf. Such an understanding will allow us to define sand resources offshore as well as the distribution of hardgrounds on the seafloor, which may play an important role in biohabitats.

*E-mail: lhogarth@ucsd.edu.

The San Diego area is west of the San Andreas fault zone and is characterized by a series of subparallel, en echelon faults including, from east to west, the San Jacinto, Elsinore, and Newport–Inglewood–Rose Canyon fault zones. In the La Jolla region, the Rose Canyon fault zone is a dextral strike-slip fault zone with complex surface expression (Treiman, 1993). The fault zone passes through La Jolla, forming Mount Soledad, a pop-up structure with a maximum uplift of ~150 m (Fig. 1); pop-up structures are areas of local uplift due to transpression or compression created when lateral motion on a strike-slip fault is interrupted by a bend or a jog in that fault. In the case of Mount Soledad, a left-stepping jog on the right-lateral Rose Canyon fault creates compression and uplift (Kennedy, 1975; Kennedy et al., 1979). Seismic surveys reveal that the Rose Canyon fault zone extends northwest 60 km offshore (Moore, 1972). Evidence of Holocene activity on the Rose Canyon fault zone comes from both offshore seismic data (Moore, 1972) and onshore trenches (Lindvall and Rockwell, 1995). Lindvall and Rockwell (1995) estimated that the total horizontal component of slip ranges from 1 to 2 mm/yr during the Holocene. In addition to the Rose Canyon fault system, Kennedy (1975) identified several other inactive northeast-southwest–trending oblique faults with vertical offset of ~10 m in the cliffs of Torrey Pines Beach (Fig. 1).

Our objective is to image the transgressive surface, overlying sands, and fault structures to better understand the processes influencing sediment accumulation and preservation on the shelf near La Jolla. Here we describe the observed morphology of the transgressive surface. We propose that our observation of a pop-up structure offshore, created by a constraining bend along the right-lateral Rose Canyon fault zone, controls the long-term accumulation of sediment in this region of the nearshore.

METHODS

In 2002, ~300 km of Compressed High-Intensity Radar Pulse (CHIRP) seismic data were acquired offshore from La Jolla Cove north to Del Mar (Fig. 1). We used a CHIRP sonar (Edgetech) with a swept frequency of 1–5.5 kHz yielding submeter vertical resolution. During the nearshore survey, the CHIRP seismic system was mounted on a surface tow frame with an attached global positioning system receiver, thus minimizing navigation error. We generated an isopach map by tracing the transgressive surface and differencing it from the seafloor throughout the seismic grid. A nominal velocity of 1500 m/s was used to convert travel-

time to sediment thickness. Bathymetric data were acquired, processed, archived, and distributed by the Seafloor Mapping Lab of California State University Monterey Bay (http://seafloor.csumb.edu/SFMLwebDATA.htm).

RESULTS

Layers in the units below the transgressive surface generally exhibit distinct dips to the south (Fig. 2) that are consistent with the local dips of the Ardath Shale, Torrey Sandstone, and Del Mar Formation on land (Kennedy, 1975). The transgressive surface is identified in the profiles by marked truncation (Figs. 2 and 3), which was formed by wave-base erosion during the sea-level rise, and is mantled by a basal unit and an overlying acoustically transparent layer. This part of the shelf has been subaerially exposed during many sea-level lowstands during the Pleistocene; the erosion and truncation on this surface probably reflect multiple sea-level cycles, not just the last sea-level rise. The poorly laminated basal unit is only observed in the mid- to outer-shelf region and appears to record the early transgression in the region. The overlying transparent unit might reflect the early stage of the highstand systems tract, which exhibits cross-shelf thinning with a maximum depocenter in the mid-shelf. The acoustically transparent character, however, precludes identification of a downlap surface, and thus our ability to confidently discern whether this package is part of the late transgressive systems tract or the early highstand systems tract.

Seismic images from our survey show that the transgressive surface exhibits an overall southward dip, and the overlying sediment thickness decreases along strike to the north of Scripps Canyon (Figs. 2 and 4). A local reversal of dip also exhibits a change in acoustic reflectivity that might imply a more resistive hardground and may be fault controlled (Fig. 2A). It is difficult, however, to trace the fault laterally shoreward from line S10 to adjacent lines because of the limited acoustic penetration beneath the transgressive surface (Fig. 2A). The dip lines show that the maximum sediment thickness above the transgressive surface is located on the mid-shelf and systematically diminishes both landward and seaward (Fig. 3). The extent of the isopach map is limited by data density; it captures the edge of the mid-shelf depocenter and delineates the south-to-north thinning.

The isopach map of sediment thickness shows a depocenter between the La Jolla and Scripps canyons, as well as to the north of Scripps Canyon (Fig. 4). Sediment thickness systematically decreases along strike to the north from ~20 m just north of Scripps Canyon to zero offshore Torrey Pines (Figs. 2 and 4). Perpendicular to shore, sediment thickness ranges from ~0–5 m nearshore to maximum thicknesses of 10–20 m

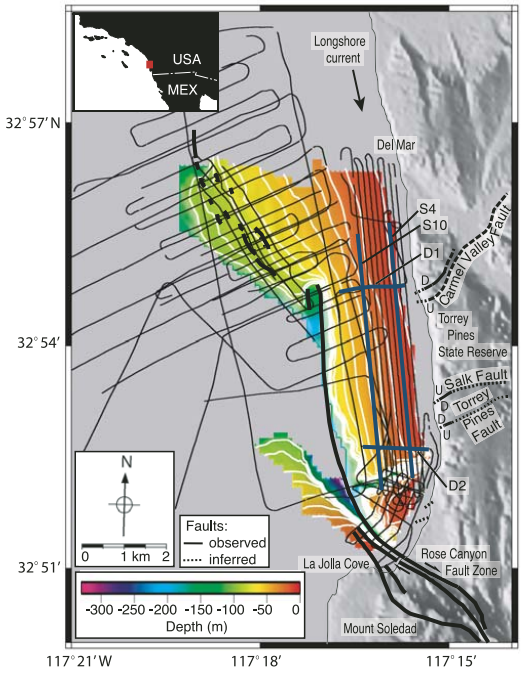


Figure 1. Survey ship track (black lines) superimposed on 2 m gridded bathymetry (data used in this study were acquired, processed, archived, and distributed by Seafloor Mapping Lab of California State University Monterey Bay: http://seafloor.csumb.edu/SFMLwebDATA.htm). White lines on bathymetry are contours (10 m intervals) to 100 m. Faults are shown in bold black: dashed for inferred location, D and U for downthrown and upthrown side, and right-lateral sense of strike-slip motion is shown with arrows. Left-stepping bend in Rose Canyon fault zone creates uplift of Mount Soledad. S4, S10, D1, and D2 (bold blue lines) indicate locations of strike lines shown in Figure 2 and dip lines shown in Figure 3. Local faults shown are based on Kennedy (1975).

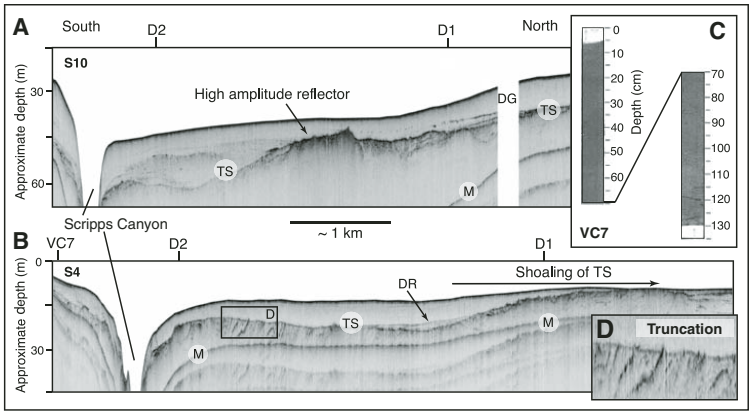


Figure 2. CHIRP along-shelf strike lines. A: Profile S10 from offshore shows shoaling of transgressive surface (TS) to north of Scripps Canyon. At this depth, Holocene sediments mantle transgressive surface. B: Nearshore profile S4 shows truncation of underlying layers as consequence of wavebase erosion, which is interpreted to occur during sea-level transgression. TS is exposed at seafloor to north. Vibracore VC7 is projected onto line S4 south of Scripps Canyon. D1 and D2 are locations of crossing dip lines. See Figure 1 for locations (M—multiple, DG—data gap, DR—dipping reflector). C: Inset shows Vibracore VC7, which recovered fine-grained to very fine grained, olive-green, homogeneous sands. In upper 135 cm of Holocene sediment there is no evidence for event beds associated with storms or floods. See Figure 4 for core location. D: Inset shows detail of TS and associated truncation.

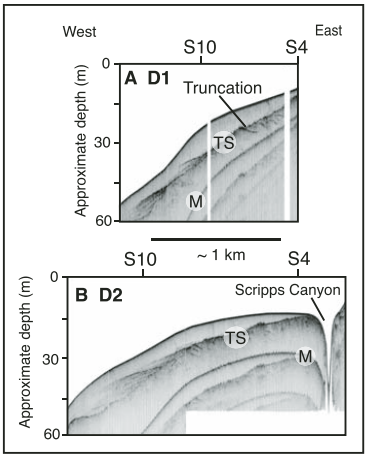


Figure 3. CHIRP cross-shelf dip lines. A: Profile D1 shows truncation along interpreted transgressive surface. Basal reflective package is interpreted as part of early transgression, and thickness of overlying acoustically transparent unit is greatest in mid-shelf, thinning both landward and seaward. B: Profile D2, farther to south, also shows mid-shelf depocenter of acoustically transparent unit. S4 and S10 are locations of crossing strike lines. TS—transgressive surface; M—multiple. See Figure 1 for locations.

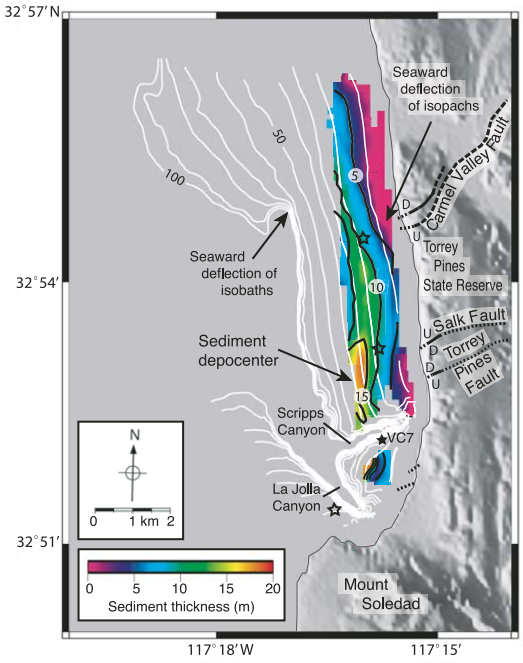


Figure 4. Holocene sediment thickness above transgressive surface (contour interval = 5 m) superimposed on bathymetric contours (contour interval = 10 m). Extent of isopach map is limited to mid-shelf and shoreward by data density shown in Figure 1. Isopachs show depocenter of Holocene sediments directly north of Scripps Canyon, where sediments are nearly 20 m thick. Along strike to the north, sediments thin to zero, whereas bathymetry does not change. Note spatial correlation between the step offshore of isobaths >60 m and that of isopachs. Stars represent locations of Vibracores; solid for this study (2005) and unfilled for previous study (Darigo and Osbourne, 1986).

in the mid-shelf region before thinning again as water depth increases (Figs. 3 and 4).

The area where hardgrounds crop out to the north correlates with the deflection of bathymetric contours offshore at water depths >60 m (Fig. 4). Note that the nearshore contours do not exhibit this deflection, even though the slope of the isopach surface changes in this area from west dipping to southwest dipping.

A 135-cm-long Vibracore acquired in 2005 (Figs. 2 and 4) recovered fine-grained to very fine grained, olive-green, homogeneous sands consistent with the sediment recovered in longer Vibracores from the region (Darigo and Osbourne, 1986; Fig. 4). Mud horizons or coarse layers indicative of flood or storm events are not observed in this homogeneous upper layer. Beneath the sand is a slightly coarser unit that is not as well sorted, and includes larger clasts and more abundant shell fragments (units II and III of Darigo and Osbourne, 1986), which may be a transgressive lag deposit. The major fluvial input to this littoral cell is by the Santa Margarita and San Luis Rey rivers to the north, with predominant southern longshore transport (Inman and Jenkins, 1999). Wave reworking and longshore transport winnow out the fine-grained particles, resulting in a homogeneous nearshore deposit, consistent with the transparent acoustic character observed in the seismic data. Early Holocene floods may have contributed coarser material, but fine-grained to very fine grained sand likely resulted from the past 5 k.y. of enhanced El Niño–driven wave energy and consequent southern sand transport (Masters, 2006).

DISCUSSION

Several faulting trends in the La Jolla area could potentially explain the observed seafloor structure and sediment distribution. For example, one possible scenario is that the relief on the transgressive surface is only controlled by steeply dipping northeast-southwest–trending normal faults, such as those observed onshore at the southern end of Torrey Pines State Reserve (e.g., Carmel Valley fault, Fig. 1). On the basis of terrace offsets, these faults are older than 120 ka (Treiman, 1993). If such a fault caused uplift of the more resistant Del Mar Formation to the north with respect to the less resistant Scripps Formation to the south, we would expect a jog of isobaths seaward as the more resistant Del Mar Formation formed a promontory. If this scenario were correct, it would not predict that the isobaths should return shoreward north of the fault (Fig. 5A), and the faults would cause a marked local thickness change across the fault from the downdropped to the upthrown block (e.g., Fig. 2A). The lateral extent of the depocenter exhibits a wavelength longer than that of the onshore downdropped block bounded by the Salk and Torrey Pines faults (Figs. 1 and 4). Furthermore, the Carmel Valley fault onshore is down to the north; i.e., the sense of motion across the fault is opposite to that predicted by the observed sediment thickness. Alternatively, in a pop-up or constraining bend scenario, a left jog in a right-lateral fault zone would cause the thickness of the transgressive deposits to thin systematically from the depocenter toward the structural high without a sharp local thickness change (Fig. 5B). Such a constraining bend would predict that the isobaths shift seaward at the south end and return shoreward at the north end of the pop-up structure, which is consistent with the isobaths deeper than ~60 m (Fig. 4; see also the regional National Oceanic and Atmospheric Administration (NOAA) National Geophysical Data Center 3-arc-second coastal relief model [http://www.ngdc.noaa.gov/mgg/coastal/grddas06/grddas06.htm]). A gentle, long-wavelength uplift of the transgressive surface is observed in the seismic images, consistent with a left jog along the Rose Canyon fault zone. The relief on the transgressive surface is largest in the west near the jog in the Rose Canyon fault (e.g., 26.5 m; Fig. 2A) and diminishes eastward away from the jog (e.g., 21.5 m; Fig. 2B), as would be predicted by the pop-up hypothesis (Fig. 5). Seismic data recently acquired (2005 R/V *New*

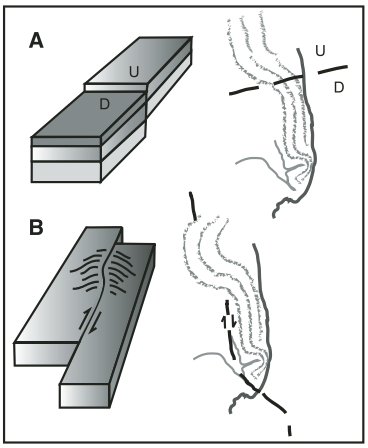


Figure 5. Two models of possible faulting mechanisms and expected bathymetry. A: Offset with more resistant Del Mar Formation exposed on upthrown block, along predominantly strike-slip fault, would cause bathymetry to step offshore. B: In case of left step on dextral strike-slip fault (e.g., Rose Canyon fault), we would expect bathymetric contours to deviate seaward on south end of fault and return landward on north end of fault, which we observe in both local bathymetry (California State University Monterey Bay 2 m) and regional bathymetry (National Oceanographic and Atmospheric Administration 3-arc-second model: http://www.ngdc.noaa.gov/mgg/coastal/grddas06/grddas06.htm). Black lines indicate fault trace; sense of motion is illustrated by arrows or D and U for downthrown and upthrown blocks.

Horizon cruise, unpublished data) to the north of the pop-up structure, where the isobaths shift shoreward, reveal that the transgressive surface has a northward dip, which is also consistent with the pop-up model. The relief on this surface may be augmented by the differential erodibility of the Eocene subsurface rocks, more indurated in the north than in the south (Kennedy, 1975).

The thickness of sediments between the canyons and directly north of Scripps Canyon, along with the near absence of sediments on the structural high to the north, suggest that uplift along constraining bends of the Rose Canyon fault plays an important role in long-term sediment accumulation in the region. The relief on the transgressive surface that predates sea-level incursion is difficult to constrain, and thus prevents reliable estimates for the deformation rate after sea-level incursion. Any relict relief would have created promontories and embayments. The dip of the reflector (DR) overlying the transgressive surface observed in line S4 can be explained by either post-transgression tilting or as backfill associated with erosion of the relict promontory (Fig. 2B). If we assume that all the relief postdates the sea-level rise, the estimated uplift rate will be biased toward a maximum. For example, if this differential relief is the consequence of tectonic uplift and tilting since inundation (ca. 10 ka), it yields deformation rates an order of magnitude larger than previous estimates of uplift rate in the region (0.13–0.14 mm/yr; Legg and Kennedy, 1979). Given that it is difficult to determine what portion of the relief is pre-incursion or post-incursion, long cores are required to place further constraints on the local tectonic uplift rates.

CONCLUSIONS

High-resolution geophysical data suggest that uplift offshore La Jolla, California, results from a left jog along the Rose Canyon right-lateral fault system, similar to the process responsible for forming Mount Soledad onshore. CHIRP seismic profiles show a shoaling of the transgressive surface from south to north. The seaward deflection of isobaths in the bathymetric data correlates with the change in slope of the transgressive surface and the change in overlying sediment thickness observed in the isopach map. Seismic profiles reveal that the sediments thin to zero above the uplifted bedrock, while the thickest sediments occur to the south of the pop-up structure. The observed sediment thicknesses suggest that tectonics control long-term sediment accumulation in the region, and hydrodynamics control sediment dispersion. Strain accommodation between right-lateral fault segments offshore Southern California results in marked thickness variability of the Holocene sediments. This new insight into controls on sediment accumulation and preservation may advance the understanding of our offshore sand resources and exposure of hardgrounds in the California Borderlands.

ACKNOWLEDGMENTS

This research was funded by the Office of Naval Research and the Kavli Institute. Reviews from Paul Liu, Dan Orange, and Glen Spinelli improved the manuscript.

REFERENCES CITED

Darigo, N.J., and Osbourne, R.H., 1986, Quaternary stratigraphy and sedimentation of the inner continental shelf, San Diego County, California, *in* Knight, R.J., and McLean, J.R., eds., Shelf sands and sandstones: Canadian Society of Petroleum Geologists Memoir II, p. 73–98.

Driscoll, N.W., and Hogg, J.R., 1995, Stratigraphic response to basin formation; Jeanne d'Arc Basin, offshore, Newfoundland, *in* Lambiase, J.J., ed., Hydrocarbon habitat in rift basins: Geological Society of London Special Publication 80, p. 145–163.

Fairbanks, R.G., 1989, A 17,000-year glacio-eustatic sea level record: Influence of glacial melting rates on the Younger Dryas event and deep-ocean circulation: Nature, v. 342, p. 637–642, doi: 10.1038/342637a0.

Inman, D.L., and Jenkins, S.A., 1999, Climate change and the episodicity of sediment flux of small California rivers: Journal of Geology, v. 107, p. 251–270, doi: 10.1086/314346.

Kennedy, M.P., 1975, Western San Diego metropolitan area; Del Mar, La Jolla, and Point Loma 7 1/2 minute quadrangles: California Division of Mines and Geology Bulletin, v. 200, p. 9–39.

Kennedy, M.P., Clarke, S.H., Greene, H.G., and Legg, M.R., 1979, Recency and character of faulting offshore from metropolitan San Diego, California: California Division of Mines and Geology, 37 p.

Legg, M.R., and Kennedy, M.P., 1979, Faulting offshore San Diego and northern Baja, California, *in* Abbott, P.L., and Elliott, W.J., eds., Earthquakes and other perils, San Diego region: San Diego, California, San Diego Association of Geologists, p. 29–46.

Lindvall, S.C., and Rockwell, T.K., 1995, Holocene activity of the Rose Canyon fault zone in San Diego, California: Journal of Geophysical Research B, Solid Earth and Planets, v. 100, p. 24,121–24,132, doi: 10.1029/95JB02627.

Masters, P.M., 2006, Holocene sand beaches of southern California: ENSO forcing and coastal processes on millennial scales: Palaeogeography, Palaeoclimatology, Palaeoecology, v. 232, p. 73–95, doi: 10.1016/j.palaeo.2005.08.010.

Moore, G.W., 1972, Offshore extension of the Rose Canyon fault, San Diego, California: U.S. Geological Survey Professional Paper P 0800-C, p. 113–116.

National Oceanic and Atmospheric Administration (NOAA) National Geophysical Data Center (NGDC) 3-arc-second coastal relief model: http://www.ngdc.noaa.gov/mgg/coastal/grddas06/grddas06.htm (July 2006).

Orange, D.L., 1999, Tectonics, sedimentation, and erosion in northern California; Submarine geomorphology and sediment preservation potential as a result of three competing processes; The formation of continental-margin strata: Marine Geology, v. 154, p. 369–382, doi: 10.1016/S0025–3227(98)00124–8.

Treiman, J.A., 1993, The Rose Canyon fault zone, southern California: California Division of Mines and Geology Open File Report 93–02, 45 p.

Manuscript received 25 July 2006
Revised manuscript received 21 October 2006
Manuscript accepted 29 October 2006

Printed in USA

Chapter 2, in full, is a reprint of the material as it appears in Geology 2007. Hogarth, Leah J., Babcock, Jeffrey; Driscoll, Neal W.; Le Dantec, Nicolas; Haas, Jennifer K.; Inman, Douglas L.; Masters, Patricia M. “Long-term tectonic control on Holocene shelf sedimentation offshore La Jolla, California”. The dissertation author was the primary investigator and author of this paper.

3

Tectonic Controls on Nearshore Sediment Accumulation and Submarine Canyon Morphology Offshore La Jolla, Southern California

Marine Geology 268 (2010) 115–128

Contents lists available at ScienceDirect

Marine Geology

journal homepage: www.elsevier.com/locate/margeo

Tectonic controls on nearshore sediment accumulation and submarine canyon morphology offshore La Jolla, Southern California

Nicolas Le Dantec [a,*], Leah J. Hogarth [a], Neal W. Driscoll [a], Jeffrey M. Babcock [a], Walter A. Barnhardt [b], William C. Schwab [b]

[a] Scripps Institution of Oceanography, UCSD, 9500 Gilman Drive, La Jolla, CA 92093-0208, USA
[b] U.S. Geological Survey, Woods Hole, MA 02543, USA

ARTICLE INFO

Article history:
Received 11 February 2009
Received in revised form 15 October 2009
Accepted 25 October 2009
Available online 10 November 2009

Communicated by J.T. Wells

Keywords:
tectonic deformation
submarine canyon morphology
nearshore sediment accumulation

ABSTRACT

CHIRP seismic and swath bathymetry data acquired offshore La Jolla, California provide an unprecedented three-dimensional view of the La Jolla and Scripps submarine canyons. Shore-parallel patterns of tectonic deformation appear to control nearshore sediment thickness and distribution around the canyons. These shore-parallel patterns allow the impact of local tectonic deformation to be separated from the influence of eustatic sea-level fluctuations. Based on stratal geometry and acoustic character, we identify a prominent angular unconformity inferred to be the transgressive surface and three sedimentary sequences: an acoustically laminated estuarine unit deposited during early transgression, an infilling or "healing-phase" unit formed during the transgression, and an upper transparent unit. Beneath the transgressive surface, steeply dipping reflectors with several dip reversals record faulting and folding along the La Jolla margin. Scripps Canyon is located at the crest of an antiform, where the rocks are fractured and more susceptible to erosion. La Jolla Canyon is located along the northern strand of the Rose Canyon Fault Zone, which separates Cretaceous lithified rocks to the south from poorly cemented Eocene sands and gravels to the north. Isopach and structure contour maps of the three sedimentary units reveal how their thicknesses and spatial distributions relate to regional tectonic deformation. For example, the estuarine unit is predominantly deposited along the edges of the canyons in paleotopographic lows that may have been inlets along barrier beaches during the Holocene sea-level rise. The distribution of the infilling unit is controlled by pre-existing relief that records tectonic deformation and erosional processes. The thickness and distribution of the upper transparent unit are controlled by long-wavelength, tectonically induced relief on the transgressive surface and hydrodynamics.

© 2009 Elsevier B.V. All rights reserved.

1. Introduction

The importance of underlying structures in controlling the formation and evolution of morphological features and sediment accumulation has long been appreciated (Shepard and Emery, 1941; Emery, 1958). Several studies illustrate the influence of tectonic deformation on geomorphology, such as continental slope morphology on tectonically active margins (Pratson and Haxby, 1996) or drainage patterns and formation of fluvial terraces (Peters and van Balen, 2007). Long-term retreat of modern beaches (Honeycutt and Krantz, 2003), the preservation and evolution of barrier-island systems (Belknap and Kraft, 1985; Schwab et al., 2000; Thieler et al., 2001; Harris et al., 2005), and short-term dynamic processes such as the position and stability of sandbars in the nearshore (McNinch, 2004), are also affected by underlying structures. Here we present new geophysical and geological data that show the importance of tectonic deformation in controlling canyon location and morphology and modern sediment distribution offshore La Jolla, California.

The sedimentary and morphological evolution of continental margins depends on many factors, three of which are eustasy, sediment supply, and tectonic deformation (Christie-Blick and Driscoll, 1995; Posamentier and Allen, 1999). Discerning how these parameters affect sediment accumulation is often difficult even when the factors are operating at different spatial scales (Sommerfield and Lee, 2003, 2004). On active margins tectonics plays a large role in controlling the nearshore physiography. In our study site, the shore-parallel deformation caused by transpression and transtension associated with the dextral Rose Canyon Fault (Fig. 1) can be isolated from the cross-shore oriented base-level changes imparted by regional tectonic uplift and eustatic sea-level fluctuations. Our work examines how local deformation affects the relief on the transgressive surface, which in turn, plays an important role in controlling regions of sediment bypass and accumulation.

* Corresponding author. Tel.: +33 2 23 23 55 99; fax: +33 2 23 23 67 17.
E-mail addresses: nledantec@ucsd.edu (N. Le Dantec), lhogarth@ucsd.edu (L.J. Hogarth), ndriscoll@ucsd.edu (N.W. Driscoll), jbabcock@ucsd.edu (J.M. Babcock), wbarnhardt@usgs.gov (W.A. Barnhardt), bschwab@usgs.gov (W.C. Schwab).

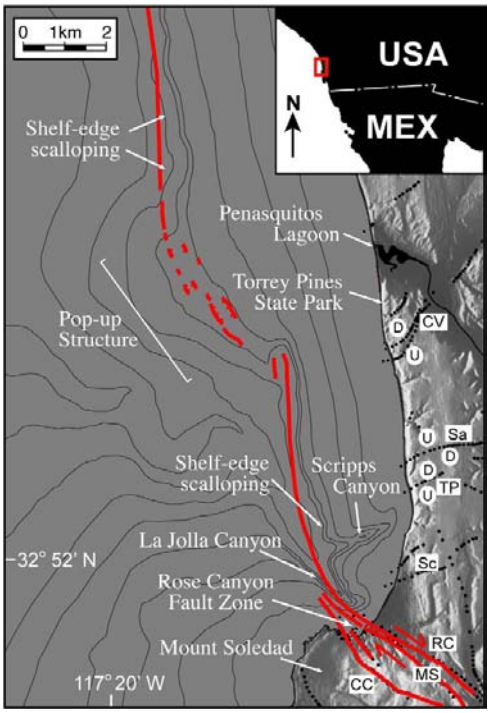


Fig. 1. Regional map showing the left jog along the right-lateral Rose Canyon Fault and the consequent structural high on the inner shelf. Arrows indicate sense of strike-slip motion on the fault. Fault-induced scalloping is observed where the Rose Canyon Fault coincides with the shelf edge north and south of the pop-up structure. Bathymetry is modified from Dartnell et al. (2007) with a 20-m contour interval. Local faults shown in dotted black lines are based on Kennedy (1975) with D and U for downthrown and upthrown sides. CC = Country Club, MS = Mount Soledad, RC = Rose Canyon, Sc = Scripps, TP = Torrey Pines, Sa = Salk, and CV = Carmel Valley faults.

The Rose Canyon Fault Zone (RCFZ; Moore, 1972; Treiman, 1993), a right-lateral, strike-slip fault system in the California Borderlands, is a major tectonic feature in the area. Although long assumed to continue offshore beneath the Pacific Ocean from its onshore expression in La Jolla, the first map of the offshore location of the feature was made by Moore (1972) using subbottom profiling. The acoustic reflection profiles imaged the fault for ~60 km to the northwest, but did not resolve its finer scale morphology, especially in the area of the La Jolla submarine canyon. Treiman (1993) combined subbottom profiles and land-based maps to refine the geometry of the RCFZ from San Diego Bay north to Oceanside. His focus was on Holocene seismicity, determining a slip rate of at least 1.0 mm/yr (Treiman, 1993). Transpression has occurred around westward jogs on the fault and created localized areas of uplift, two of which are expressed in the topography of Mount Soledad and the bathymetry and subbottom structure offshore Torrey Pines State Park (pop-up structure of Hogarth et al., 2007; Fig. 1). Wave-cut notches are observed along the shelf at various water depths and appear to record still-stands during the last sea-level rise (Emery, 1958; Byrd et al., 1975; Henry, 1976; Waggoner, 1979; Darigo and Osbourne, 1986).

La Jolla Bay is located at the southern end of the Oceanside littoral cell, which is delineated by Mount Soledad (Fig. 1). In this region, sediment transport is predominantly to the south (Inman and Chamberlain, 1960). Multiple studies have examined the Holocene sediment distribution (Henry, 1976; Waggoner, 1979), origin, age, transport mechanisms, and transport pathways (Everts and Dill, 1988; Hass, 2005; Young and Ashford, 2006), particularly in relation to the dynamics of littoral cells (Inman and Masters, 1991a, 1991b). Research on the Quaternary sediment cover on the shelf off San Diego County has also focused on coastal management, protection of marine habitats, and resource inventory for mining purposes (Darigo and Osbourne, 1986). The sediment thickness exhibits a wedge-shaped cross-shore profile with a mid-shelf depocenter (Byrd et al., 1975; Henry, 1976; Hogarth et al., 2007). Sediment input mostly consists of sand and silt derived from river discharge to the north and widespread cliff erosion (Stow and Chang, 1987; Hass, 2005; Young and Ashford, 2006).

Previous work on La Jolla Canyon has yielded fundamental scientific advances in the understanding of canyon morphology and architecture (Buffington, 1964; Shepard and Dill, 1966), the role of canyons for transport between deep oceans and shallow waters, submarine fan stratigraphy (Covault et al., 2007), turbidity flows and bottom canyon currents (Inman et al., 1976), erosive processes accompanying the formation and persistence of canyons (Shepard, 1981), sedimentation and erosion at canyon heads (Dill, 1964; Chamberlain, 1964), and interactions between canyons and biota (Vetter, 1994). The canyon has two branches, the Scripps Branch and the La Jolla Branch. Because the entire canyon has been termed the La Jolla Canyon, for clarity purposes, we will refer to the entire canyon as the La Jolla Canyon System. The La Jolla and Scripps canyon heads extend into shallow water (~8–10 m) and as such they modify nearshore circulation, surface wave patterns, and littoral sediment transport (Shepard and Inman, 1950; Thomson et al., 2005). In addition, currents measured along the floor of the canyons show a strong tidal component (Inman et al., 1976; Shepard et al., 1977).

In this study, high-resolution seismic and bathymetric data acquired offshore La Jolla, California between the surf zone and the shelf break (Fig. 2) allow us to examine the tectonic control on the locations of the La Jolla and Scripps submarine canyons as well as the impact of tectonics on postglacial sedimentation on the inner shelf offshore La Jolla. We will first present the results for the canyon morphology and then we will discuss the stratigraphic packages observed along the margin from oldest to youngest based on the first comprehensive maps of their aerial distribution.

2. Methodology

2.1. Data acquisition

In 2002 and 2003, high-resolution swath bathymetry and seismic data were acquired offshore La Jolla, Southern California during three cruises. The surveys covered the narrow shelf from Point La Jolla north to Penasquitos Lagoon. The survey tracks mostly consist of strike lines with about 150-m line spacing, augmented with four dip lines (Fig. 2). We used a SwathPlus-L (formerly Submetrix) interferometric swath bathymetric sonar by SEA Ltd (http://www.sea.co.uk) and the Scripps subbottom reflection sonar system (SUBSCAN), which is a modified EdgeTech (http://www.edgetech.com/) CHIRP system that consists of a dual-transducer X-Star sonar with an ADSL link from the towfish to the topside computers.

The SwathPlus-L sonar, which operates at 117 kHz and has a nominal cross-track resolution up to 15 cm, yielded better than 50-cm horizontal resolution even over the steep topographic features of the survey area, up to at least 75 m depth. The SUBSCAN sonar uses a 50 ms swept pulse across a 1.5 to 5 kHz range with 24° beam width, yielding sub-meter vertical resolution to sub-seafloor depths of approximately 50 m. During the nearshore surveys in 2002 onboard the *RV Saikhon*, the SwathPlus-L system was attached to a side-mount while the SUBSCAN system was 'floated' on a surface tow frame. The deployment configuration was complemented with an onboard motion sensor and a global positioning system (GPS) receiver to measure attitude and position. Navigation for the seismic data was

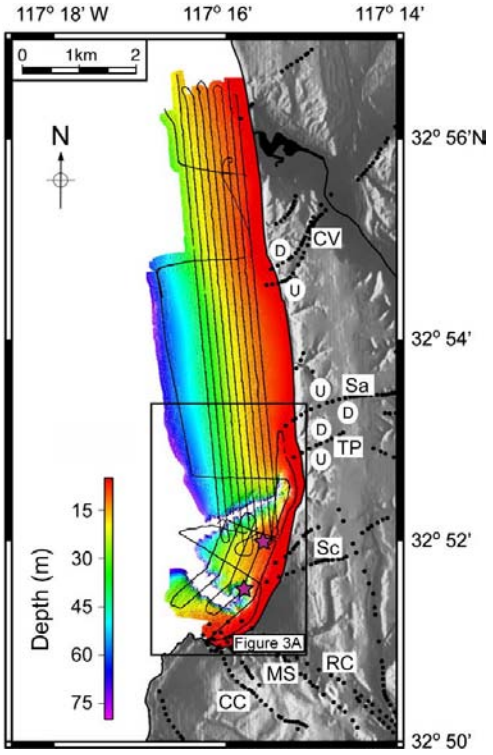


Fig. 2. Ship tracks are shown (black lines) superimposed on high-resolution bathymetry. Core locations are denoted by purple stars (push core near La Jolla Canyon head and vibracore near the Scripps Pier south of Scripps Canyon). See Fig. 1 for abbreviations. (For interpretation of the references to color in this figure legend, the reader is referred to the web version of this article.)

measured using a second GPS receiver mounted on the surface tow frame. During the offshore survey in 2003 onboard the *R/V Sproul*, only seismic data were collected and the SUBSCAN system was towed at approximately 10 m above the seafloor. Winch cable payout records were used to correct layback offsets during post-processing. Data were acquired at a ship speed of approximately 4–5 knots during both surveys.

During a scuba dive on Dec 14th 2007, a short push core was acquired from a layer that outcrops along a ridge at 23 m water depth near the head of La Jolla Canyon (Figs. 2 and 3B). The site was selected to ground-truth one of the stratigraphic packages identified in the seismic data, which has a laminated acoustic character and outcrops in this area. A 2-inch diameter clear plastic tube with a tapered extremity was pushed into the seafloor and capped before pulling it out to create suction and improve sediment recovery. The lower end of the core was capped underwater so that the sample was well preserved. The core was split, described and photographed. Other vibracores referenced in relation to geophysical interpretations were collected and processed by Hogarth et al. (2007) and by Darigo and Osbourne (1986).

2.2. Data processing

Processing the raw bathymetry data involved numerous steps. The soundings were corrected incorporating the acquisition parameters – attitude and position – as well as water level fluctuations with the tides using observations from the NOAA tide gauge installed at the Scripps Pier. The vertical datum was shifted from MLLW to NAVD 88. The sound speed in water was adjusted using CTD data, which were collected during the survey to account for density variations between nearshore, shelf, and deeper waters within the submarine canyons. The data volume was gridded at 50-cm resolution with a continuous curvature spline in tension. Finally, the data were smoothed using a linear convolution filter of 11.5 m averaging window size in both horizontal directions.

The seismic data were converted into standard SEG-Y, heave-corrected, processed, and plotted using SIOSEIS (Henkart, 2003) and SeismicUnix (Cohen and Stockwell, 2002) seismic processing software. In addition, depths to various acoustic reflectors identified in each profile were digitized. The corresponding horizons were then gridded at 10 m resolution and used to generate isopach maps of the stratigraphic packages. In order to convert travel time to sediment thickness, a velocity of 1720 m/s was used for non-silty sediments and a velocity of 1520 m/s was used for water and mud-dominated sediments (Jackson et al., 1996; Williams et al., 2002; Buckingham and Richardson, 2002). We used the software Fledermaus by Interactive Visualization Systems (IVS 3D, http://www.ivs3d.com) to merge all graphic elements into three-dimensional perspective views of the seafloor and subbottom.

3. Results

3.1. Bathymetry

3.1.1. Canyon morphology

The two canyons, as revealed by high-resolution bathymetry, exhibit very different morphologies (Fig. 3). La Jolla Canyon is much wider than Scripps Canyon, especially near its head. Scripps Canyon is ~150 m wide at its seaward extent, but narrows to ~30 m wide near its head. In contrast, the width of La Jolla Canyon is ~250 m along its length, and widens to nearly 500 m at its shoreward extent where incisions form a bowl-shaped head. In addition, Scripps Canyon is very linear, whereas La Jolla Canyon curves gently to the north with a 30° change in its azimuth from the canyon head to where it intersects Scripps Canyon. The Scripps Canyon head is narrow and steep-walled. Conversely, the La Jolla Canyon head is characterized by a concave upwards morphology with moderate slopes. The upper reaches of La Jolla Canyon are dissected by a number of ridges and gullies (Fig. 3). Some of these ridges extend quite far into the canyon acting as promontories separating the bowl-shaped canyon heads.

3.1.2. Side canyons

The morphology of side canyons incised into the walls of the two canyons is also dissimilar. For example, a few large side canyons have incised the margins of La Jolla Canyon deeply enough to intersect consolidated basement rocks. Near or within the head of the canyon, these channels are long and remarkably tortuous, with one in particular taking two well-defined and opposite turns ("S"; Fig. 3). The incision located on the northern wall of La Jolla Canyon, south of the intersection with Scripps Canyon is wide and rounded, resembling the scalloping on the shelf edge north of Scripps Canyon ("I"; Fig. 3). The northern most incision observed in Fig. 3 causes a shoreward inflexion of the 75 m isobath, that appears as a depression in the bathymetry (northern most "I"; Fig. 3A). In contrast with La Jolla Canyon, the side canyons of Scripps Canyon are shallower, smoother-walled, and are primarily incised into unconsolidated sediments. Side canyons have generally incised oblique to the axis of Scripps Canyon, and some extend far away from its axis (~500 m, Fig. 3) despite their gentle slopes. Farther north along the margin, a structure resembling a side canyon is observed in the bathymetry, which defines the southeast corner of the pop-up structure and is where the Rose Canyon Fault takes a westerly jog (Fig. 1).

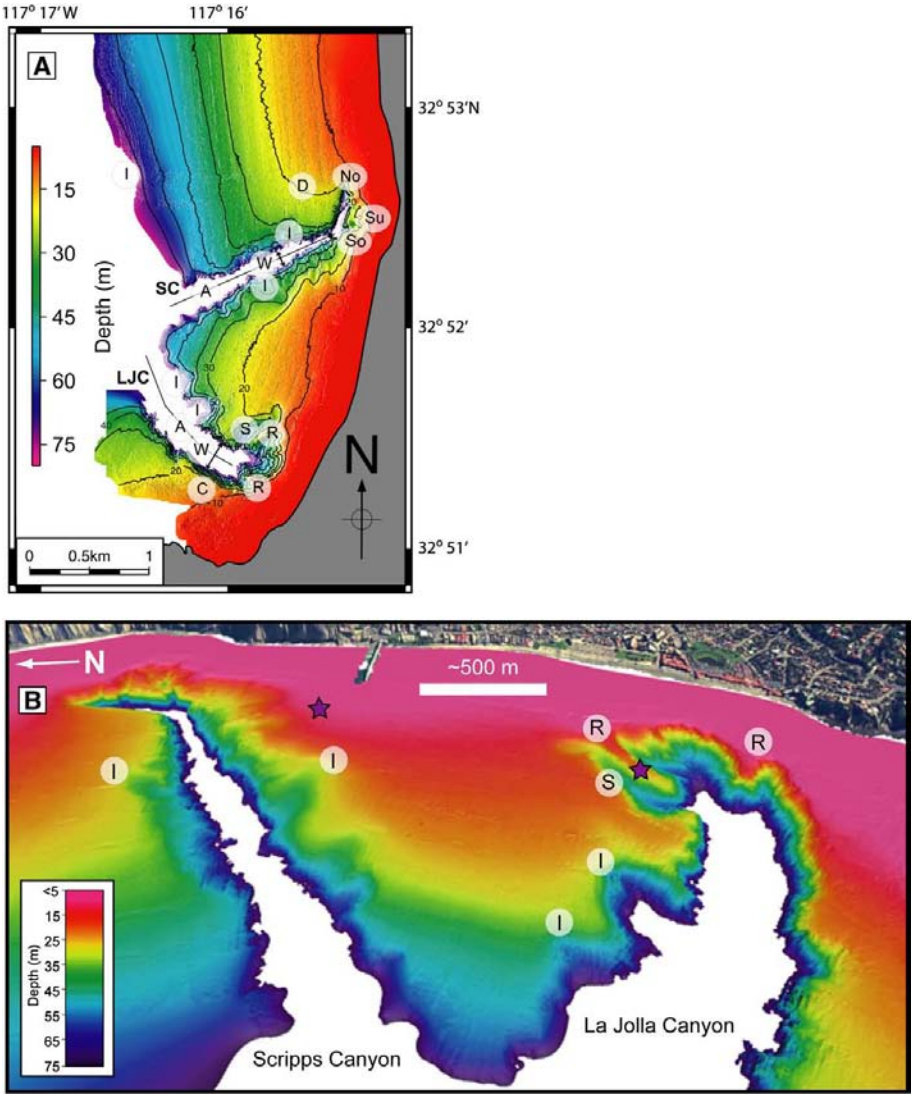


Fig. 3. High-resolution bathymetry near La Jolla Canyon System. A: View of high-resolution bathymetry near La Jolla and Scripps canyons. SC = Scripps Canyon, LJC = La Jolla Canyon, A = Canyon thalweg, W = Width of canyon thalweg, I = Incision into canyon wall (side channel), S = Sinuous side channel, C = Cretaceous hard grounds, R = Ridge within La Jolla Canyon head, D = Deflection of isobath shoreward, So = South Branch of Scripps Canyon, Su = Sumner Branch of Scripps Canyon, No = North Branch of Scripps Canyon. B: Perspective view looking east with core locations. Bathymetry has a vertical exaggeration of 6:1, while the land has none. (For interpretation of the references to color in this figure legend, the reader is referred to the web version of this article.)

3.1.3. Asymmetry between the north and south walls

The canyon walls exhibit marked asymmetry (Fig. 3). For example, most of the ridges and side canyons of La Jolla Canyon occur on its north wall. Conversely, the south wall has few or no secondary incisions, especially in the shallow section near the canyon head. In Scripps Canyon, secondary incisions are more frequent, larger, and deeper along the south wall. Despite these differences, the canyons also share some morphologic features. One similarity is the northward orientation of their heads. As the canyons trend shoreward across the shelf, their shallow-water extensions are preferentially developed towards the north. Another common trait is that, except for the head of La Jolla Canyon, the slopes of the walls are very steep in both canyons.

3.2. Regional angular unconformity

A regional angular unconformity is identified in seismic profiles and mapped throughout the study area. The surface is typically identified by dipping and truncated reflectors below (Fig. 4) and is overlain by relatively flat-lying reflectors or an acoustically transparent unit (Fig. 5). Regionally, the bedding beneath the angular unconformity dips to the south, but three areas exhibit reversals in this trend (Fig. 4). The major

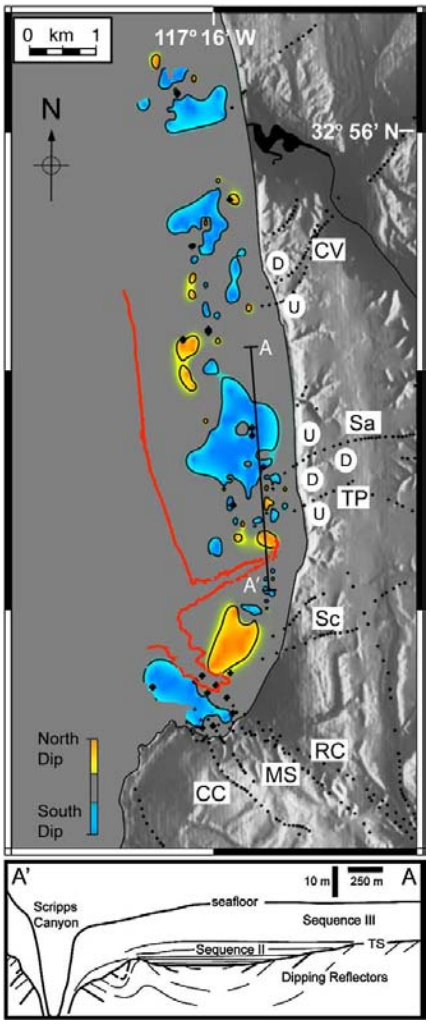


Fig. 4. Regional bedding dips. Black diamonds mark faults identified in seismic profiles. See Fig. 1 for abbreviations. The outline of the canyon is superimposed in red. Cross-section from A to A′ shows dipping reflectors beneath the transgressive surface (TS), inferred synforms and antiforms, and their relationship to Scripps and La Jolla canyons. Sequences II and III are shown. (For interpretation of the references to color in this figure legend, the reader is referred to the web version of this article.)

regions where bedding dips to the north are the following: 1) directly north of La Jolla Canyon, 2) directly north of Scripps Canyon, and 3) in the localized offshore high aligned with the Carmel Valley Fault (Fig. 4). Where the reversal of dip is observed offshore, the units dip more steeply to the north (~15–20°) than those measured onshore (~5–10°; Kennedy, 1975).

In areas where the unconformity was difficult to identify based on stratal geometry, it was traced laterally from regions where it could be confidently identified. Deposition above the angular unconformity exhibits much variability ranging from acoustically laminated onlapping deposits to acoustically transparent deposits (Fig. 5). In some areas the angular unconformity becomes the seafloor (Figs. 6 and 7B). Hogarth et al. (2007) identified this unconformity as the transgressive surface from the last deglaciation (~21 ka to present). Throughout much of the study area, the transgressive surface coalesces with the underlying sequence boundary formed during the last sea-level fall (~120 to 21 ka), but the two surfaces appear to diverge in the canyon regions.

The transgressive surface shows much variability in topography and roughness in the along-shore and cross-shore directions. It has relatively high relief on either side and in the immediate proximity of the La Jolla and Scripps canyons. To the south of La Jolla Canyon, the transgressive surface shallows where Cretaceous mudstones outcrop on the seafloor. Between the two canyons the transgressive surface is relatively flat, uniformly slopes to the northwest, and is overlain by up to 20 m of sediments. The high in the transgressive surface near Scripps Canyon is more pronounced to the north of the canyon (Figs. 7A, 8, and 9B). A constraining bend in the Rose Canyon Fault creates a structural high in the transgressive surface in the northern portion of our study area. A saddle along the transgressive surface is observed between the high coincident with Scripps Canyon and the high associated with the pop-up structure (Figs. 5, 8, and 9B). Within this low, strike profiles show a localized high offshore with an along- and cross-shore extent of ~1 km and moderate vertical relief of a few meters (Fig. 5). Dip lines show several notches or wave-cut terraces on the transgressive surface that have relief on the order of several meters (Fig. 7B).

A notable decrease in roughness along the transgressive surface is observed from offshore to onshore (Fig. 5). The onshore trends of the Carmel Valley, Salk, and Torrey Pines faults appear to be aligned with the deformation observed in water depths >~45 m (Figs. 2, 4, and 5). At shallower depths, the expression of the fault on the transgressive surface is subtle and only delineated by changes in bedding orientation below the transgressive surface. Furthermore, wave-cut terraces on the transgressive surface are confined to water depths >20–30 m and their relief increases with depth (Fig. 7B).

Observations from the sea cliffs in our survey area offer an ideal opportunity to examine the along-shore variability of the tectonic landscape, which complements our offshore observations. In the northern part of our study area, Legg and Kennedy (1979) identified a system of east–west trending oblique faults, including the Carmel Valley and Salk faults. Sea cliffs between the south extremity of La Jolla Shores beach and Point La Jolla are of particular significance because they lie within the RCFZ, where trench studies suggest Holocene deformation (Lindvall and Rockwell, 1995). Along the seacliffs, we observe three strike-slip faults, namely the Country Club, Mount Soledad, and Rose Canyon faults from south to north (Fig. 2; Treiman, 1993), as well as a number of more diffuse fault splays. The change in coastal relief from the low-lying La Jolla Shores to the uplifted and deformed sea cliffs along Mount Soledad parallels the change in seabed type from sandy bottom to the kelp-bearing rocky substrate observed around Point La Jolla (Fig. 2). This transition from mobile sands to hardgrounds is associated with the Rose Canyon Fault, which lines up with La Jolla Canyon, and delineates the northern extent of Mount Soledad. In turn, the Country Club Fault correlates with a zone of increased seafloor roughness that occurs immediately south of La Jolla Canyon. The Country Club Fault is also associated with differences in erosion patterns along the sea cliffs. South of the Country Club Fault and north of the Mount Soledad Fault, rocks are sand-dominated whereas in between these two faults the rocks are mud-dominated.

3.3. Sedimentary units offshore La Jolla

3.3.1. Sequence I: Canyon-edge deposits

The lowest unit interpreted in the seismic profiles is characterized by parallel, highly reflective horizons inter-bedded with acoustically transparent sediments. Sequence I onlaps existing topography, is locally truncated by the overlying transgressive surface, and is deposited above

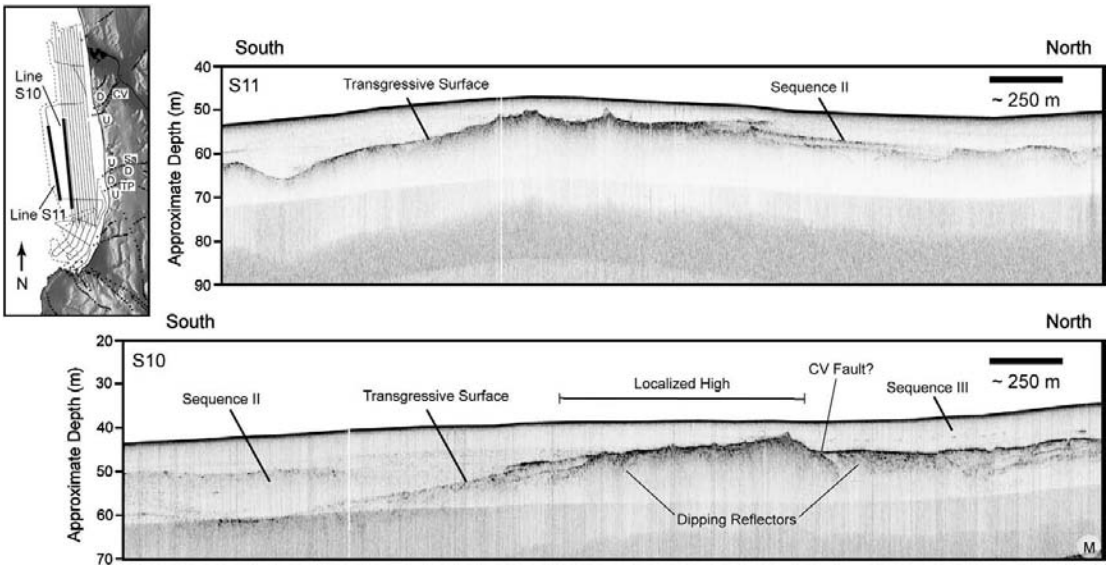


Fig. 5. Transgressive surface roughness increases with water depth. A: The offshore line, strike line 11, exhibits more roughness on the transgressive surface due to deformation on the Carmel Valley, Salk, and Torrey Pines faults. B: Strike line 10 is slightly shallower and exhibits significant smoothing of the transgressive surface. (M = multiple). Note Sequence II infills the lows. In location map, dotted line shows extent of bathymetry data and bold lines show profile locations.

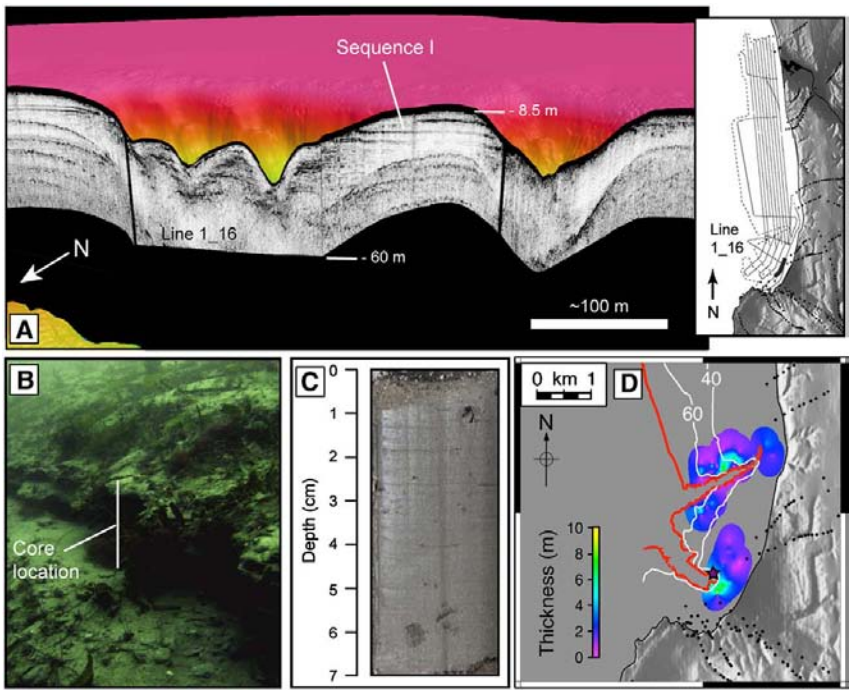


Fig. 6. A: Perspective image showing Sequence I outcropping at the seafloor. Bathymetry and seismic profile have vertical exaggeration of 6:1. Bold line on inset shows the profile location and dotted line shows extent of bathymetry survey. B: Underwater photograph showing layers of Sequence I where push core was collected. C: Fine-grained sediment recovered in push core. D: Sequence I isopach map shows distribution and thickness of this unit and push core location. Red line outlines canyons and white lines are structure contours to the top of the transgressive surface. (For interpretation of the references to color in this figure legend, the reader is referred to the web version of this article.)

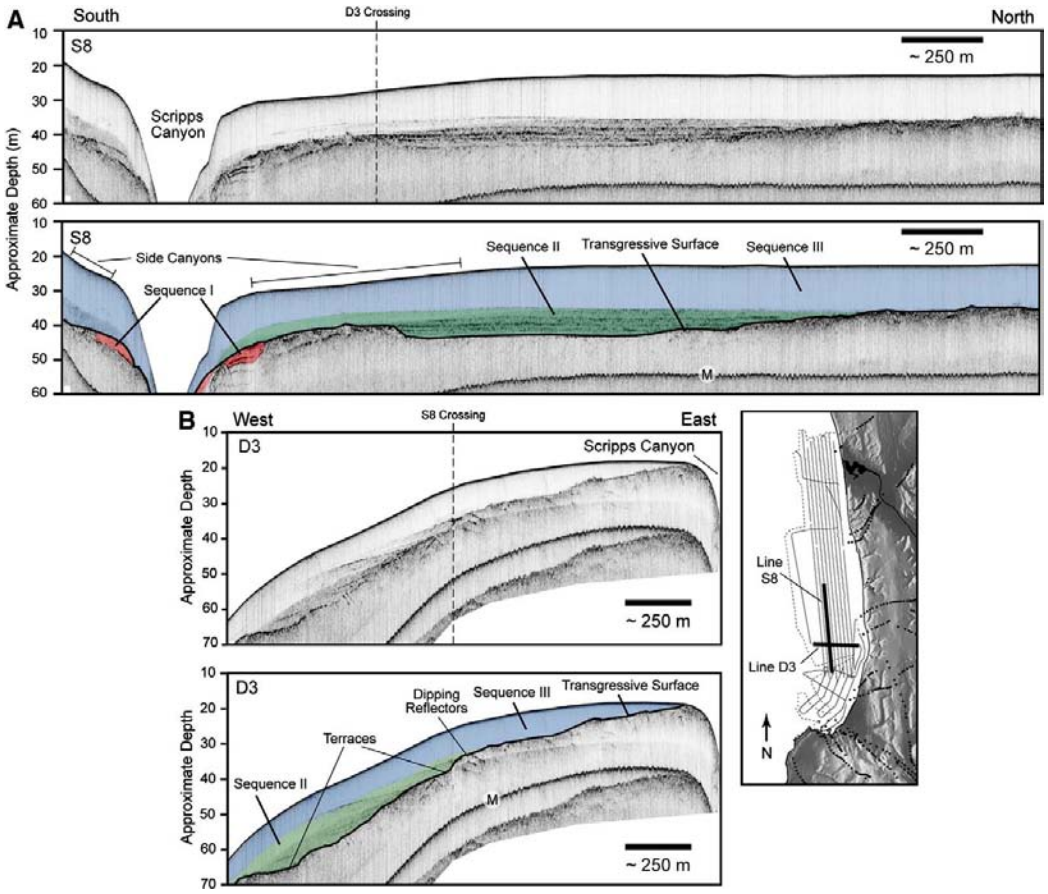


Fig. 7. CHIRP profiles. A: Strike line 8 uninterpreted (top) and interpreted (bottom) shows Sequences I, II, and III. Note that Scripps Canyon is located within a high in the transgressive surface. B: Dip line 3 uninterpreted (top) and interpreted (bottom) shows Sequences II and III. The terraces formed during relative sea level still stands are more prominent at greater depths. (M = Multiple). Color code is as follows: red = Sequence I, green = Sequence II, and blue = Sequence III. Thick black line traces the transgressive surface. In the location map, dotted line shows extent of bathymetry survey and bold lines show profile locations. (For interpretation of the references to color in this figure legend, the reader is referred to the web version of this article.)

the inferred sequence boundary (Figs. 6A, 7A, and 8). These layers tend to attenuate the acoustic source energy, which generally precludes imaging of deeper stratigraphic units. Divers sampled Sequence I at ~23 m depth in the head of La Jolla Canyon and recovered push cores containing fine-grained muds inter-bedded with silts and sands (Figs. 2, 3B, and 6C). An isopach map of these laminated sediments shows that they occur along the canyon edges (Fig. 6D). These sediments have a large spatial extent at the head of La Jolla Canyon, whereas they are confined to the edges of Scripps Canyon. Furthermore, the sediments of this unit are thicker near La Jolla Canyon (>10 m thick) than in Scripps Canyon.

3.3.2. Sequence II: Infilling unit

Within the sediments overlying the transgressive surface, a basal unit exhibiting distinct lamination is observed (Fig. 7). The acoustic character of these sediments is different from the unit observed near the canyons; as they are sub-parallel, highly reflective horizons inter-bedded with unevenly reflective layers. The unit is spatially limited to the lows in the transgressive surface between the two canyons and to the north of Scripps Canyon (Figs. 5, 7, and 8). These laminated sediments are thickest, up to 12 m thick, seaward of the 30 m isobath. Moreover, these deposits infill lows and diminish relief on the transgressive surface (Figs. 5 and 7B). In dip lines, between ~70 m and 35 m water depth, the onlapping reflectors within Sequence II have high acoustic amplitudes at their landward terminations, but the amplitudes diminish seaward, where they eventually become acoustically transparent. Some of the layers exhibit down-lap onto older deposits within this sequence or onto the underlying transgressive surface.

The isopach map in Fig. 10B details the thickness and distribution of Sequence II deposits. The thickest accumulation fills a structural low on the transgressive surface just to the north of Scripps Canyon (Figs. 8 and 9B). Sequence II is absent landward of the 20-m bathymetry contour (Figs. 8 and 10B). Although the thickness of the entire sedimentary sequence above the transgressive surface is variable (Fig. 10A), most of the observed lateral variability is associated with Sequence II (Fig. 10B).

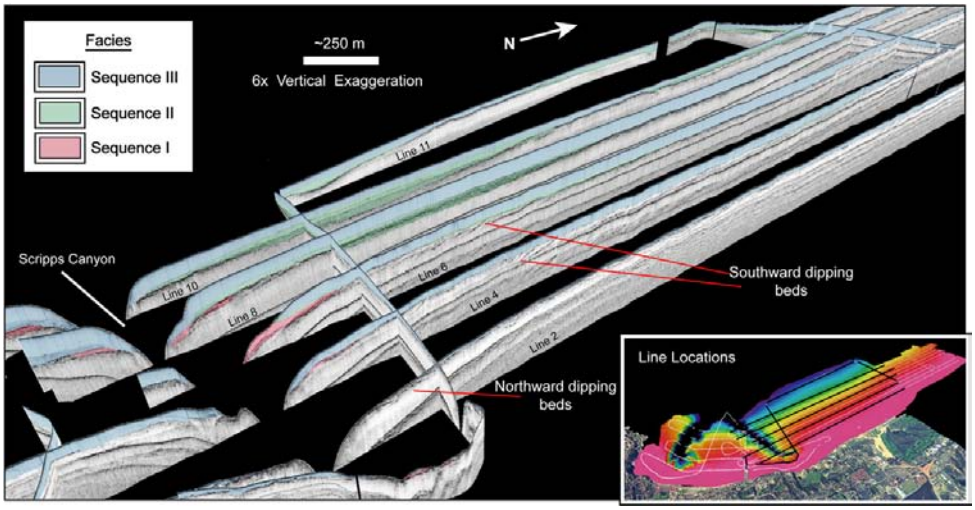


Fig. 8. Seismic fence diagram revealing the regional distribution of Sequences I, II, and III. Sequence I (red unit) in this region is confined to the edges of Scripps Canyon. Dipping and truncated reflectors are observed beneath the transgressive surface and their dip varies along strike as shown in Fig. 4. Sequence II (green unit) preferentially infills lows along the transgressive surface and thins landward. Northward thinning of Sequence III (blue unit) is observed in the study region. Profiles have a vertical exaggeration of 6:1. Inset shows figure location and seismic lines shown. (For interpretation of the references to color in this figure legend, the reader is referred to the web version of this article.)

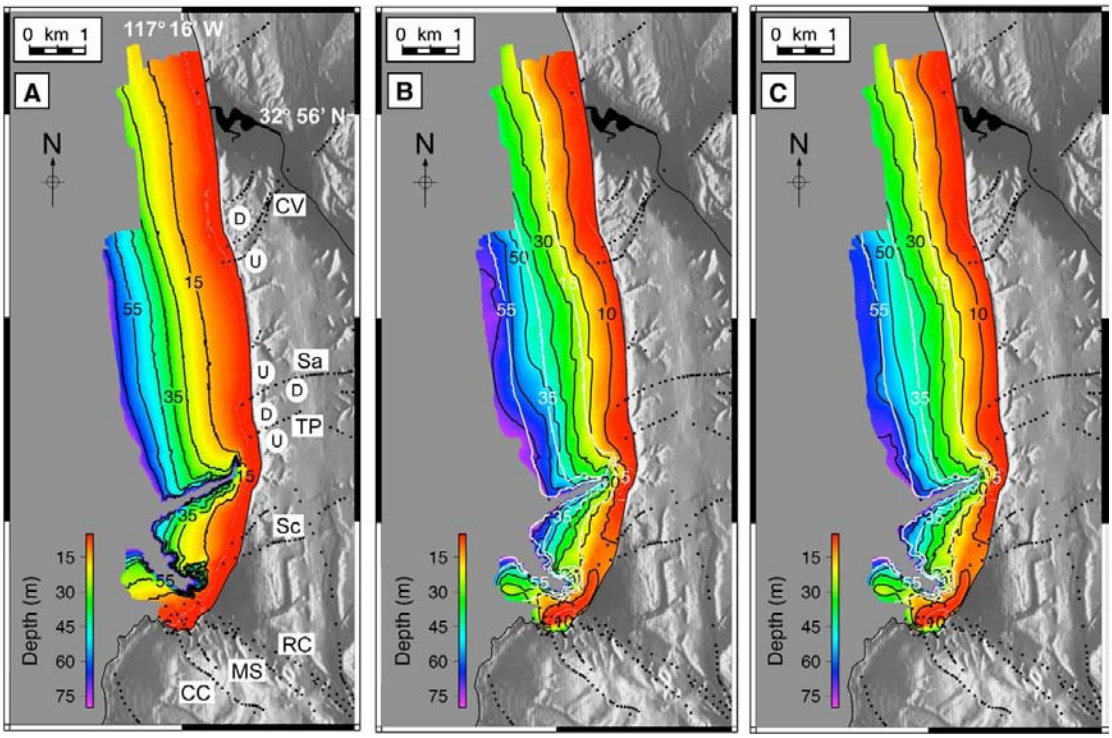


Fig. 9. Structure contour maps. A: Bathymetry with 10 m contour interval in black. B: Depth to the transgressive surface with contours in black. C: Depth to the top of Sequence II with contours in black. For maps B and C, bathymetry contours are superimposed in white. (For interpretation of the references to color in this figure legend, the reader is referred to the web version of this article.)

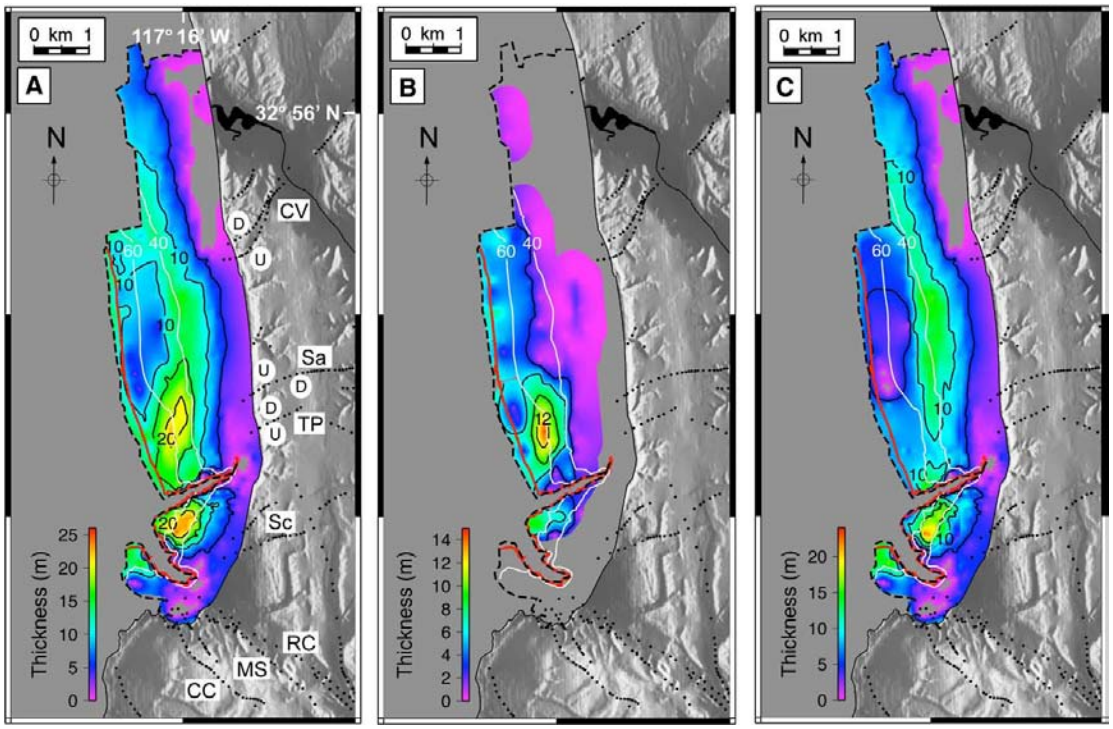


Fig. 10. A: Isopach map of Sequences II and III. B: Isopach map of Sequence II. C: Isopach map of Sequence III. Note that Sequence II makes up most of the northern depocenter observed in A, whereas the inter-canyon depocenter is predominantly Sequence III. Isopach thicknesses are shown in black. For reference, the 40 m and 60 m structure contours to the top of the transgressive surface (white) and the outline of canyon (red) are superimposed. Note thickness scales vary for the different panels and were selected to highlight along-strike variability. Survey area is shown by dashed line, and gray regions within survey area are regions with zero sediment thickness. (For interpretation of the references to color in this figure legend, the reader is referred to the web version of this article.)

3.3.3. Sequence III: Upper unit

The uppermost unit is acoustically transparent, exhibits cross-shelf thickness variability with a mid-shelf depocenter, and makes up the majority of sediment overlying the transgressive surface (Figs. 7 and 8). The unit is fine-grained to very fine-grained, homogenous sands based on cores acquired in the area (Fig. 2; Darigo and Osbourne, 1986; Hogarth et al., 2007). In areas where these acoustically transparent sediments overlie the transgressive surface, there is a clear transition, but the transition between Sequences II and III can be less distinct. The laminations of Sequence II grade upward into the transparent Sequence III and in some areas fade into the transparent unit approaching their lateral terminations (Fig. 7). Thus, the boundary between the basal unit and the overlying sediments was selected at the uppermost identifiable reflector. Despite being acoustically transparent, the unit does contain several subtle, oblique or occasionally curved reflectors. In strike lines at the canyon edges, as the seabed slope increases, these reflectors dip towards the canyon axis and, where curved, are generally concave upwards. In general, the reflectors originate at or near the seabed, and sometimes occur in sets of two or three reflectors. The geometry of these features is similar to the shape of the seafloor observed along the modern canyon edges. Where the reflectors intercept the basal highly reflective package (Sequence II) near the canyon edges, they appear to truncate the underlying reflectors and also exhibit a change in trend from concave up to concave down. Several profiles exhibit an apparent increase in thickness of the transparent sediment unit in close proximity to the canyon due to the oblique orientation of side channels (Figs. 3B and 7A). This creates a concave-up geometry of the seabed in strike profiles crossing the canyon, reflecting the three-dimensionality of these side channels.

An isopach map showing the combined thickness of Sequences II and III (Fig. 10A) illustrates how these sequences infill topographic relief along the transgressive surface (Fig. 9B). In the isopach map (Fig. 10A), from south to north, we observe the following: 1) Holocene sediment is absent on top of the hard grounds south of La Jolla Canyon, 2) a depocenter containing >20 m of sediment overlies the erosional surface between the two branches of the canyon, 3) a second depocenter north of Scripps Canyon also contains >20 m of sediment, and 4) sediment thickness thins to ~5 m across the zone that extends between Scripps Canyon and the northern extent of the study area, which corresponds to the pop-up structure identified by Hogarth et al. (2007).

As previously mentioned, much of the variability in the thickness of the Holocene unit (Fig. 10A) corresponds to variability in the basal, reflective package (Fig. 10B). This basal unit makes up most of the depocenter north of Scripps Canyon (Fig. 10B), whereas the upper transparent unit accounts for the majority of sediment in the depocenter between the two canyons (Fig. 10C). In addition, to the north of Scripps Canyon, the overlying acoustically transparent unit (Fig. 10C) reveals a well-developed mid-shelf depocenter along the 40 m depth contour. Note the slight seaward deflection of the mid-shelf depocenter toward the north offshore Torrey Pines State Park, reflecting deformation on the constraining bend and uplifted pop-up structure (Hogarth et al., 2007).

4. Discussion

4.1. Tectonic control on canyon location

Although researchers have long proposed that the RCFZ controls the location of La Jolla Canyon (e.g., Shepard, 1981; Treiman, 1993), the seismic and swath data provide new constraints on regional tectonic deformation and the distribution of post-Last Glacial Maximum (LGM, ~21 ka) sedimentary sequences. Bedding planes beneath the transgressive surface exhibit widespread dip reversals to the north of La Jolla Canyon (Fig. 4). The relatively steep dip of these units near La Jolla Canyon appears to be the result of compression along the constraining bend north of Mt. Soledad (Fig. 4). Farther east onshore, bedding mapped by Kennedy (1975) dips more shallowly because the fault is more translational in this region. Similar dip reversals have been observed in other regions where folding and faulting have been documented (e.g., Gulick and Meltzer, 2002).

The seismic and bathymetric data suggest that Scripps Canyon formed at the apex of a structural antiform (Fig. 4). While other rectilinear canyons extending close to the coastline appear to be fault-controlled (e.g., the Redondo Canyon; Gardner et al., 2002), none of the en-echelon oblique faults observed in adjacent sea cliffs project offshore to the location of Scripps Canyon (Fig. 2). Shoaling of the transgressive surface associated with the antiform that appears to control Scripps Canyon is best expressed on the northern limb (Figs. 4 and 9B). Anticlinal folding causes extension above the neutral surface and consequent fracturing parallel to the axis of the fold. In contrast, synclines as observed between the canyons and to the north of Scripps Canyon engender compression above the neutral surface that would minimize fracturing. We propose that erosion at the apex of this antiform would be enhanced due to the fractured and structurally weakened nature of the rock (Davis and Reynolds, 1996). Enhanced erosion along this shore-normal zone of fractures may have initiated formation of Scripps Canyon. The linear morphology of Scripps Canyon has led previous researchers to invoke a tectonic origin. Specifically, fractures related to the Torrey Pines Fault have been purported to exert a structural control on the orientation of the shallow-water branches at the head of the canyon (Webb, 1988; Rindell, 1991). However, there is no evidence in seismic profiles of faults intersecting the heads of Scripps Canyon. In our scenario, these fractures are not fault-controlled, but are rather associated with folding and consequent extension across the crest of an antiform.

La Jolla Canyon is also located in an area with pronounced dip reversal, which is the result of the RCFZ (Fig. 4). Onshore observations of the three main faults and of their offshore extensions imaged in the seismic data refine our understanding of the structural control on the formation of La Jolla Canyon (Fig. 4). The thalweg of La Jolla Canyon occurs along a thrust fault in the RCFZ that separates lithified Cretaceous mudstones from less consolidated Eocene sands and gravels. The Country Club Fault, despite having large horizontal offset on land, has little influence on the location of the La Jolla submarine canyon because the Cretaceous rocks on both sides of the fault are well indurated. It appears that the canyon exploits the northernmost fault, which is the boundary between the competent Cretaceous formations and the less lithified Eocene sands and gravels.

4.2. Tectonic control on canyon morphology

Tectonically induced structure governs the characteristics of the side channels that intersect La Jolla Canyon. The marked asymmetry exhibited by these side channels, being much larger on the northern wall, is likely controlled by lithologic differences across the Rose Canyon Fault (Fig. 3). Short, arcuate cuts in the south wall of La Jolla Canyon occur where highly resistive Cretaceous lithified units are exposed. Side canyons on the northern wall of La Jolla Canyon incised more deeply into the adjacent shelf due to the less indurated Eocene substrate. One of the larger incisions on the northern side of La Jolla Canyon appears to be controlled by the northeast–southwest trending Scripps Fault (Fig. 2 and "S" in Fig. 3). This side canyon trends to the northeast for ~500 m, but abruptly curves to the north at its head.

In contrast to La Jolla Canyon, the side canyons along Scripps Canyon incise only the upper surficial sediments that are unlithified, and as a result are much less steep (Fig. 2). Observations of recurring sediment accumulation and subsequent catastrophic slump events indicate that some of the secondary canyon tributaries are active (Dill, 1964; Marshall, 1978). The oblique intersection of these secondary incisions with the thalweg of Scripps Canyon suggests formation by downslope-eroding sediment flows, rather than by retrogressive failure alone, which would yield a more orthogonal geometry (Farre et al., 1983). In addition, Mastbergen and van den Berg (2003) recently proposed a breaching model based on negative pore pressure build-up and tested it on a well-documented slide in the south wall of Scripps Canyon (Marshall, 1978). The role of slope failure in forming these channels is apparent in the shape of the canyon edges. The steep upper walls appear to be formed by failure of unconsolidated Holocene deposits. In addition, there is no observed down-lap in the strike lines across Scripps Canyon that would be indicative of the non-deposition and sediment bypass associated with strong axial canyon currents (Fig. 7).

The influence of the canyon on the adjacent morphology as observed in the bathymetry is over a much greater distance than would be predicted by slope stability (Figs. 3 and 7A). In the upper walls of Scripps Canyon and along the north side of La Jolla Canyon, the slopes should not exceed the angle of repose for saturated sands as the sediments are unconsolidated. It is interesting to note, the slopes of the side canyons are significantly below the angle of repose yet they extend up to 1 km away from the thalweg. These observations suggest that other factors in addition to slope stability may shape the side canyons.

4.3. Tectonic control on sediment distribution and thickness

Three sedimentary units and their relative ages have been identified in the seismic data based on stratal geometry, acoustic character, and analyses of sediment samples where available. We interpret Sequence I, the highly reflective unit observed near the canyons and sampled by push core, as an estuarine or lagoonal deposit, consistent with previous findings that the sediments within the head of La Jolla Canyon were deposited in an estuarine environment (Shepard and Dill, 1966; Holden 1968; Judy 1987). The presence of ostracods in sediment samples recovered from the head of La Jolla Canyon at water depths of 23 m (Holden, 1968) is indicative of deposition within a brackish water environment. Radiocarbon dates of root structures within the same horizon yielded ages of 8270 ± 500 years b.p. (Shepard and Dill, 1966; Holden, 1968). Often age dates derived from woody debris overestimate the age of deposition as wood can have some residence time in the watershed, however, this does not apply to in situ root structures. The ostracods were found in sediments outcropping from 16 to 27 m water depth (Holden, 1968), which is consistent with the sediment thickness observed in CHIRP seismic data from this region. During transgression, the canyons may have acted as inlets to low lying areas landward of the beach similar to what is observed at Penasquitos Lagoon today. These low areas are potential locations where late-lowstand or early-transgressive subaerial deposits may be preserved between the sequence boundary and overlying transgressive surface. Similar estuarine units appear to be deposited along Scripps Canyon in similar water depths (Fig. 6).

Farther offshore, we interpret Sequence II, the basal sediments infilling lows or notches in the transgressive surface (Figs. 5 and 7), as a transgressive deposit, often referred to as a healing-phase wedge (Posamentier and Allen, 1999). Healing-phase deposits have been referred to as transgressive backfill or transgressive lag (e.g., Cattaneo

and Steel, 2003 and references therein). Darigo and Osbourne (1986) interpreted this unit to be several different marine and nonmarine deposits of late Pleistocene age. Sequence III, the upper acoustically transparent unit is interpreted to be a late-transgressive to highstand unit comprising unconsolidated sands, consistent with Hogarth et al. (2007).

The geometries and locations of the three sedimentary units in the area reflect the interplay of tectonics, eustasy, and sediment supply. We are able to distinguish the influences of eustasy and local transpressional tectonics based on geometry; transpression on the RCFZ imparts a shore-parallel trend while effects due to sea-level change and long-term, regional tectonic deformation engender a cross-shore trend (Hogarth et al., 2007). As sea level rises and a shoreline transgresses, areas of the coastal plain landward of the shoreline become potential areas of aggradation. In the case where sediment supply outpaces upper shoreface erosion, estuarine deposits can be preserved, in particular within channel incisions and embayments. As sea level continues to rise, erosion of the upper shoreface provides sediments to infill, or "heal," the lows in the lower shoreface and on the shelf (Posamentier and Allen, 1999; Catuneanu, 2006). These lows usually occur seaward of notches that are likely a consequence of relative sea level still stands (Fig. 7B). In some cases, the location of these notches is also influenced by the presence of back-tilted blocks, which allowed for differential erosion (Fig. 7B). The lows are subsequently backfilled as the shoreline migrates landward, eroding the coastline, with the consequent coarse-grained lag deposited offshore. As the transgression continues, so-called healing-phase deposits overlie the preserved estuarine sediments, as observed in strike lines (>20 m) around Scripps Canyon (Figs. 7A and 8).

As the Scripps and La Jolla submarine canyons cut across the entire shelf into the nearshore, the upper reaches of these features constitute embayments that are conducive to the deposition of estuarine sediments. In the case of La Jolla Canyon (Fig. 6), estuarine deposits found at shallow depths (~10–15 m) are inferred to be late-Holocene in age as a lagoon still occupied this site only 100 years ago and extended ~1 mile to the east of the current La Jolla Shores Beach (Moriarty, 1964). These thick estuarine deposits crop out in some areas, in particular along isolated ridges within the head of La Jolla Canyon (Fig. 6). Most likely, wave and tidal energy efficiently reworks sediments or prevents the deposition of modern sands over the estuarine units that outcrop at shallow water depths.

Beyond the primary features controlled by eustasy and long-term tectonic deformation, we observe tectonically induced secondary relief on the transgressive surface. The pop-up structure associated with the constraining bend on the Rose Canyon Fault generates a local northward shoaling trend on the transgressive surface (Fig. 8). The antiform through which Scripps Canyon is incised is an influential secondary structure as well. Operating at smaller wavelengths, deformation and offset bedding associated with east–west trending faults create along-shore variability in the transgressive surface and appear to influence the pattern of modern sediment deposition. The most significant example of this deformation is the localized structural high north of Scripps Canyon associated with the Carmel Valley and Salk faults on land (Figs. 4 and 8). The area between these two oblique faults appears to be uplifted relative to the surrounding area (Figs. 1 and 5). Both the large-wavelength uplift associated with the pop-up structure and the short-wavelength deformation associated with these oblique faults create along-shore relief in the transgressive surface (Figs. 4, 5, and 9B).

The healing-phase wedge is confined to the saddle region away from the canyons. Similar infilling of lows in the antecedent topography during transgression has been observed elsewhere (e.g., on the northern California shelf, Sommerfield and Wheatcroft, 2007). North of Scripps Canyon, the northern Holocene depocenter and much of the along-shore thickness variability observed in the Holocene sequence correspond to variations in the basal healing-phase unit (Fig. 10A and B). Such a correlation is not observed in the inter-canyon shelf where the transparent upper sands appear to account for the majority of the sediment thickness in the depocenter (Fig. 10A, B, and C). The depression in the transgressive surface is more pronounced north of Scripps Canyon than in the inter-canyon shelf (Fig. 9B). This is likely due to the positive uplift associated with the pop-up structure to the north and the shoaling of the transgressive surface towards the RCFZ in the south. The reflectors observed in the healing-phase deposits of the northern depocenter are horizontal and on-lap the transgressive surface (Fig. 7A). This indicates that offset on the Carmel Valley and Salk faults, and more importantly, uplift of the pop-up structure pre-date deposition of the healing-phase unit.

Some of the relief on the transgressive surface is modified by wave erosion in the nearshore, which enhances the smoothness of the seafloor as coarse-grained sediments eroded from the shoreface are transported to the low areas offshore (Fig. 10B). For example, fault-induced roughness in the transgressive surface is preserved in deeper water because these areas were more rapidly transgressed. We interpret the overall decrease in the relief on the transgressive surface from offshore to onshore, which greatly influences the location of healing-phase deposits, as a consequence of the varying rates of sea-level rise during the last transgression (Fig. 5; Fairbanks, 1989). With decreasing rate of sea-level rise, the shallower part of the shelf was exposed to wave-based erosion over a longer period and existing structures were more effectively leveled. This pattern of increased roughness offshore is likely enhanced by the overprinting of erosion during several sea-level cycles.

4.4. Hydrodynamic control on modern sediment accumulation

The distribution of the upper Holocene sediment package in the along-shore direction is affected by hydrodynamic factors (wind, waves, and currents), sediment supply, and antecedent topography. Based on acoustic character and limited core data, we infer that the change in acoustic character between Sequences II and III records a change in sediment sorting from coarse-grained, poorly sorted sediment to fine-grained, well sorted sands. Given the 8270 y.b.p. age for underlying estuarine sediments (Shepard and Dill, 1966; Holden, 1968), this sets the upper age limit for the overlying acoustically transparent sequence. The structure contour map of the top of Sequence II (Fig. 9C) shows that the relief along the transgressive surface (Fig. 9B) has been diminished by the healing-phase wedge, leaving a relatively smooth inner shelf profile with a seaward dip and minor along-shore variability. North of Scripps Canyon, unconsolidated sediments are thickest at ~40 m water depth (Fig. 10C) and thin both seaward and landward (Figs. 7B, 8, 10A, and C). The depocenter records the depth from which average waves can no longer resuspend sediment (Fig. 10C). Transport beyond the depocenter only occurs infrequently during larger storm events, which may explain the observed offshore thinning (e.g., Henry, 1976; Zhang et al., 1999; Harris and Wiberg, 2001).

In the northern part of our survey area, offshore Torrey Pines State Park, very little modern sediment deposition occurs at shallow water depths as the mid-shelf thickness high is deflected seaward due to the shoaling of the transgressive surface (Fig. 10A and C). The marked thinning of Sequence II in the deeper area of our survey corresponds to the deformation associated with oblique faults as little sediment has accumulated over the transgressive surface high (Fig. 5). Because the healing-phase infilled and reduced relief across the transgressive surface offshore, minimal thickness variation in the overlying transparent package is observed in this region (Figs. 9C and 10C).

Our work questions the efficiency of Scripps Canyon in capturing and transporting sediment offshore during the most recent sea-level rise and challenges the prevailing views of Holocene sediment transport and deposition offshore La Jolla. Observation of sediment wasting events in the heads of Scripps Canyon (Dill, 1964; Chamberlain, 1964) and related studies involving mass balance estimates for littoral cell sediment

budgets (Inman and Chamberlain, 1960; Inman and Masters, 1991b) have led the research community to conclude that the majority of sediment is captured and transported offshore by Scripps Canyon. However, our data shows that modern sediment accumulation offshore La Jolla may be more complex. The well-defined thickness maximum in the upper acoustically transparent layer, which corresponds to the inter-canyon Holocene depocenter, requires a net influx of sediment to this region since ~6–8 ka.

Mass balance calculations by Chamberlain (1964) suggested that much of the sediment supplied by longshore drift escaped the littoral cell via Scripps Canyon. Nevertheless, our observations suggest that large amounts of sediment have bypassed Scripps Canyon, despite the narrow pathway between the canyon head and the beach. The large along-shore variation in wave heights observed near Scripps Canyon may be a mechanism for enhanced sediment transport within the surf zone shoreward of the Scripps Canyon head. Thus, we need to reassess the role of the La Jolla Canyon System on sediment accumulation on the inner shelf and evaluate the proportion of sand captured by the canyon versus that shunted southward to the inter-canyon depocenter.

Observations of modern sediment accumulation on the San Diego County shelf, which provide a perspective on the regional pattern, confirm that the inner shelf offshore La Jolla, California is generally a depocenter of modern sediments. Regional studies reveal that exposed bedrock is common between the mid-shelf wedge and the beach, except at river mouths (Henry, 1976). Outside of the two areas of uplift due to the RCFZ, there are no bedrock exposures offshore La Jolla between the mid-shelf wedge and the beach. Our study area appears to be characterized by an atypically large accumulation of young sediment. The westward step of the coastline at the southern extremity of the Oceanside littoral cell may act as a jetty and promote sediment accumulation. The well-developed rip currents consistently observed south of the Scripps Pier at La Jolla Shores beach (Shepard and Inman, 1950) and also immediately north of the Scripps Pier (Smith and Largier, 1995) are likely contributing to this net accumulation. These currents redistribute modern sediments seaward on the inter-canyon shelf (Inman, 1952; Inman, 1953) and contribute to the formation of the depocenter observed in the isopach maps.

Repeated sounding surveys performed between 1949 and 1950 (Shepard and Inman, 1951; Inman, 1952; Inman, 1953) and seismic surveys conducted in 1976 and 1979 with a 3.5 kHz seismic profiler (Henry, 1976; Waggoner, 1979) indicate that sand levels are fairly stable on short time scales (1 to 3 years) at the location where we have identified the upper Holocene depocenter in the inter-canyon shelf. However, both accretion and erosion dynamics have been reported (Inman, 1953; Marshall, 1978; Dayton et al., 1989). This would imply that the Holocene sediment depocenter is currently in near equilibrium, with little net influx or outflux over at least the last few decades. A well-defined scour mark due to dredging is observed at 20 m water depth to the north of our study area (see Dartnell, et al., 2007). The preservation of this feature after the dredging occurred indicates that longshore drift is currently limited to the nearshore region. Sediment transport in the littoral cell may be highly episodic with sediment transport occurring during abnormally stormy climatic regimes.

5. Conclusions

High-resolution three-dimensional coverage of the shelf in the vicinity of the La Jolla and Scripps submarine canyons, obtained from CHIRP seismic and swath bathymetry data, highlights the structural control on the observed stratigraphy and morphology. The faulted and folded tectonic landscape associated with constraining bends in the Rose Canyon Fault Zone plays a critical role in canyon location and morphology as well as in the distribution of modern facies offshore La Jolla, California. In addition to the northward shoaling of the transgressive surface, our high-resolution seismics reveal much cross-shore and along-shore structural variability. We observe widespread dip reversals in the bedrock and an increased dip of offshore units compared to those observed onshore. We propose that the observed structural deformation offshore La Jolla is the expression of the compressional component of the transpressional strain regime associated with the RCFZ. We also propose that an antiform controls the location of Scripps Canyon, contrary to the previous hypothesis of fault control. Furthermore, the action of wave-based erosion is reflected in leveling and smoothing of bedrock highs and subsequent infilling of lows with reworked shelf materials. There is also an overall decrease of relief and small-scale roughness in the transgressive surface landward of ~25 m water depth due to a decrease in the rate of sea-level rise and longer exposure to wave-base erosion.

The detailed bathymetry reveals morphological differences between La Jolla Canyon and Scripps Canyon at various scales, from overall canyon shape to morphology of secondary incisions. The asymmetric development and deep side channels of La Jolla Canyon are indicative of differential erosion due to deformation near the RCFZ. The longitudinal variability of the unconsolidated modern sediment cover on the upper walls of Scripps Canyon appears to result from erosion of shallow gullies by failure processes. Ancient failures or sliding planes within the upper Holocene unit record the evolutionary history of the canyon edges.

We identify three stratigraphic sequences overlying the acoustic bedrock offshore La Jolla: 1) estuarine deposits, 2) a healing-phase wedge, and 3) homogeneous sands. We interpret the spatial distribution of these modern stratigraphic units in light of the complex interaction between sea-level rise, tectonics, and sediment supply. The primarily along-shore variation in the local tectonic structure allows us to distinguish the influences of eustasy and transpressional tectonics. The deposition pattern of the two older packages appears to be structurally controlled, with lagoonal deposits limited to the shallow upper reaches of the canyons and the healing-phase deposits infilling the lows seaward of wave-cut notches. The accumulation of the younger sand unit is controlled in large part by local hydrodynamics, with a typical mid-shelf depocenter north of Scripps Canyon and between the canyons. The identification of this depocenter raises questions about the efficiency of Scripps Canyon in capturing sediments and refines our conceptual model for the Holocene sediment transport and deposition offshore La Jolla.

Acknowledgements

This research was funded by the Office of Naval Research, the Southern California Coastal Ocean Observing System (SCCOOS), and an Achievement Rewards for College Scientists (ARCS) fellowship. We thank William W. Danforth for his help processing the Submetrix data, Warren L. Smith for his assistance in analyzing cores, Captain Eddy Kisfaludy for operating the *R/V Saihkon*, the crew of the *R/V Sproul*, and Douglas Inman for numerous discussions on the topics in this manuscript. We would also like to thank Wayne Baldwin, Daniel Belknap, and an anonymous reviewer for their comments, which improved the manuscript. The authors also acknowledge the use of software packages for data processing. The Generic Mapping Tools (GMT, Smith and Wessel, 1990; Wessel and Smith, 1998; http://gmt.soest.hawaii.edu) and Mirone (Luis, 2007; http://w3.ualg.pt/~jluis/mirone) are available online free of charge. Kingdom Suite (http://www.seismicmicro.com) is a commercial software made available for educational use at no charge.

References

Belknap, D.F., Kraft, J.C., 1985. Influence of antecedent geology on stratigraphic preservation potential and evolution of Delaware's barrier systems. Marine Geology 63, 235–262.

Buckingham, M.J., Richardson, M.D., 2002. On tone-burst measurements of sound speed and attenuation in sandy marine sediments. IEEE Journal of Oceanic Engineering 27 (3), 429–453.

Buffington, E.C., 1964. Structural control and precision bathymetry of La Jolla submarine canyon, California. Marine Geology 11, 44–58.
Byrd, R.E., Berry, R.W., Fischer, P.J., 1975. Quaternary geology of the San Diego–La Jolla underwater park. Studies of the geology of Camp Pendelton and Western San Diego County, CA. San Diego Association of Geologists, pp. 77–79.
Catuneanu, O., 2006. Principles of Sequence Stratigraphy. Elsevier, Amsterdam. 375 pp.
Cattaneo, A., Steel, R.J., 2003. Transgressive deposits: a review of their variability. Earth Science Reviews 62 (3–4), 187.
Chamberlain, T.K., 1964. Mass transport of sediment in the heads of Scripps submarine canyon, California. In: Miller, R.L. (Ed.), Papers in Marine Geology, Shepard Commemorative Volume. Macmillan Company, New York, pp. 42–64.
Christie-Blick, N., Driscoll, N.W., 1995. Sequence stratigraphy. Annual Review of Earth and Planetary Sciences 23, 451–478.
Cohen, J.K., Stockwell Jr., J.W., 2002. CWP/SU: Seismic Unix release 36, a free package for seismic research and processing. Center for Wave Phenomena. Colorado School of Mines, Golden, Colorado. www.cwp.mines.edu/cwpcodes.
Covault, J.A., Normark, W.R., Romans, B.W., Graham, S.A., 2007. Highstand fans in the California borderland: the overlooked deep-water depositional systems. Geology 35, 783–786.
Darigo, N.J., Osbourne, R.H., 1986. Quaternary stratigraphy and sedimentation of the inner continental shelf, San Diego County, California. Shelf sands and sandstones: In: Knight, R.J., McLean, J.R. (Eds.), Canadian Society of Petroleum Geologists Memoir II, pp. 73–98.
Dartnell, P., Normark, W.R., Driscoll, N.W., Babcock, Gardner, J.M., Kvitek, J.V., Rikk, G., Iampietro, P.J., 2007. Multibeam bathymetry and selected perspective views offshore San Diego, California. U.S. Geological Survey Scientific Investigations Map 2959, 2 sheets, version 1.0, June 14, 2007, http://pubs.usgs.gov/sim/2007/2959/.
Davis, G.H., Reynolds, S.J., 1996. Structural Geology of Rocks and Regions. Wiley and Sons, New York. 776 pp.
Dayton, P.K., Seymour, R.J., Parnell, P.E., Tegner, M.J., 1989. Unusual marine erosion in San Diego County from a single storm. Estuarine, Coastal and Shelf Science 29 (2), 151–160.
Dill, R.F., 1964. Sedimentation and erosion in Scripps submarine canyon head. In: Miller, R.L. (Ed.), Papers in Marine Geology, Shepard Commemorative Volume. Macmillan Company, New York, pp. 23–41.
Emery, K.O., 1958. Shallow submerged marine terraces of Southern California. Geological Society of America Bulletin 69 (1), 39–60.
Everts, C.H., Dill, R.F., 1988. Sedimentation in submarine canyons, San Diego County, California, 1984–1987. US Army Corps of Engineers, Coastal Engineering Research Center, Waterways Experiment Station, Reference No. CSTWS 88-2.
Fairbanks, R.G., 1989. A 17,000-year glacio-eustatic sea-level record: influence of glacial melting rates on the Younger Dryas event and deep-ocean circulation. Nature 342, 637–642.
Farre, J.A., McGregor, B.A., Ryan, W.B.F., Robb, J.M., 1983. Breaching the shelf break: passage from youthful to mature phase in canyon evolution. In: Stanley, D.J., Moore, G.T. (Eds.), The shelfbreak: critical interface on continental margins. Society of Economic Paleontologists and Mineralogists (SEPM) Special Publication No. 33, pp. 25–40. Tulsa, Oklahoma.
Gardner, J.B., Dartnell, P., Stone, C.J., Mayer, L.A., Hughes Clarke, J.E., 2002. Bathymetry and selected perspective views offshore greater Los Angeles, California. USGS – Water Resource Investigations Report 02-4126, 1 map sheet, http://walrus.wr.usgs.gov/pacmaps/pubs.html.
Gulick, S.P.S., Meltzer, A.S., 2002. Effect of the northward-migrating Mendocino triple junction on the Eel River forearc basin, California: structural evolution. Geological Society of America Bulletin 114 (12), 1505–1519.
Harris, C.K., Wiberg, P.L., 2001. A two-dimensional, time-dependent model of suspended sediment transport and bed reworking for continental shelves. Computers and Geosciences 27 (6), 675–690.
Harris, M.S., Gayes, P.T., Kindinger, J.L., Flocks, J.G., Krantz, D.E., Donovan, P., 2005. Quaternary geomorphology and modern coastal development in response to an inherent geologic framework: an example from Charleston, South Carolina. Journal of Coastal Research 21 (1), 49–64.
Hass, J.K., 2005. Grain size and mineralogical characteristics of beach sand in the Oceanside Littoral Cell, Southern California: implications for sediment provenance. Thesis (M. S.)–University of California, San Diego.
Henkart, P., 2003. SIOSEIS software. Scripps Institution of Oceanography, La Jolla, California. http://sioseis.ucsd.edu.
Henry, M.J., 1976. The unconsolidated sediment distribution on the San Diego County mainland shelf, California. Masters thesis, San Diego State University.
Hogarth, L.J., Babcock, J., Driscoll, N.W., Le Dantec, N., Hass, J.K., Inman, D.L., Masters, P.M., 2007. Long-term tectonic control on Holocene shelf sedimentation offshore La Jolla, California. Geology 35 (3), 275–278.
Holden, J.C., 1968. Brackish water ostracods from La Jolla submarine canyon 7200 (plus/minus) 500 years before present. Paleobios, vol. 5. Museum of Paleontology, University of California, Berkeley.
Honeycutt, M.C., Krantz, D.E., 2003. Influence of the geologic framework on spatial variability in long-term shoreline change, Cape Henlopen to Rehoboth Beach, Delaware. Journal of Coastal Research 147–167 (Special Issue No. 38).
Inman, D.L., 1952. Areal and seasonal variations in beach and nearshore sediments at La Jolla, California. Ph. D. Thesis, University of California, Los Angeles.
Inman, D.L., 1953. Areal and seasonal variations in beach and nearshore sediments at La Jolla, California. US Dept of the Army, Corps of Engineers, Office of the Chief of Engineers, Beach Erosion Board, Technical Memorandum No. 39.
Inman, D.L., Chamberlain, T.K., 1960. Littoral sand budget along the southern California coast. Volume of Abstracts, Report of the 21st International Geological Congress, Copenhagen, Denmark, pp. 245–246.
Inman, D.L., Nordstrom, C.E., Flick, R.E., 1976. Currents in submarine canyons; an air–sea–land interaction. Annual Review of Fluid Mechanics 8, 275–310.
Inman, D.L., Masters, P.M., 1991a. Coastal sediment transport concepts and mechanisms. Coast of California Storm and Tidal Waves Study, State of the Coast Report. U.S. Army Corps of Engineers, Los Angeles.
Inman, D.L., Masters, P.M., 1991b. Budget of sediment and prediction of the future state of the coast. State of the Coast Report, San Diego Region, Coast of California Storm and Tidal Waves Study, vol. 5. U.S. Army Corps of Engineers, p. 43.
Jackson, D.R., Briggs, K.B., Williams, K.L., Richardson, M.D., 1996. Tests of models for high-frequency seafloor backscatter. IEEE Journal of Oceanic Engineering 21 (4), 458–470.
Judy, T.C., 1987. Reconnaissance geology of the Holocene lagoonal deposits in the La Jolla submarine canyon and their relationship to the Rose Canyon Fault. Undergraduate Research Report, San Diego State University.
Kennedy, M.P., 1975. Western San Diego metropolitan area: Del Mar, La Jolla, and Point Loma, 7 1/2 minute quadrangles. Bulletin, California, Division of Mines and Geology, vol. 200, pp. 9–39.
Legg, M.R., Kennedy, M.P., 1979. Faulting offshore San Diego and Northern Baja, California. In: Abbott, P.L., Elliott, W.J. (Eds.), Earthquakes and other perils, San Diego region, San Diego, California, United States. San Diego Association of Geologists, pp. 29–46.
Lindvall, S.C., Rockwell, T.K., 1995. Holocene activity of the Rose Canyon Fault zone in San Diego, California. Journal of Geophysical Research, B, Solid Earth and Planets 100, 24121–24132.
Luis, J.F., 2007. Mirone: a multi-purpose tool for exploring grid data. Computers and Geosciences 33, 31–41.
Marshall, N.F., 1978. Large storm-induced sediment slump reopens an unknown Scripps submarine canyon tributary. In: Stanley, D.J., Gilbert, K. (Eds.), Sedimentation in submarine canyons, fans, and trenches. Dowden, Hutchinson and Ross, Stroudsburg, Pa, pp. 73–84.
Mastbergen, D.R., van den Berg, J.H., 2003. Breaching in fine sands and the generation of sustained turbidity currents in submarine canyons. Sedimentology 50 (4), 625–637.
McNinch, J.E., 2004. Geologic control in the nearshore: shore-oblique sandbars and shoreline erosional hotspots, Mid-Atlantic Bight, USA. Marine Geology 221, 121–141.
Moore, G.W., 1972. Offshore extent of the Rose Canyon Fault, San Diego, California. U.S. Geological Survey Professional Paper P 0800-D, pp. 113–116.
Moriarty, J.R., 1964. The use of oceanography in the solution of problems in a submarine archaeological site. In: Miller, R.L. (Ed.), Papers in Marine Geology. Macmillan, New York, pp. 511–522.
Peters, G., van Balen, R.T., 2007. Tectonic geomorphology of the northern Upper Rhine Graben, Germany. Global and Planetary Change 58, 310–334.
Posamentier, H.W., Allen, G.P., 1999. Siliciclastic sequence stratigraphy: concepts and applications. SEPM, Concepts in Sedimentology and Paleontology, vol. 7. 210 pp.
Pratson, L.F., Haxby, W.F., 1996. What is the slope of the U.S. continental slope? Geology 24, 3–6.
Rindell, A.K., 1991. An investigation of Scripps submarine canyon: its geology, sedimentary regime, and bubbling gases. Masters Thesis, San Diego State University.
Schwab, W.C., Thieler, E.R., Allen, J.R., Foster, D.S., Swift, B.A., Denny, J.F., 2000. Influence of inner-continental shelf geologic framework on the evolution and behavior of the barrier-island system between Fire Island Inlet and Shinnecock Inlet, Long Island, New York. Journal of Coastal Research 16 (2), 408–422.
Shepard, F.P., Emery, K.O., 1941. Submarine topography off the California coast: canyons and tectonic interpretation. Waverly Press, Baltimore MD.
Shepard, F.P., Inman, D.L., 1950. Nearshore water circulation related to bottom topography and wave refraction. Transactions of the American Geophysical Union 31 (2), 196–212.
Shepard, F.P., Inman D.L., 1951. Sand movement on the shallow inter-canyon shelf at La Jolla, California. US Dept of the Army, Corps of Engineers, Office of the Chief of Engineers, Beach Erosion Board, Technical Memorandum No. 26.
Shepard, F.P., Dill, R.F., 1966. Submarine canyons and other sea valleys. Rand McNally, Chicago.
Shepard, F.P., McLoughlin, P.A., Marshall, N.F., Sullivan, G.G., 1977. Current-meter recordings of low-speed turbidity currents. Geology 5 (5), 297–301.
Shepard, F.P., 1981. Submarine canyons: multiple causes and long-time persistence. American Association of Petroleum Geologists Bulletin 65 (6), 1062–1077.
Smith, W.H.F., Wessel, P., 1990. Gridding with continuous curvature splines in tension. Geophysics 55 (3), 293–305.
Smith, J.A., Largier, J.L., 1995. Observations of nearshore circulation—rip currents. Journal of Geophysical Research—Oceans 100 (6), 10967–10975.
Sommerfield, C.K., Lee, H.J., 2003. Magnitude and variability of Holocene sediment accumulation in Santa Monica Bay, California. Marine Environmental Research 56, 151–176.
Sommerfield, C.K., Lee, H.J., 2004. Across-shelf sediment transport since the Last Glacial Maximum, southern California margin. Geology 32 (4), 345–348.
Sommerfield, C.K., Wheatcroft, R.A., 2007. Late Holocene sediment accumulation on the northern California shelf: oceanic, fluvial, and anthropogenic influences. Geological Society of America Bulletin 119 (9–10), 1120–1134.
Stow, D.A., Chang, H.H., 1987. Coarse sediment delivery by coastal streams to the Oceanside Littoral Cell, California. Shore and Beach 55 (1), 30–40.
Thieler, E.R., Pilkey, O.H.J., Cleary, W.J., Schwab, W.C., 2001. Modern sedimentation of the shoreface and inner continental shelf at Wrightsville beach, North Carolina, USA. Journal of Sedimentary Research 71 (6), 958–970.
Thomson, J., Elgar, S., Herbers, T.H.C., 2005. Reflection and tunneling of ocean waves observed at a submarine canyon. Geophysical Research Letters 32 (10), L10602.
Treiman, J.A., 1993. The Rose Canyon Fault Zone, southern California. California Division of Mines and Geology, Open File Report 93-02. 45 pp.
Vetter, E.W., 1994. Hotspots of benthic production. Nature 372, 47.
Waggoner, J.A., 1979. Unconsolidated shelf sediments in the area of Scripps and La Jolla submarine canyons. Masters of Science in Geology, San Diego State University.

Webb, D.A., 1988. A structural interpretation of Scripps submarine canyon. Advances in Underwater Science, Proceedings of the American Academy of Underwater Sciences, 8th Annual Scientific Diving Symposium, La Jolla, CA: American Academy of Underwater Sciences, pp. 213–220.
Wessel, P., Smith, W.H.F., 1998. New, improved version of Generic Mapping Tools released. EOS Transactions of the American Geophysical Union 79 (47), 579.
Williams, K.L., Jackson, D.R., Thorsos, E.I., Tang, D., Schock, S.G., 2002. Comparison of sound speed and attenuation measured in a sandy sediment to predictions based on the Biot theory of porous media. IEEE Journal of Oceanic Engineering 27 (3), 413.
Young, A.P., Ashford, S.A., 2006. Application of airborne LIDAR for seacliff volumetric change and beach-sediment budget contributions. Journal of Coastal Research 22 (2), 307–318.
Zhang, Y., Swift, D., Fan, S., Niedoroda, A., Reed, C., 1999. Two-dimensional numerical modeling of storm deposition on the northern California shelf. Marine Geology 154 (1–4), 155–167.

Chapter 3, in full, is a reprint of the material as it appears in Marine Geology 2009. Le Dantec, Nicolas; Hogarth, Leah J.; Driscoll, Neal W.; Babcock, Jeffrey M. “Tectonic controls on nearshore sediment accumulation and submarine canyon morphology offshore La Jolla, Southern California”. The dissertation author was a primary investigator and co-author of this paper.

4

New Seismic Evidence for Active Deformation and its Control on Long-term Sediment Accumulation on the Eel Margin, Northern California

4.1 ABSTRACT

New high-resolution CHIRP seismic data acquired along the Eel Margin, northern California, reveal that stratal architecture and sediment thickness of the Holocene transgressive deposits are, in large part, controlled by tectonic deformation and sediment supply. A thick (> 20 m) transgressive systems tract is observed across the Eel Margin, a forearc basin that is undergoing active folding perpendicular to the coastline at mm/yr rates. The transgressive systems tract on the Eel Margin exhibits marked thickness variation in the along shore direction; being thickest in the Eel River Syncline and thinnest over the Eureka Anticline. The divergent character of the infill suggests that deposition in the syncline is syntectonic. The relief observed along the transgressive surface is consistent with deformation rates measured onshore. The transgressive surface is offset across the Eureka Anticline suggesting it has been active since ~10 ka. An outer shelf depocenter (~80 m water depth) thins both landward and seaward. Along the outer shelf the transgressive surface coalesces with the underlying sequence boundary. Moving landward, however, the two surfaces diverge. Two distinct acoustic units have been identified within the transgressive systems tract; a basal healing-phase deposit overlying the transgressive surface and an upper onlapping unit. The healing-phase deposit infills structural lows along the outer shelf with a maximum thickness of 8 m and is separated from the overlying acoustically well laminated unit by a pronounced surface of onlap. Moving shoreward along the inner shelf (< 60 m water depth) the transgressive sequence thins and becomes acoustically transparent, which suggests that the finer-grained material is bypassing the inner shelf and being sequestered on the middle to outer shelf. Despite bathymetric evidence that the highstand systems tract has begun to form along the coast adjacent to river sediment sources, gas wipe out and wave-base reworking obscure seismic evidence for the characteristic downlap.

4.2 INTRODUCTION

Three independent variables: eustatic sea-level fluctuation, tectonic subsidence/ uplift, and sediment supply control the development of stratigraphic patterns and associated facies (e.g., Sloss, 1963). In addition, climate and physiography of the margin play an important role in the generation of stratigraphic architecture (Christie-Blick and Driscoll, 1995). Numerous attempts have been made to understand how changes in these variables affect the stratigraphic record; that is, trying to define the link between process and product. Sequence stratigraphy is an approach to determine layer-by-layer how sedimentary successions are put together, from the smallest elements to the largest, as well as to understand the origin of the physical surfaces that bound depositional building blocks. Despite many efforts to understand how changes in these variables affect the stratigraphic record, controversy remains regarding the importance of tectonics versus eustatic sea-level change on generating sequence architecture.

The general concepts of sequence stratigraphy represent a distillation of numerous observations along many passive margins (Vail et al., 1977; Jervey, 1988; Posamentier et al., 1988, Van Wagoner et al., 1990). One of the major assumptions of the sequence stratigraphic model is that there is a constant subsidence rate that increases uniformly from the hinge zone basinward or seaward in response to cooling and contraction of the mantle or sediment loading. Furthermore, sediment input during a sea-level cycle is assumed to be constant or experience a slight increase during sea-level fall as a result of increased erosion and incision (Vail et al., 1977). Even though it is explicit that local factors such as tectonic deformation and variations in sediment supply must be considered when applying the sequence stratigraphic model, it remains unclear how such local factors will modify the formation of discontinuities and the stratigraphic sequences they bound. In this manuscript, we will present new data acquired as part of the Office of Naval Research (ONR) STRATAFORM project that will illustrate how variations in

tectonic deformation and sediment supply modify the architecture of the transgressive sequence on the northern California margin.

Following Christie-Blick and Driscoll (1995), the depositional sequence is defined as a relatively conformable succession of genetically related strata bounded by unconformities and their correlative conformities. Although an unconformity is generally defined as a buried surface of erosion and/or non-deposition, in the application of sequence stratigraphy it has been restricted to those surfaces that are related (or are inferred to be related) at least locally to the lowering of depositional base level and hence to subaerial erosion or bypassing (Van Wagoner et al., 1988). According to this definition, intervals bounded by marine erosion surfaces that do not pass laterally into subaerial discontinuities are not sequences and the bounding unconformities are not sequence boundaries. In the standard sequence stratigraphic model, “parasequences” and “parasequence sets” are the building blocks that make up the three different “systems tracts” (Brown and Fisher, 1977) that compose a sequence. Parasequences are characterized by overall upward shoaling of depositional facies bounded by marine flooding surface and their correlative surfaces (Fig. 1; Vail 1987; Van Wagoner et al., 1988, 1990; Swift et al., 1991). The balance between sediment supply and accommodation governs their overall stacking patterns and facies arrangements, and these factors determine which systems tract they compose. For example, when sediment supply outpaces the creation of new accommodation the sedimentary sequences prograde across the margin with a seaward migration of the shoreline and associated facies (e.g., LST, Fig. 1). Conversely, if the creation of new accommodation outpaces the sediment supply there will be a shoreward migration of parasequences and associated facies (e.g., TST, Fig. 1). It is these stacking patterns that define the various system tracts and provide important linkages between facies assemblages and stratal geometry. One of the main goals of this research is to examine the relationship between facies assemblages and

stratal geometry on a tectonically active margin.

Subdivision of sequences into the three different systems tracts, highstand, transgressive, and lowstand, depends on the phase lag between transgressive-regressive cycles and the development of sequence boundaries (Fig. 1). In the standard model for a siliciclastic environment with a shelf-slope break, the regressive part of any cycle includes both the highstand and lowstand (or shelf margin) systems tracts, with the highstand below the sequence boundary and the lowstand above. On the shelf, alternating transgressive and highstand units predominate, but are not always easy to distinguish (Christie-Blick and Driscoll, 1995). Furthermore, the transgressive systems tract can be nearly absent or relatively thick depending on the depositional environment. For example, low-gradient settings typically have thin transgressive sequences, but these deposits can be thick if transgression is punctuated by short, regressive intervals (Cattaneo and Steel, 2003). Conversely, in high-gradient, high sediment supply settings, transgressive deposits can develop up to tens of meters thick locally above a high-gradient wave ravinement surface (Cattaneo and Steel, 2003). Other factors such as inherent physiography, tidal and wave energy, and dominant sediment grain size of a margin can play a role in transgressive deposit geometry. The nested approach of the northern California STRATAFORM focus site provides the ideal opportunity for us to examine how the stratal patterns along an active margin respond to different rates of tectonic deformation, variations in sediment supply, and different sediment source regions.

Researchers have attempted to develop modified versions of the standard sequence stratigraphic model with case studies in a variety of settings. Examples include settings where sedimentation is accompanied by growth faulting (Brown and Fisher, 1977); carbonate platforms and ramps (Brown and Fisher, 1977; Sarg, 1988; MacNeil and Jones, 2006); and nonmarine settings such as fluvial, eolian, and lacustrine environments (Dam and Surlyk, 1992; Lawton et al., 2003). The main emphasis of this work has been

to document variations in the arrangement of facies and associated stratal geometry. Researchers have also sought deeper understanding by integrating outcrop and subsurface geology from seismic records with flume experiments (Koss et al., 1994; Wood et al., 1993) and computer simulations (e.g., Jervey, 1988; Ross et al., 1990; Driscoll and Karner, 1999). Some have even used computer simulations to predict facies distributions and geometries in areas unconstrained by well-log or seismic data (e.g., Warrlich et al., 2008) and numerical models to test sequence stratigraphic model assumptions (e.g., Swenson and Muto, 2007). Among the more interesting results of this work are the new ideas and concepts concerning the origin of sequences and their bounding unconformities. The high-resolution data acquired during the STRATAFORM project has provided an opportunity to test and refine some of these new concepts regarding strata formation.

Using the sequence stratigraphic approach (Vail et al., 1977, 1991; Vail, 1987; Christie-Blick et al., 1990; Van Wagoner et al., 1990; Driscoll and Hogg, 1995; Christie-Blick and Driscoll, 1995; Driscoll and Karner, 1998) to interpret the preserved stratal geometry in a basin allows a chronostratigraphic framework to be established with which to examine the preserved basinal lithostratigraphy. Vail et al. (1991) state that the most important criteria necessary to discern between tectonic activity, eustatic sea-level fluctuations, and sediment supply are the distribution in time and space of their effects on accommodation. Furthermore, these authors suggest that these processes can be differentiated by examining their rates, their duration, their rate of change or pattern of change, and finally the spatial extent of the modification (Posamentier, 1988; Vail et al., 1991). However, in actively deforming regions, such as the northern California margin, the rates of these disparate processes can have similar magnitudes of millimeters per year (Underhill, 1991; Driscoll, 1992; Driscoll and Hogg, 1995; Christie-Blick and Driscoll, 1995; Driscoll and Karner, 1998). Consequently, caution should be used when using rates to infer process because rates are not always the key to discern between tectonics

and eustasy. Furthermore, Posamentier et al. (1988) and Posamentier and James (1993) emphasize that sequence stratigraphic models are generally applicable and that the effects of local factors such as climate, sediment supply, and tectonics must be incorporated into these models before they can be applied to a particular basin. While this is an easy caveat to mention, it requires an a priori geologic understanding of a given region. This type of reasoning places the proverbial cart in front of the horse because it is the technique of sequence stratigraphy that is used to understand the interplay between, and importance of, regional (allocyclic) versus local (autocyclic) processes.

On active margins such as the west coast of North America, tectonics plays an important role in generating morphology and subsequent stratigraphic architecture on the continental shelf (e.g., Orange, 1999; Burger et al., 2002; Hogarth et al., 2007). The Eel River Basin in northern California is an ideal location to investigate the different influences of tectonics, eustasy, and sediment supply. Northeast-southwest compression due to the encroachment of the Mendocino Triple Junction generates folds and high-angle reverse faults with axes oriented at a high angle to the shoreline. The tectonic signal has variable sign and amplitude parallel to the coastline, providing an opportunity to examine how tectonic deformation affects stratigraphic architecture and facies assemblages. In addition, the large, episodic sediment yield to the margin results in thick sedimentary packages with well-preserved geometry. The localization of sediment sources in subsiding synclines also enhances along-shore variability in sedimentation, which improves understanding of the role of sediment supply in generating sequence geometry.

In 1994 the ONR STRATAFORM project aimed to bridge the gap between time scales of sedimentary processes and strata formation (Nittrouer, 1999). The program combined studies that examined cores, CHIRP seismics, and Multi-Channel Seismics (e.g., Burger et al., 2002) to study processes that generate marine strata spanning a range of time scales from days to millennia to hundreds of millennia. In this study, we use high

resolution CHIRP seismic data to examine the products of the most recent transgression. Taking into account our current understanding of the modern shelf depositional and erosional processes allows us to better evaluate the roles of sediment input and dispersal, tectonic deformation, eustasy, and physiography in the formation of the stratigraphic record. By interpreting high resolution CHIRP seismic data in a sequence stratigraphic context, we are able to develop a detailed understanding of the formation of the transgressive systems tract on a tectonically active shelf during the most recent sea-level rise.

4.3 REGIONAL SETTING

4.3.1 Geology

The Eel River forearc basin began to form in the Neogene between the accretionary prism overlying the Cascadia subduction zone (CSZ) to the west and Cascade magmatic arc to the east (Fig. 2; Clarke, 1992). The offshore basin is composed of up to 2.5 km of upper Miocene to Holocene sediments above Franciscan Complex basement rocks (Clarke, 1987; Gulick et al., 2002). Several episodes of deformation have occurred across the region since the Paleogene, with the last major episode of deformation occurring in the late Pleistocene. The Pacific ridge first subducted near Los Angeles ~29 ma ago and resulted in the formation of the nascent San Andreas Fault (SAF), which has been migrating north and south in response to the continued subduction. Encroachment of the Pacific Plate and the northward migration of the SAF have imparted a north-northeast compression across the basin causing major folding and high-angle reverse and thrust faulting along north-northwest tends and reactivation of older north-trending fabrics. Since ~500 ka the encroachment of the Mendocino Triple Junction (MTJ), which is the northward propagating end of the SAF, has warped the southern Eel basin (McCrory, 1996) and has produced northeast-oriented shortening of

at least 20 mm/yr (Clarke and Carver, 1992). This has resulted in thrust faults onshore (Gulick & Meltzer, 2002), and counter-clockwise rotation of north-south oriented structures to a northwest-southeast orientation. Farther onshore to the east, it appears that strike-slip structures related to the San Andreas Fault and motion between the Pacific and North America plates dominate. In addition, since the early Pleistocene, this plate motion has produced a preceding bulge of uplift and reduction of accommodation up to 80 km north of the triple junction (Gulick et al., 2002). The area between the regimes onshore and offshore, in the southeast part of the basin, is characterized by transpressive structures. Previous MCS studies have imaged upward branching flower structures, different separations and thicknesses across faults, (Gulick & Meltzer, 2002), and offset of incised channels (Burger et al., 2002).

The basin is segmented by rising anticlines that are underlain by active thrust faults (Figs. 3 and 4), and the synclines are filled with Middle Pleistocene sediments of the Wildcat Group, which onlap the underlying marine sediments of the Franciscan and Yager Complexes (Clarke, 1992). The northwest folds and faults are clearly imaged in the topography data and rotate from the predominant fabric away from the MTJ (Fig. 2; McLaughlin, 1994; McCrory, 2000; Gulick and Meltzer, 2002). The folds and faults are also imaged in offshore bathymetry and backscatter data with the Little Salmon Anticline delineating the northern boundary of the large slope failure in the region (Fig. 4). Modern sediment accumulation rates on the shelf vary with maximum accumulation rates an order of magnitude grater than the rates of tectonic deformation inferred from uplifted marine terraces (Orange, 1999; Vick, 1988).

In the study area at the southeast end of the offshore basin, several structures that appear to be rotated by the encroaching triple junction are oriented nearly perpendicular to shore (Figs. 3 and 4). The three main areas of uplift, from north to south, are the following: 1) Patrick's Point to the Mad River Fault, 2) Eureka Anticline to Table Bluff

Anticline, and 3) Centerville Beach to the Russ Fault. The intervening areas of subsidence are: 1) Freshwater Syncline, 2) the Little Salmon Fault, and 3) Eel River Syncline (Figs. 2 and 3; Vick, 1988). Vertical rates of motion on these structures ranges from 2.3 mm/yr uplift at Russ Fault to 3 mm/yr subsidence in the Eel River Syncline. Onshore, the Little Salmon Fault (LSF) has been placed either (1) coincident with Table Bluff Anticline (McLaughlin et al., 2000) or (2) coincident with the south side of Humboldt Hill (Clarke, 1992; Kelsey and Carver, 1988) with the Table Bluff Fault Zone being an active branch of the Little Salmon Fault (McCrory, 2000). Onshore the LSF exhibits dip slip motion (McCrory, 2000; Gulick & Meltzer, 2002), but offshore in shallow water it appears to be deformed by transpressive tectonics (Gulick & Meltzer, 2002). The slip rate on the LSF ranges from 4.6±2.1 mm/yr estimated offshore (McCrory, 2000) to 6.1±2.3 mm/yr estimated onshore (Clarke & Carver, 1992).

Continued deformation along the Eel margin is evidenced by earthquakes, uplifted marine terraces, and subsidence and flooding of peat horizons. Tectonic deformation and recurrence intervals in the Humboldt area were constrained by examining peat sequences in the intertidal areas (Vick, 1988). Four depositional cycles of abruptly terminated peat overlain by massive muds that gradually graded upward into peats were observed in a 3 m core. The abrupt terminations and gradual regrowth of peat layers is interpreted to result from large earthquakes causing rapid subsidence (~2 m) in the bay and then gradual refilling of the bay over time. Dates of the horizons indicate a recurrence interval for these large earthquakes of 700-1000 years (Vick, 1988). Clarke and Carver also found evidence for late Holocene paleoseismicity on the LSF and in the Mad River Fault Zone (1992). They examined fault displacements and several other indicators such as driftwood and fossil mollusk shells on raised land and submerged and buried marshes and forests. They concluded that movements on the Little Salmon Fault and the Mad River Fault Zone were associated with events on the CSZ megathrust, and future events could be up

to Mw=9.5 (Clarke and Carver, 1992).

4.3.2 Modern Hydrodynamics and Sediment Dispersal

The Eel River, located in the south of the study area, has a relatively small drainage basin area of 8640 km^2 and steep headwater terrain up to ~2000 m in elevation (Nittrouer, 1999). It is the largest sediment source to the California margin, yielding ~2232x10^3 $kg/km^2/yr$ of suspended sediment to the coast, while the smaller Mad River (1290 km^2) to the north has a comparably large sediment yield of ~2070x10^3 $kg/km^2/yr$ (Wheatcroft and Sommerfield, 2005). Both rivers occupy subsiding synclines; the Eel River in the Eel River Syncline and the Mad River in the Freshwater Syncline (Fig. 3). Easily erodable sedimentary and metamorphic rocks such as weakly lithified siltstone and mudstone of the Eel River Basin supply the shelf with a total suspended sediment (TSS) load of 10-30 Mt/yr of silt and clay (Syvitski and Morehead, 1999), with ~25% of the river's TSS as fine sands (Sommerfield and Nittrouer, 1999), and bedload is estimated to be ~10-20% of TSS (Brown and Ritter, 1971). The Eel River is a storm-dominated system with over 90% of its annual runoff occurring between November and May (Sommerfield and Nittrouer, 1999). Large sediment discharge events are often coincident with energetic ocean conditions that act to redistribute previous flood deposits and transport ~80% of the silt and clay alongshore to the ends of the shelf and beyond the outer shelf (Sommerfield and Nittrouer, 1999; Wheatcroft et al., 1997). The dispersal environments resulting from the waves, winds, and gravity-driven flows characteristic of the Eel margin result in three characteristic sediment provinces: sand, muddy sand, and mud. The surficial sand facies grades from medium-grained sand on the beach to finer sand around the 50 m isobath. Between ~50 m and 60 m sand is interbedded with mud, and in deeper waters mud is dominant. Varying degrees and depths of biological mixing, accumulation rates, and original bed thickness across the shelf results in

variable preservation potential over the shelf. Due to the episodic, thick nature of storm beds, stratification is preserved on the central shelf, but seaward of the 75 m isobath, stratification is not preserved (Sommerfield and Nittrouer, 1999; Zhang et al., 1999). Over a 100-yr sediment record, maximum deposition occurred on the mid-shelf centered on the 70-m isobath (Sommerfield and Nittrouer, 1999).

4.4 METHODS

In 1998, 1999, and 2000 over 1000 km of CHIRP seismic data were acquired offshore from the Eel River in northern California as part of the STRATAFORM project (Fig. 4). Nearshore strike lines were collected in 1998 onboard the R/V Coral Sea, and regional dip lines were acquired in 1999 and 2000 onboard the R/V Thompson. The regional dip lines coincided with coring transects, and vibracore numbers indicate their locations on survey lines as well as their water depths. For example, core Q45 was collected coincident with dip line Q at 45 m water depth (Fig. 4). Vibracores, box cores, and piston cores collected across the study area provide some information about the nature of facies and contacts observed in seismic data. The cruise tracks were designed to provide (a) detailed dip line coverage (~1.75 km line spacing) from the outer shelf/upper slope across the shelf into shallow water (~20 m) and (b) detailed strike line coverage (~250 m line spacing) of the fold/fault system and overlying sediment thickness on the inner shelf. For the regional dip and strike lines a 1-5.5 kHz chirp signal with a 50 ms sweep was used, while for the nearshore surveys a 1-15 kHz chirp signal with a 10 ms sweep gave better vertical resolution and minimized time between shots. These signals yielded submeter vertical resolution to subsurface depths up to 50 m. Data were corrected for ship heave using SIOSEIS (Henkart, 2003) and further processed using Seismic Unix (Cohen and Stockwell, 1999). To correct for layback, one set of survey lines collected at one azimuth was held constant and the navigation for other lines was shifted to match the

fixed lines. The total offset between lines was up to ~ 200 m, which was not significant enough to influence correlation with structures onshore. Kingdom Software (Seismic Micro Technology http://www.seismicmicro.com) was used to determine depths to interpreted surfaces as well as thickness of intervening units. An average of 1500 m/s was used to convert two way travel time to depth. Generic Mapping Tools (GMT; http://gmt.soest.hawaii.edu/) was used to apply a continuous curvature surface algorithm and interior tension of 0.35 to convert data points to grid surfaces. Fledermaus software by Interactive Visualization Systems (IVS 3D, http://www.ivs3d.com) was used to combine seismic profiles for three-dimensional perspective views.

4.5 RESULTS

4.5.1 Major Structures and Features

An angular unconformity is imaged throughout the study area (Figs. 5, 6 and 7). However, this surface is not mapped at depths deeper than ~30 m below the seafloor in the southern half of the data set where gas limits acoustic penetration. The angular unconformity is interpreted to be the transgressive surface formed during the sea level rise following the last deglaciation (~21 ka–present) as it truncates underlying bedding, has relatively high acoustic reflectivity, and overlying sediments onlap the surface progressively landward. The surface exhibits much variability in roughness and acoustic character, being smooth with high acoustic amplitude in most areas, but rough with variable acoustic amplitude in other regions. For example, the surface is quite rough ~40 m water depth adjacent to the Mad River. Still other areas are obscured by gas, such as above a prominent anticline (Fig. 6). Deposition above the surface ranges from acoustically transparent, to distinctly laminated or irregular. Deposits below are also variable, transparent to highly reflective, with wide, channel-like surfaces, anticline structures, and laminations. The overall topography of the transgressive surface in

the northern half of the study area is marked by a broad high extending ~10-15 km along strike, adjacent to the Mad River Fault, the Freshwater Syncline, and the Eureka Anticline onshore (Fig. 2). In the northernmost dip lines, T and V, the surface is covered by ~4 m of sediment at 30 m water depth (Fig. 5A). Farther south, however, sediment cover decreases to a minimum of ~2 m over a prominent fault and anticline (Fig. 5B). The anticline and fault are well imaged in several lines (Fig. 6B), but are obscured by gas in other lines (Figs. 6A and 6C). In strike line 15N, the angular unconformity surface is visibly offset ~0.5 m across this structure (Fig. 7). To the south of the fault the transgressive surface deepens and is covered with over 30 m of sediment (Fig. 6). A structure contour map of the transgressive surface shows that the trend of the distinct southern edge of the structural high is coincident with the projection of the northern branch of the Little Salmon Fault onshore, which coincides with the Humboldt Hill Anticline (HHA), and as such we will refer to this entire suite of faults as the Little Salmon Fault Complex (LSF complex; Fig. 8). The fault/fold anticline within the structural high coincides with the Eureka Anticline onshore. The LSF complex delineates the topographic high in the north from the structural low in the south and is outlined by the eastward deflection of the 60 m contour (Fig. 8). Within the southern low, we observe a local high adjacent to the Table Bluff Anticline (Fig. 8A). Vibracores along the LSF structural high penetrated the angular unconformity surface (Q45; Figs. 9 and 10). Sediments recovered in core Q45 sampled the transgressive surface, which separated a layer of coarse-grained, rounded pebbles and cobbles overlying fine-grained deposits with a sharp erosive contact between the two units (Fig. 9).

4.5.2 Sequence I

Above the regional unconformity that we interpret as the transgressive surface, we identify two distinct acoustic units. The lower unit, Sequence I, mantles the angular

unconformity and is characterized by chaotic to transparent reflectors that appear to coincide with the rough areas of the transgressive surface (Figs. 5 and 8). The transgressive surface in regions coincident with Sequence I exhibits more roughness than in areas lacking Sequence I. The shoreward limit of Sequence I is defined by a prominent surface of onlap with shoreward terminations (Fig. 5). Sequence I is most distinct in dip lines between ~60 and 100 m water depth and at shallower depths in strike lines to the south and north of the Eureka Anticline (Figs. 6, 7, 10). Across the margin, the unit thickens from zero meters to a maximum of ~8 m at ~90 m water depth and then continues to thin offshore (Fig. 11A). In northern dip lines, such as line T, there are a few reflectors within Sequence I that dip less steeply than the transgressive surface (Fig. 5A). In the southern dip lines, such as Line 4p , Sequence I is thicker and the acoustic character of the sediments is more chaotic with concave-up, closely spaced, and truncated reflectors that decrease in number seaward and eventually fade to two subparallel reflectors (Figs. 5B and 10). In strike, the unit appears to infill lows, pinching out near the Eureka Anticline (Figs. 6 and 10). For example, in several strike lines to the north of the Eureka Anticline Sequence I infills a broad low ~5 m deep and extending ~2-3 km (Fig. 6). In strike lines, the onlap surface that forms the upper boundary of Sequence I is smooth with high-amplitude acoustic character (Fig. 6). The southern extent of Sequence I is difficult to discern as gas obscures the subsurface reflectors. An isopach map of Sequence I shows that it is thin to absent over the structural high, it has a maximum thickness in the water depth range of 60-100 m, and its distribution has linear trends parallel to the contours (Figure 10A). Its maximum thickness of ~8 m is located to the southwest of the structural high (Fig. 10A), which coincides with an embayment delineated by the 100 m contour on the structural contour map for the transgressive surface (Fig. 8A). Note there is very little structural control associated with the Freshwater Syncline (FS) on either the depth to the transgressive surface (Fig.

8A) or on the sediment thickness of Sequence I (Fig. 11A). In fact, the largest control on both sediment thickness and depth to the transgressive surface appears to be the southern boundary of the LSF complex that separates a broad high to the north from a structural low to the south (Fig. 8)

4.5.3 Sequence II

Sequence II is observed throughout the study area above Sequence I and the transgressive surface, but its acoustic character is highly variable along and across the margin. At deep water depths (> 60 m) there are several parallel, high-amplitude reflectors in Sequence II (Figs. 6, 7, and 10). Nearshore areas are characterized by transparent sediment, and some regions are obscured by high-amplitude reflections indicative of gas or fluid in the sediment (e.g., Fig. 5A). Still other areas of Sequence II have a blotchy acoustic character (e.g., Fig. 6). In line V, the northernmost dip line, which is located offshore of the modern Mad River, Sequence II sediments are relatively thick, onlap Sequence I, and thin progressively shoreward and seaward. Immediately to the south, in line T, the thickness of sediment overlying the transgressive surface appears to be consistent until ~60 m water depth at which point the sediments begin to thicken seaward to a maximum thickness at ~80-90 m water depth (Figs. 5A and 10). In the nearshore, the unit is acoustically transparent, but displays distinct acoustic laminations moving seaward towards the middle to outer shelf (> 50 m water depth). Even though Sequence II thins seaward from the 80 m depocenter there is no observed downlap or shoreward migration of the downlap position in this region of the shelf. Rather, the reflectors appear to terminate at the seafloor by truncation (Figs. 5 and 10). The acoustic reflectivity of the transgressive surface increases coincident with the increase in reflectivity of the overlying layers. Farther south, Lines R and Q exhibit very thin sediment cover (~1 m) to ~60 m water depth at which point the sediment thickness

increases seaward to a maximum again at ~80-90 m water depth, beyond which, sediment thickness decreases relatively rapidly (Fig. 10). The acoustic character of the transgressive surface and overlying sequence in the southern dip lines displays the same characteristics observed in the northern lines, that is, large lateral variability in acoustic amplitude of the transgressive surface and variation from acoustically well-laminated reflectors along the outer and mid-shelf to acoustically transparent on the inner shelf (e.g., Line 4p, Fig. 5B). The deformation within the fault complex can be observed as line 4p crosses the fold/fault axis very obliquely (Fig. 5B). Line O is located along the southern limb of the Eureka Anticline (Figure 4). To the south, Sequence II thickness continues to increase systematically towards the Eel River Syncline, but the maximum thickness is not imaged due to the occurrence of gas that obscures reflectors from the underlying surfaces (Fig. 10). Along strike Sequence II exhibits as much variability as there is observed across the margin; it is thin over the northern structural high and thickens into the Eel River Syncline (Fig. 11B). The high amplitude horizons in Sequence II onlap the inclined transgressive surface as it deepens into the Eel River Syncline. The onlapping reflectors exhibit divergence and their dip systematically increases with depth to the south (Fig. 12). The mid-shelf thickness maximum of Sequence II observed in dip lines between 80 and 90 m water depth is delineated in an isopach map of the sequence (Fig. 11B) and is also revealed by the entire thickness of the transgressive deposit (i.e., Sequences I and II, Fig. 11C). Although the structure map of the transgressive surface shows little variation to the north of the LSF complex (Fig. 8A), sediments over the transgressive surface thicken gradually from ~1-2 m to ~5 m over a distance of ~10 km towards the Mad River Delta at water depths shallower than 60 m (Fig. 11B). The isopach map also shows the northeast margin of a sediment depocenter located to the south of the LSF complex and the pronounced eastward jog in the depocenter (Fig. 11). Within the area adjacent to the Eel River Syncline, where the transgressive surface is locally high directly offshore of the

Table Bluff Anticline, a sediment thickness minimum is observed (Fig. 11B). As shown in the isopach map of Sequence II, sediments are thinnest over the structural highs and thickest in the lows.

In summary, the CHIRP data show that the late Pleistocene and Holocene succession on the Eel shelf is a seaward- and landward-thinning unit bounded by the transgressive surface and the sea floor (Figs. 5, 6, and 10). Sequence II onlaps on to the basal sequence (Sequence I) and the onlap position migrates landward through time, a stratal geometry characteristic of the transgressive systems tract. Across the shelf, this succession ranges from a few meters thick at the shelf break to almost 25 m thick near the middle to outer shelf depocenter to less that 5 m at the 25 m isobath. The folded and faulted strata beneath the transgressive surface are truncated as a result of wave-base erosion associate with the last sea-level rise. Along the shelf, the thickness of the transgressive systems tract exhibits marked variability, being thickest in the subsiding synclines (30+ m thickness), and thinning to less than 2 m across the axis of the Eureka Anticline (Figs. 5 and 6). The upper surface of the Holocene deposits slopes smoothly seaward and is poorly correlated with the relief on the underlying transgressive surface.

4.6 DISCUSSION

4.6.1 Evolution of the Transgressive Sequence

Seismic records show that the Holocene transgressive succession on the Eel Margin is a seaward and landward thinning unit defined by an underlying surface of erosion, or the transgressive surface, and the overlying seafloor. The transgressive sequence is further divided into two distinct units. We interpret Sequence I, which is bounded by the transgressive surface below and by a flooding surface characterized by backstepping, onlapping reflectors above, as a transgressive healing-phase deposit. Our interpretation of this unit is based on its aerial and stratigraphic location as well as its

acoustic character and geometry. Sequence I is thickest in water depths > 60 m, with the thickest deposition following roughly shore-parallel trends to the west of the structural high that is bounded on its southern edge by the LSF complex (Fig. 11A). In seismic profiles, this distribution is related to low areas in the transgressive surface (Figs. 5 and 6). We propose that these low areas correspond with periods of slow sea-level rise during the early deglaciation (~21-15 ka; e.g., Fairbanks, 1989; Chappell et al., 1996). For example, we observe one broad low between ~100 and 80 m water depth that could be a terrace carved when sea level was rising slowly (21-15ka; Figs. 6 and 8A). The resultant wave-cut terraces provide a change in relief from less steep where wave-base erosion occurred to more steep above the region of erosion (e.g., Hart and Plint, 1993). At the onset of meltwater pulse 1A (~15ka), sea-level began to rise rapidly to ~60 m water depth. Seaward of these depths, we observe the most roughness on the transgressive surface, which would be predicted if wave-based erosion had little to no time to erode and rework the surface. Sediment eroded from the shoreface subsequently located at <~60 m infilled, or "healed," the lows in the transgressive surface in the lower shoreface and on the shelf (Cattaneo and Steel, 2003; Posamentier and Allen, 1999). The thin veneer of coarse-grained, rounded pebbles and cobbles sampled above the transgressive surface in core Q45 reflects a high energy environment and the coarse-grained sediment lag that would be deposited (Fig. 9). The upper boundary of Sequence I is defined by the surface of onlapping marine horizons. Traditionally, the transgressive surface is identified by a progressive shoreward shift of facies (Christie-Blick and Driscoll, 1995), seen here as onlapping horizons. This is the case at shallow water depths where Sequence I is absent, however, the onlapping surface diverges from the wave ravinement surface at depth and in structural lows near shore (Fig. 10).

Spinelli and Field (2003) interpret what we have labeled Sequence I as "transgressive coastal deposits" deposited by the Mad River prior to or early in the

transgression. They have identified the lower bounding surface of this sequence as a lowstand erosion surface, or sequence boundary, and the upper, onlap surface as the transgressive surface (see their Figs. 3 and 4). In their scenario, because the unit is bounded by the sequence boundary and the transgressive surface, it must be a lowstand unit. We agree with Spinelli and Field (2003), that Sequence I is a transgressive deposit, but we propose it is a healing-phase deposit formed by wave-base erosion and is sequestered in structural lows along the transgressive surface. In near shore regions, shallower than those mapped by Spinelli and Field (2003), we imaged a channelized erosion surface truncated by the transgressive surface (Figs. 5A and 10). This erosion surface is directly under Sequences I and II, and we interpret it as a lowstand erosion surface. The intervening sediment unit exhibits broad distributary style channel incisions and thick laminations. The distributary nature of the channels, however, suggests that the surface may not be the sequence boundary. One scenario that could lead to the observed geometry is that the preexisting physiography of the shelf or timing of erosion at the shelf edge facilitated deposition in the nearshore and erosion or nondeposition farther offshore. Recent research has shown that erosion during the lowstand may not occur until sea level falls below the shelf edge (e.g., Tornqvist et al., 2006; Van Heijst and Postma, 2001). This could result in sediment deposition on the shelf during early lowstand and subsequent erosion of the shelf edge and adjacent shelf during the late lowstand (i.e., Stage 2 – maximum sea-level fall). During transgression, wave base erosion could cannibalize thin deposits near the middle to outer shelf, and the transgressive surface might coalesce with the underlying sequence boundary formed near the shelf edge, but not on the inner shelf where thicker deposits overlying the sequence boundary are observed. It is possible that the sediments of Sequence I are estuarine in nature and were deposited during early sea-level rise, but their occasional chaotic character implies a reworked nature, such as one would predict for coarse sediment shunted offshore during shoreface erosion

or, perhaps in reworked estuarine deposits. Such a scenario explains the distribution of Sequence I infilling the lows along the transgressive surface and the observation that the transgressive surface and the onlap surface coalesce landward (Fig. 5), except in lows (Fig. 6).

Spinelli and Field (2003) invoke a change in sediment source during the transgression to explain the observed geometry; the "transgressive coastal" deposits are purported to be sourced from the Mad River with the overlying acoustically well-laminated onlapping sequences being sourced from the Eel River. In their Fig. 5, they show that the sediment thickness of this unit ("transgressive coastal deposits" - Spinelli and Field, 2003) changes across the Freshwater Syncline with a maximum thickness on the northern limb of the Freshwater Syncline. Furthermore, they report that the thickness of this unit is approximately 2-3 meters across much of the shelf with maximum thickness of 8 m off the axis of a syncline directly offshore from the present location of the Mad River, which led them to believe the sediment was sourced from the Mad River (Spinelli and Field, 2003). It is difficult to understand why "transgressive coastal deposits" sourced from the Mad River would be preferentially deposited on one limb of a syncline. Furthermore, based on the CHIRP seismics, the Freshwater Syncline appears to exert no influence on the thickness or distribution of Sequence I (Fig. 8). Our results show that Sequence I infills other structural lows, the depocenter is predominantly shore parallel, and it cuts across the trend of the Freshwater Syncline suggesting that deformation associated with the syncline was inactive at this time. The isopach map shows that Sequence I is located at the edges of the structural high delineated on its southern edge by the LSF complex (Fig. 11). Based on the observed erosion and non-deposition, it appears that the Eureka Anticline and adjacent shoal was a structural high throughout the last sea-level rise. Sequence I might be eroded off the Eureka Anticline because of subsequent uplift and deformation in the region (Figs. 6, 7 and 10). At lower stands of sea level,

given the geometry of the Eureka Anticline and adjacent region, the shoreline would have taken an abrupt eastward jog along its south termination (Figs. 8 and 11). Thus, as sea level transgressed across this shoreline, healing-phase deposits would have been shunted both to the south and west of the high, consistent with our observations (Fig. 8).

Sequence II is a unit of onlapping, backstepping sediments characteristic of the transgressive systems tract. Based on their flat, laminated nature in the cross shelf direction and core samples, we interpret Sequence II as formed by deposition along an open shelf. Along strike, Sequence II shows marked divergence in the Eel River Syncline with the dip of each reflector increasing with depth (Fig. 12). As mentioned above, the thickness variations of Sequence II are as large along the margin as they are across the margin (Fig. 11); the thickness ranges from > 30 m in the subsiding Eel River Syncline to < 2 m across the axis of the Eureka Anticline. Fig. 10 illustrates the three-dimensional onlap pattern of Sequence II, onlapping Sequence I and the transgressive surface to the east and the limb of the Eel River Syncline to the north. The thickness of this deposit led Burger et al. (2002) to assign it to the highstand systems tract. Nevertheless, the depositional systems tracts are defined primarily by their architecture and facies associations (Posamentier and Vail, 1988). A transgressive systems tract is composed of backstepping beds, which terminate landward by onlap and seaward by downlap. The highstand systems tract is composed of offlapping beds with dowlapping seaward terminations that evolves from aggradational to progradational in response to available accommodation. The surface between the two tracts, known as the maximum flooding surface (Swift et al., 1991), separates discordant sets of bedding planes. By these criteria, the bulk of the deposits above the transgressive surface on the Eel shelf must be assigned to the transgressive systems tract. There is, however, some geomorphic evidence of incipient highstand. A coastal plain has developed since the late Holocene reduction in the rate of sea-level rise, and the Mad and Eel estuaries of 5000 ybp have

inverted as deltas have filled these synclinal axes and have prograded down their length. Based on sediment thickness, distribution, and acoustic character (Figs. 5, 6 and 10), it appears that the ephemeral near shore deposits are reworked and transported offshore and are sequestered on the middle to outer shelf. On the inner shelf, the transparent acoustic character of the transgressive sequence and numerous cores suggest the inner shelf is composed of homogenous sands with little to no acoustic impedance contrasts. Moving offshore, the thickness of the transgressive sequence exhibits a marked increase in concert with an increase in acoustic laminations (Figs. 5 and 10). These observations suggest that the flood deposits emplaced on the inner shelf are subsequently reworked and sequestered offshore in deeper water or along strike in the actively subsiding synclines (e.g., Eel River syncline).

4.6.2 Tectonic Controls on Sedimentation

The thickness of the transgressive sequence is predominantly controlled by the along-shore tectonic deformation and folding in the region (Figs. 2 and 10). Sediment is eroded from shoals and deposited in lows where expanded sections are observed. This pattern represents the long-term sediment accumulation controlled by tectonic accommodation. As few of the cores acquired during STRATAFORM penetrated the transgressive surface, we have examined the stratal patterns and onshore paleoseismic work to place some constraints on the relative timing of deformation (e.g., Fig. 3). For example, the offset of the transgressive surface over the Eureka Anticline indicates deformation has taken place since sea level transgressed that water depth (~50 m). Assuming wave-based erosion reworked the shoreface and subsequent deformation offset the planar surface, deformation on the Eureka Anticline has occurred since ~10 ka. Activity on the Eureka Anticline agrees with mid-Pleistocene to Holocene activity inferred by other researchers (Clarke and Carver, 1992; Gulick and Meltzer, 2002;

McCrory, 2000). In addition, the high sediment input to the margin provides a high fidelity record of the deformation, such as the diverging, highly reflective horizons within Sequence II (Figs. 6 and 12). The divergence of bedding with increasing distance away from the LSF complex records the rapid subsidence in the Eel River syncline of up to 3 mm/yr (Fig. 3). Uplift rates onshore for the LSF complex are significantly lower than subsidence of the Eel River syncline, and reflectors in the upper sediment unit do not appear to diverge seaward to the west of the anticline (Figs. 5 and 10). The divergent geometry of the reflectors in the Eel River Syncline indicates deformation and deposition have been synchronous rather than deformation predating deposition (Fig. 12). The geometry of the reflectors indicates syntectonic deposition (Fig. 13A). It is possible that deformation has been continuous, but based on previous researchers' observations of episodic events on the LSF (e.g., Clarke and Carver, 1992; Vick, 1988) it is more likely that deformation offshore has also been episodic. The high-amplitude reflectors in Sequence II, which are interpreted to represent time horizons, may not occur with high enough frequency to determine whether deformation is continuous (Fig. 13A) or episodic (Fig. 13B). The thickness of Sequence II sediments in line 10 represents ~1.3 mm/yr of deformation assuming an age of 10 ka for the transgressive surface in that location (Fig. 12). This rate of deformation at the northern side of the Eel River Syncline is likely a low estimate for the maximum rate in the syncline and is comparable to the maximum of 3 mm/yr observed onshore (Fig. 3; Vick, 1988).

Long cores are needed to provide more insight into the nature of the deformation. We predict that continuous deformation and sedimentation would result in very little grain-size change throughout the core (Fig. 13A), but episodic deformation, which would create sudden deepening, would result in a pattern of recurrent, coarsening upward units (Fig. 13B). Alternatively, flat-lying geometry and an overall coarsening upward package would be observed if deformation preceded deposition (Fig. 13C). Unfortunately cores

from the STRATAFORM project did not sample deeper than ~3 m below the seafloor on the shelf and thus were inadequate to define the grain size patterns or date the highly reflective horizons observed on the margin (Fig. 10).

Spinelli and Field (2003) claim a structural control for the location of the sediments mapped here as Sequence I. This claim is based on a rough coincidence of their Sequence I depocenter with location of the Freshwater Syncline as mapped by Clarke (1992). Evidence from Burger et al. (2002) shows that the Freshwater Syncline has likely been inactive since ~500ka and that the youngest units within it are generally flat-lying. Seismic profiles from this study also find little evidence for a syncline in the vicinity of the mapped Freshwater Syncline, nor in the location of the mapped Sequence I sediments. In addition, the sediment depocenter mapped by Spinelli and Field (2003) is confined to the northern side of the mapped Freshwater Syncline, not infilling a distinct low. The finer scale mapping of Sequence I facilitated by this study indicates that the unit is contour parallel and is thickest offshore of the high associated with the LSF complex and, if anything thickens to the south. However, due to gas it is difficult to determine with confidence how far it extends to the south. If these sediments are in fact estuarine sediments deposited during the late lowstand to early transgression prior to the sea-level incursion, it is unclear how the Mad River derived sediments could surmount this long-standing topographic high and deposit sediments to the south. Spinelli and Field (2003) propose that the Mad River must have migrated to the north over time, but this appears unlikely given the structural impediment formed by the Eureka Anticline and LSF complex (Fig. 8).

4.6.3 Sediment Source and Hydrodynamic Control on Sediment Distribution

On shorter time scales, hydrodynamic forcing likely plays a role in generating the mid-shelf sediment thickness high, and the rivers as sediment sources enhance sediment

thickness on the adjacent shelf. The mid-shelf wedge visible between ~75 and 90 m of water depth in the Eel River Basin is likely the result of hydrodynamic conditions such as wave climate and the currents that carry Eel River storm sediments to the north (e.g., Sommerfield and Nittrouer, 1999; Harris et al., 2005). As expected with slowing sea-level rise and high sediment input, accommodation has been filled or exceeded on the shelf adjacent to the Mad and Eel Rivers where sediment thickness increases above the thickness observed on the intervening structural high. Although, sediment thickness in the Eel River Syncline is largely due to the tectonic low, bathymetry and strike lines that parallel the shoreline show that there is excess sediment accumulation as part of a subaqueous delta, and it has deflected the 40 m isobath seaward in front of the Eel River mouth (Fig. 2). This observation is consistent with bathymetric observations from Goff et al. (1999). A similar observation appears to hold offshore of the Mad River, but our survey coverage did not extend far enough north to adequately document this trend. The superimposition of the sediment source on the tectonic basin results in enhanced sediment thickness and bathymetry, and thus the seafloor is poorly correlated with the relief on the underlying transgressive surface (Figs. 2 and 8).

Highly reflective layers within Sequence II are likely due to storm events that have carried large amounts of sediment to the shelf. These storm layers would have finer sediment grain sizes than the sediment layers deposited during normal conditions. Shallow lines also appear to have more mottled, highly reflective sediments in the near surface. This could be due to a higher concentration of gas at shallower depths. The location of the depocenter on the outer shelf at 80 – 90 m water depth is deeper than the water depth of the depocenter (~70 m) observed by studies of sediments deposition on time scales of 100s of years (Sommerfield & Nittrouer, 1999). The shoreward offset is most likely temporal, and with continued exposure to storm activity and reworking the short-term depocenter will eventually be transported offshore.

4.7 CONCLUSIONS

In this study, high-resolution CHIRP data provided a detailed view of sediment architecture near the seafloor, which facilitated analysis of the different controls on sediment deposition and preservation on the shelf since the Last Glacial Maximum (~21 ka). The transgressive systems tract of the Eel River shelf is composed of two acoustic units, a healing-phase deposit that smooths seafloor roughness and an upper transgressive unit of aggrading, backstepping marine deposits. On the shelf offshore of the Eel River, sediments erode off the highs and accumulate in the lows, creating expanded sections. Along-strike variability in accommodation due to tectonic deformation is the major control on long-term accumulation. Hydrodynamic forcing appears to control shorter-term sediment dispersal, but its influence is also apparent in long-term cross-shore sediment distribution. In the Eel River Basin, the location and extent of the mid-shelf thickness maximum depends on the wave climate and sediment size distribution characteristic of the margin. High sediment input and slowing sea-level rise may have brought about the transition from the transgressive systems tract to the highstand systems tract. The geometry of reflectors within the transgressive sequence indicates the relative timing of sedimentation and deformation; offset of the transgressive surface and diverging reflectors in the upper transgressive sediments indicate that deposition is syntectonic with rates of approximately 3 mm/yr. Onshore to offshore correlation of structures is tenuous as many structures onshore appear to die away offshore and those offshore appear to die off onshore, attesting to the highly three-dimensional deformation in the region.

4.8 ACKNOWLEDGEMENTS

This project was funded by ONR as part of the STRATAFORM initiative. Special thanks to Joe Kravitz and the LA ARCS Foundation.

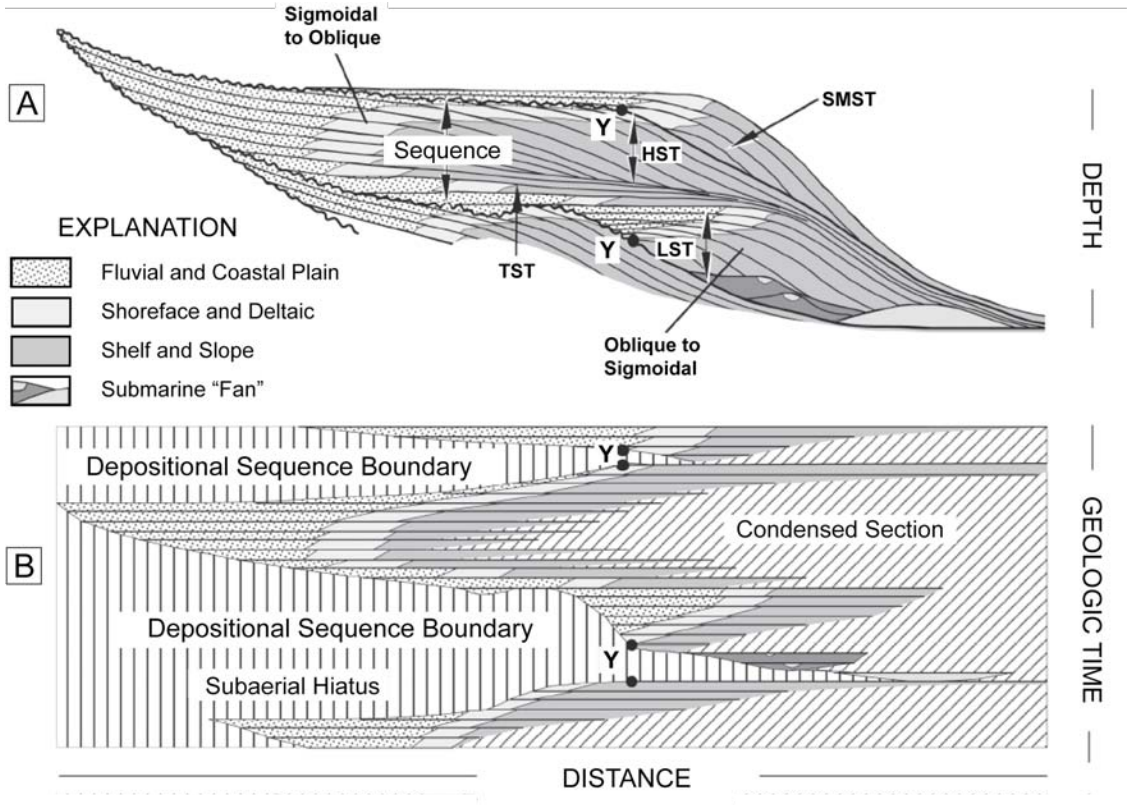
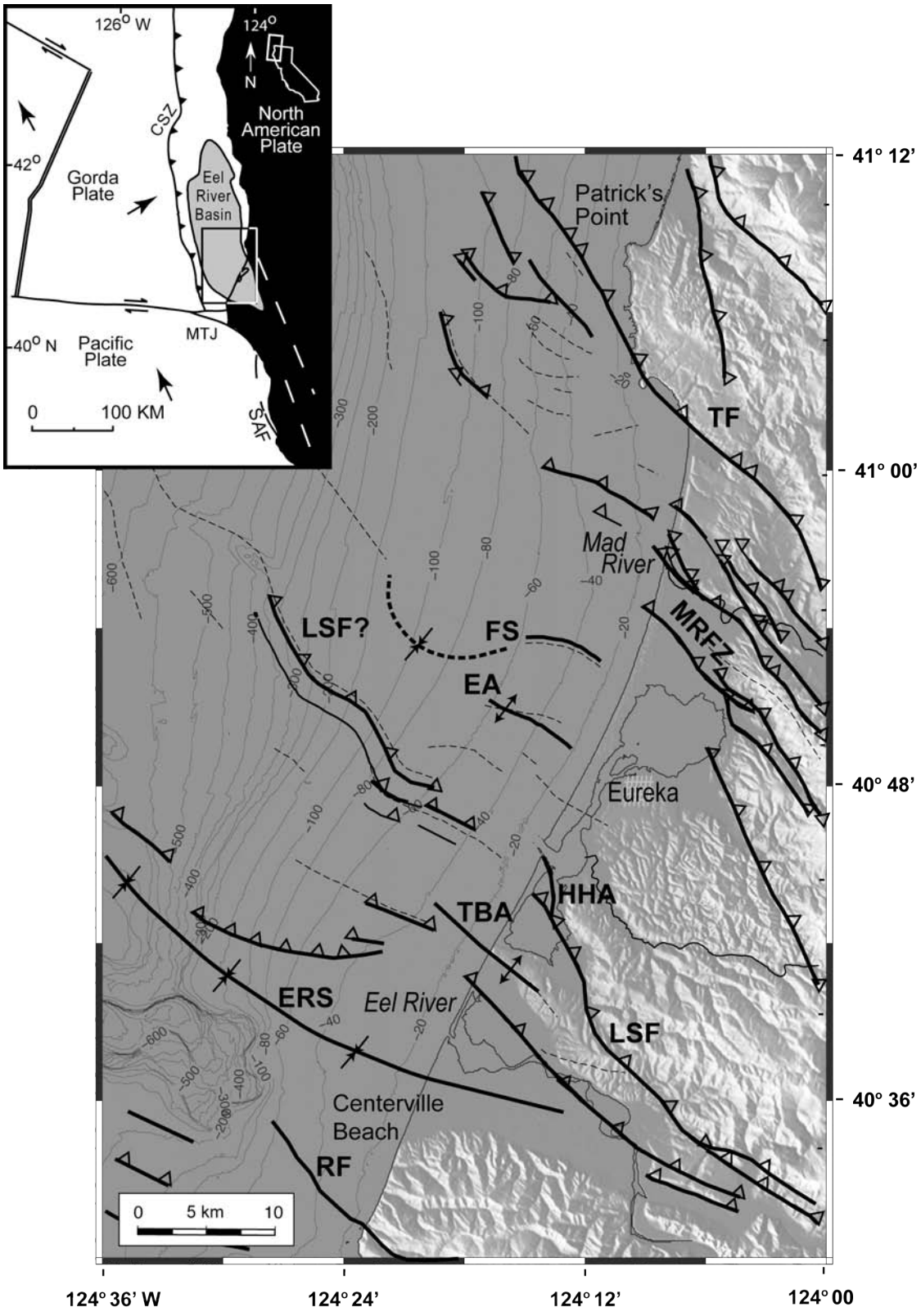


Figure 4-1: A: Chronostratigraphic and B: lithostratigraphic representation of a sequence stratigraphic profile showing a classic sequence bounded by subaerial unconformities or sequence boundaries. HST = Highstand Systems Tract, TST = Transgressive Systems Tract, LST = Lowstand Systems Tract, and SMST = Shelf Margin Systems Tract (after Christie-Blick and Driscoll, 1995).

Figure 4-2: Location map with local structural features and inset showing plate boundaries offshore northern California (after Clarke, 1992). Note that major local structures (black lines) are oriented at a higher angle to the coastline than the regional structures (e.g., San Andreas Fault (SAF), inset). CSZ = Cascadia Subduction Zone, MTJ = Mendocino Triple Junction, RF = Russ Fault, ERS = Eel River Syncline, LSF = Little Salmon Fault, TBA = Table Bluff Anticline, HHA = Humboldt Hill Anticline, EA = Eureka Anticline, FS = Freshwater Syncline, MRFZ = Mad River Fault Zone, TF = Trinidad Fault. Structures from Clarke (1992) and McLaughlin et al. (2000).


126° W
124°
N
North American Plate
CSZ
42°
Gorda Plate
Eel River Basin
40° N
Pacific Plate
MTJ
0
100 KM
SAF
41° 12’
41° 00’
40° 48’
40° 36’
Patrick’s Point
TF
Mad River
MRFZ
LSF?
FS
EA
Eureka
HHA
TBA
ERS
Eel River
LSF
Centerville Beach
RF
0
5 km
10
124° 36’ W
124° 24’
124° 12’
124° 00

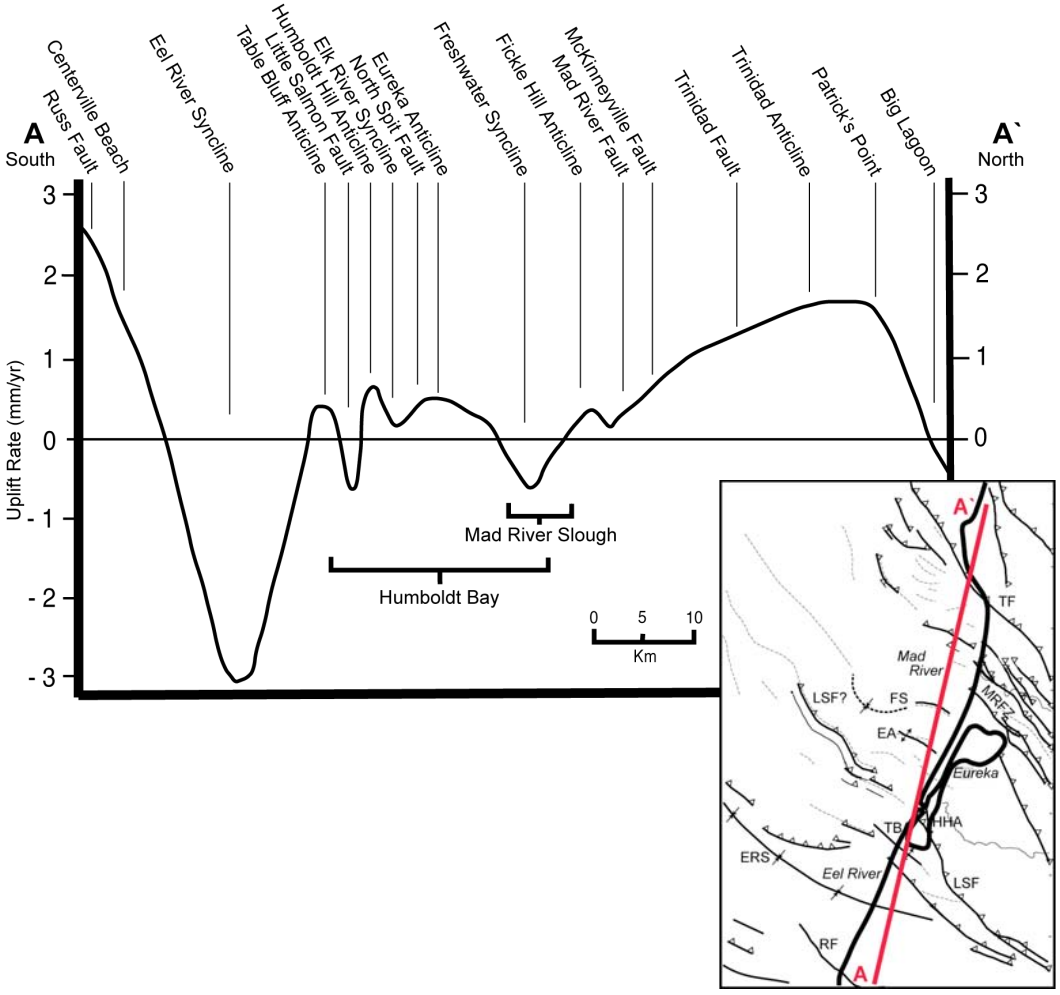


Figure 4-3: Rates of uplift and subsidence along profile A-A' (see Figure 2 for location). Note the maximum rate of deformation of ~ 3mm/yr occurs in the Eel River Syncline. After Vick (1986).

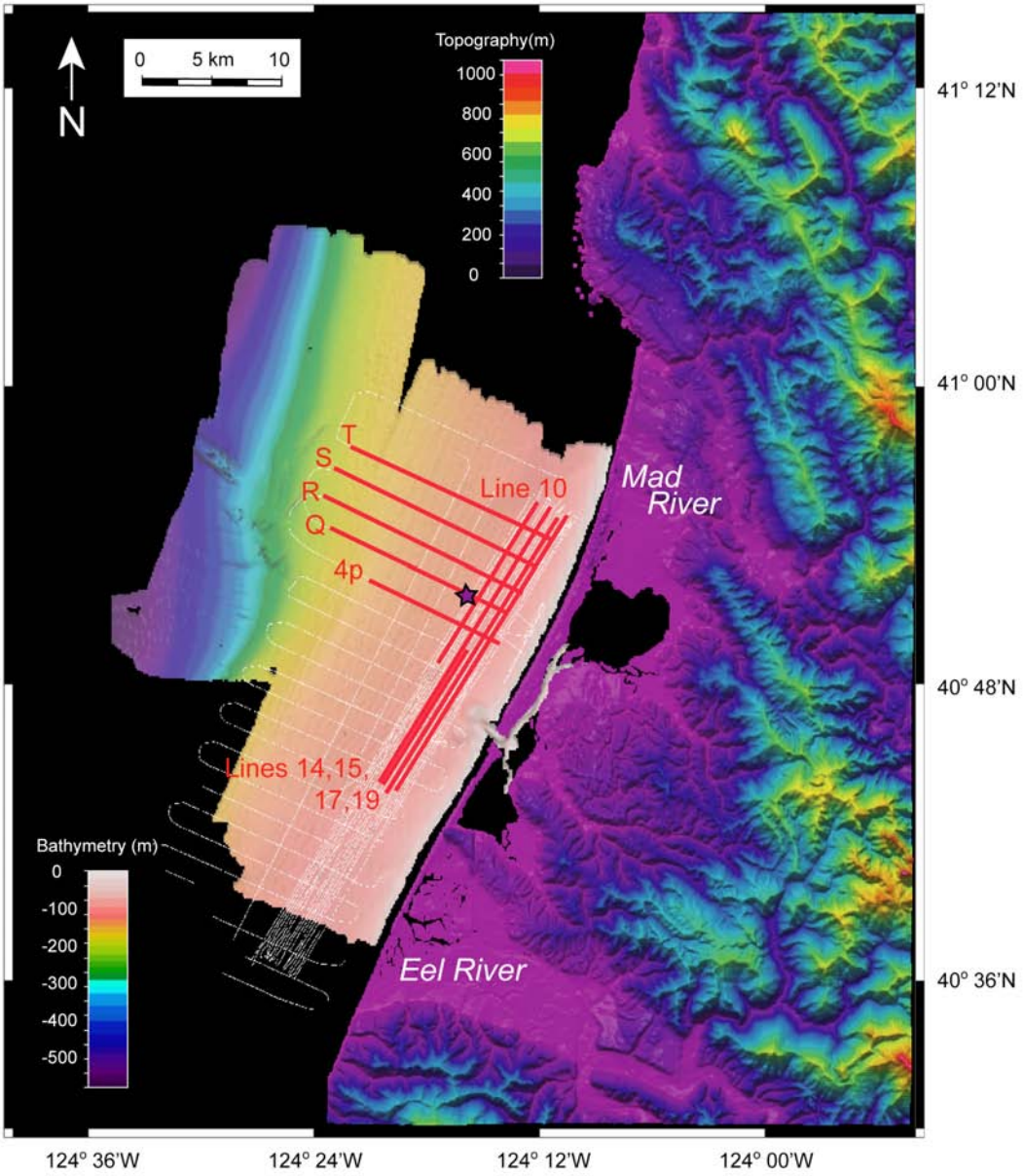
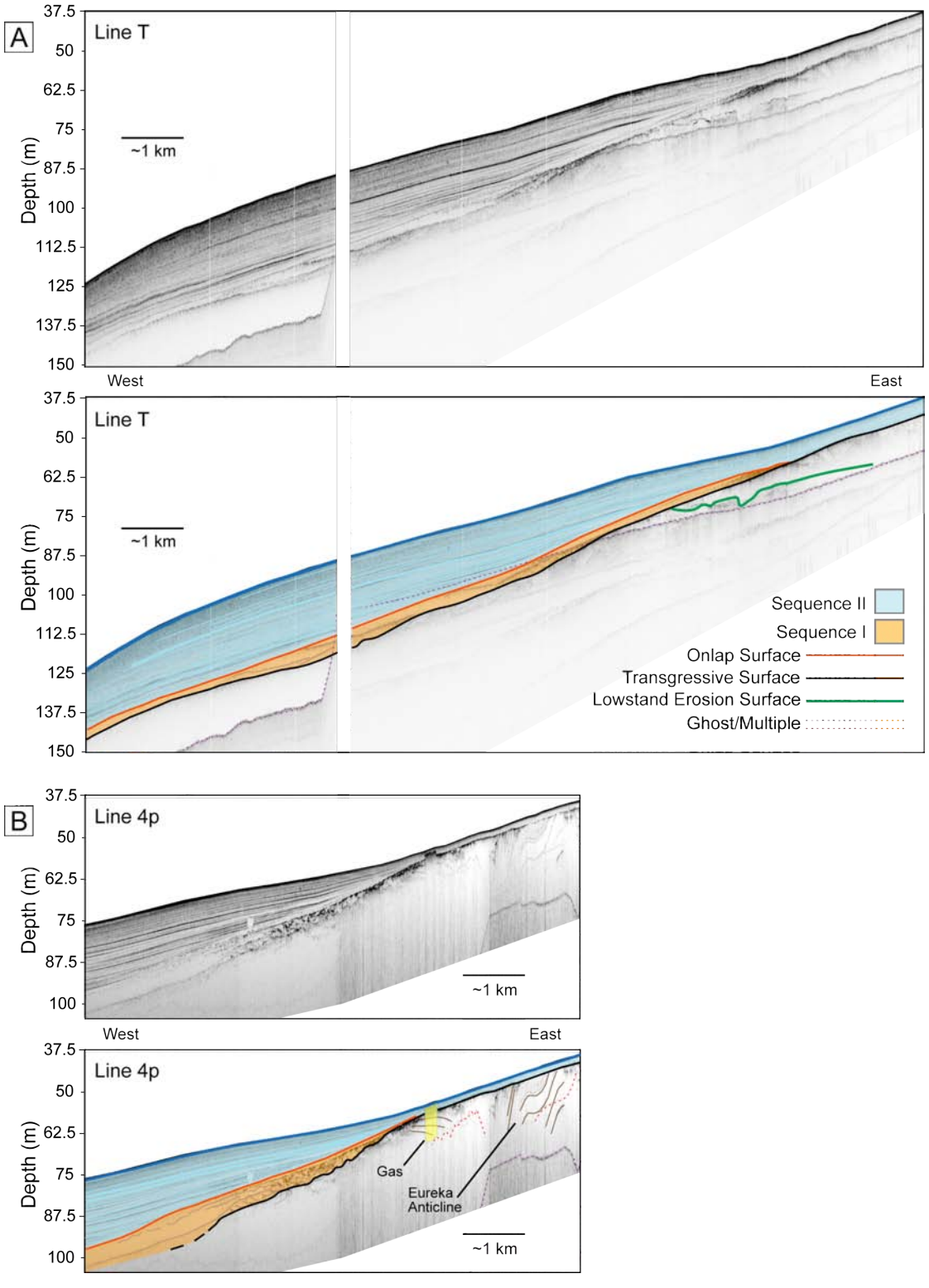


Figure 4-4: Survey ship tracks superimposed on high-resolution bathymetry (Goff et al., 1999; Ferrini and Flood, 2002) collected as part of the STRATAFORM project. Red lines indicate profiles shown in Figures 5, 6, and 10. Star indicates location of core shown in Figure 9.

Figure 4-5: Dip lines T and 4p. A: Line T uninterpreted (top) and interpreted (bottom) crosses the margin just south of the Mad River, and B: Line 4p uninterpreted (top) and interpreted (bottom) crosses the margin to the north of the Eel River Syncline and crosses the Little Salmon Fault complex and Eureka Anticline. Vertical area in white in line T is a data gap.


A
Line T
~1 km
Depth (m)
37.5
50
62.5
75
87.5
100
112.5
125
137.5
150
West
East
Line T
~1 km
Sequence II
Sequence I
Onlap Surface
Transgressive Surface
Lowstand Erosion Surface
Ghost/Multiple
B
Line 4p
~1 km
West
East
Line 4p
Gas
Eureka
Anticline
~1 km

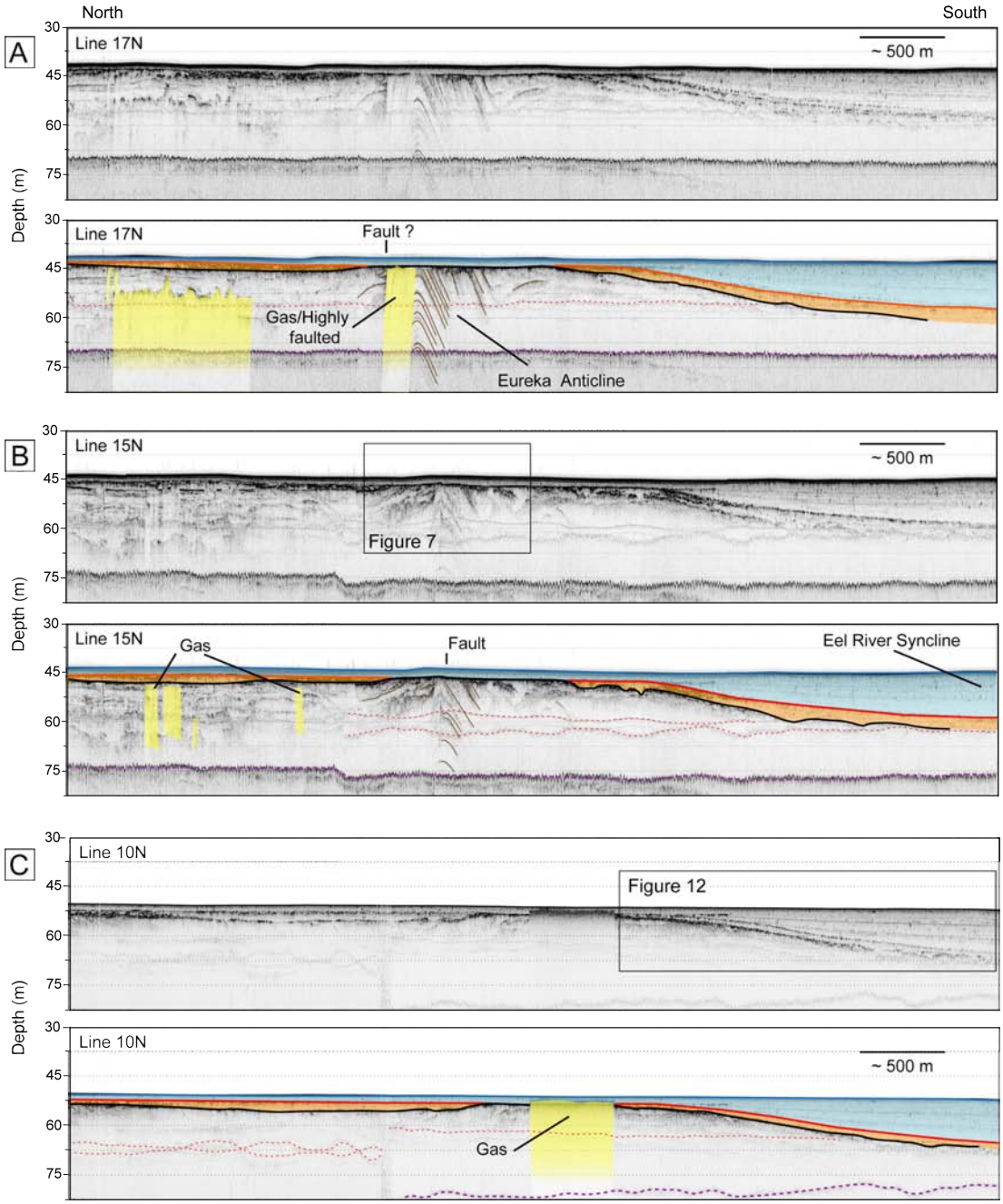


Figure 4-6: Strike lines A: 10, B: 15, and C: 17 uninterpreted (top) and interpreted (bottom). In strike lines the transgressive surface and a prominent anticline and fault are imaged. The transgressive surface deepens to the south towards the Eel River Syncline. Note reflectors are intermittently obscured by gas throughout much of the study area. Color scheme is same as shown in Figure 5.

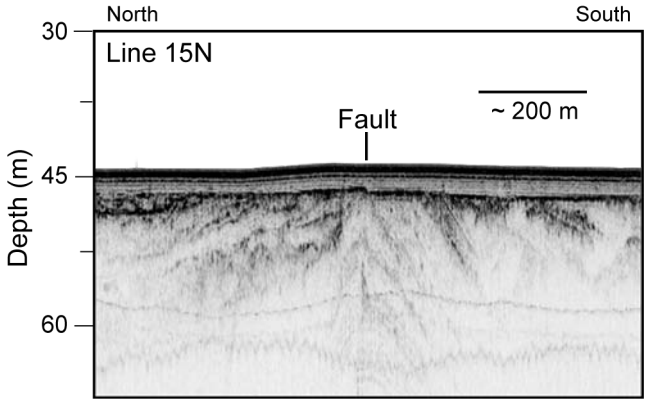


Figure 4-7: Detail of strike line 15 showing fault offset in transgressive surface above the Eureka Anticline. See Figures 4 and 6 for location.

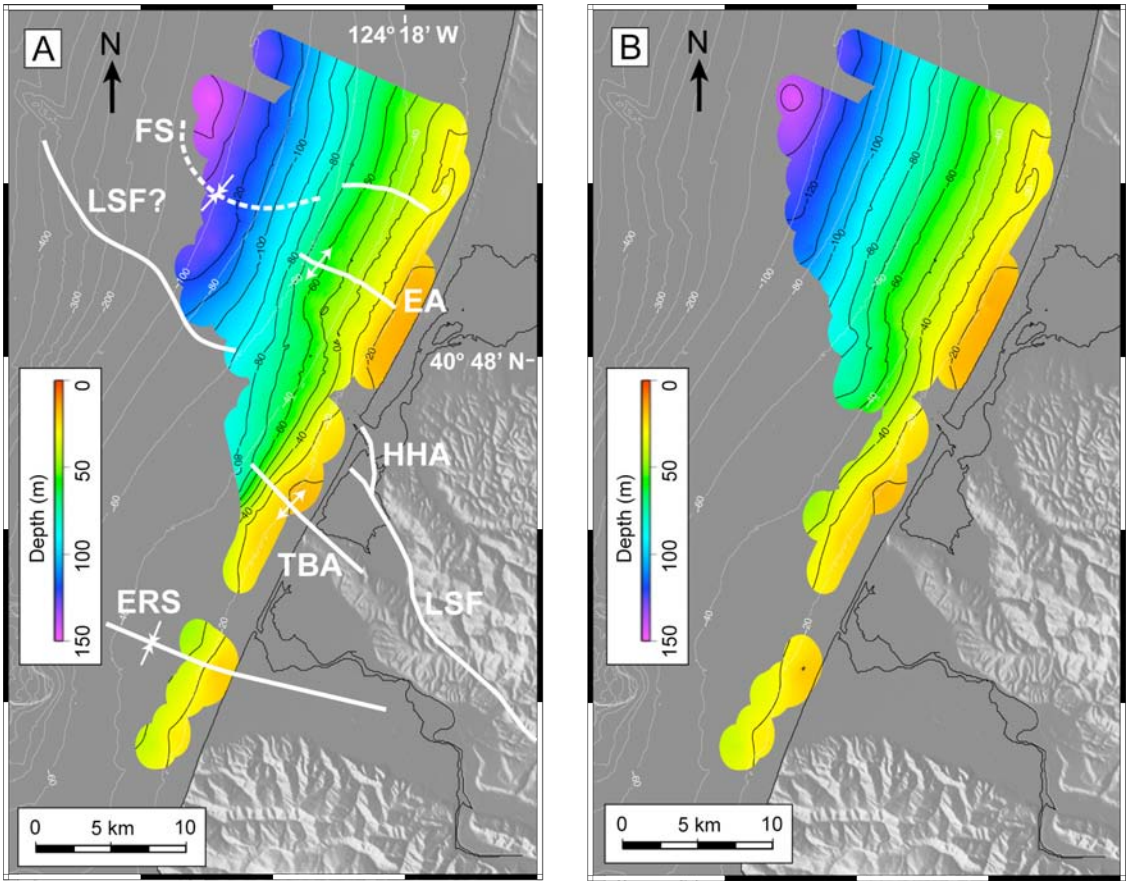


Figure 4-8: Structure contour maps. A: Depth to transgressive surface shows the abrupt eastward jog and deepening to the south of the northern high and a slight high offshore of the Table Bluff Anticline. B: Depth to top of Sequence I shows the surface is more evenly sloping than the transgressive surface at depths > 60 m. In A selected tectonic features are superimposed in white. ERS = Eel River Syncline, LSF = Little Salmon Fault, TBA = Table Bluff Anticline, HHA = Humboldt Hill Anticline, EA = Eureka Anticline, FS = Freshwater Syncline.

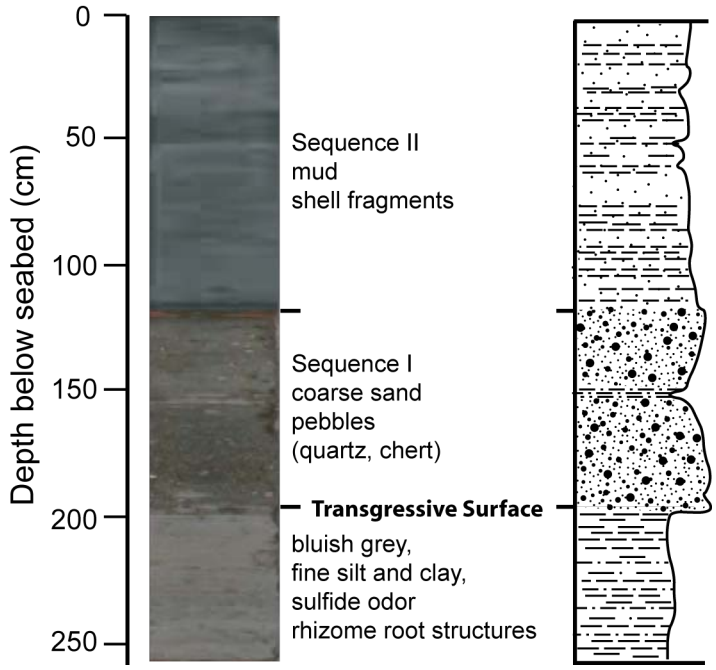
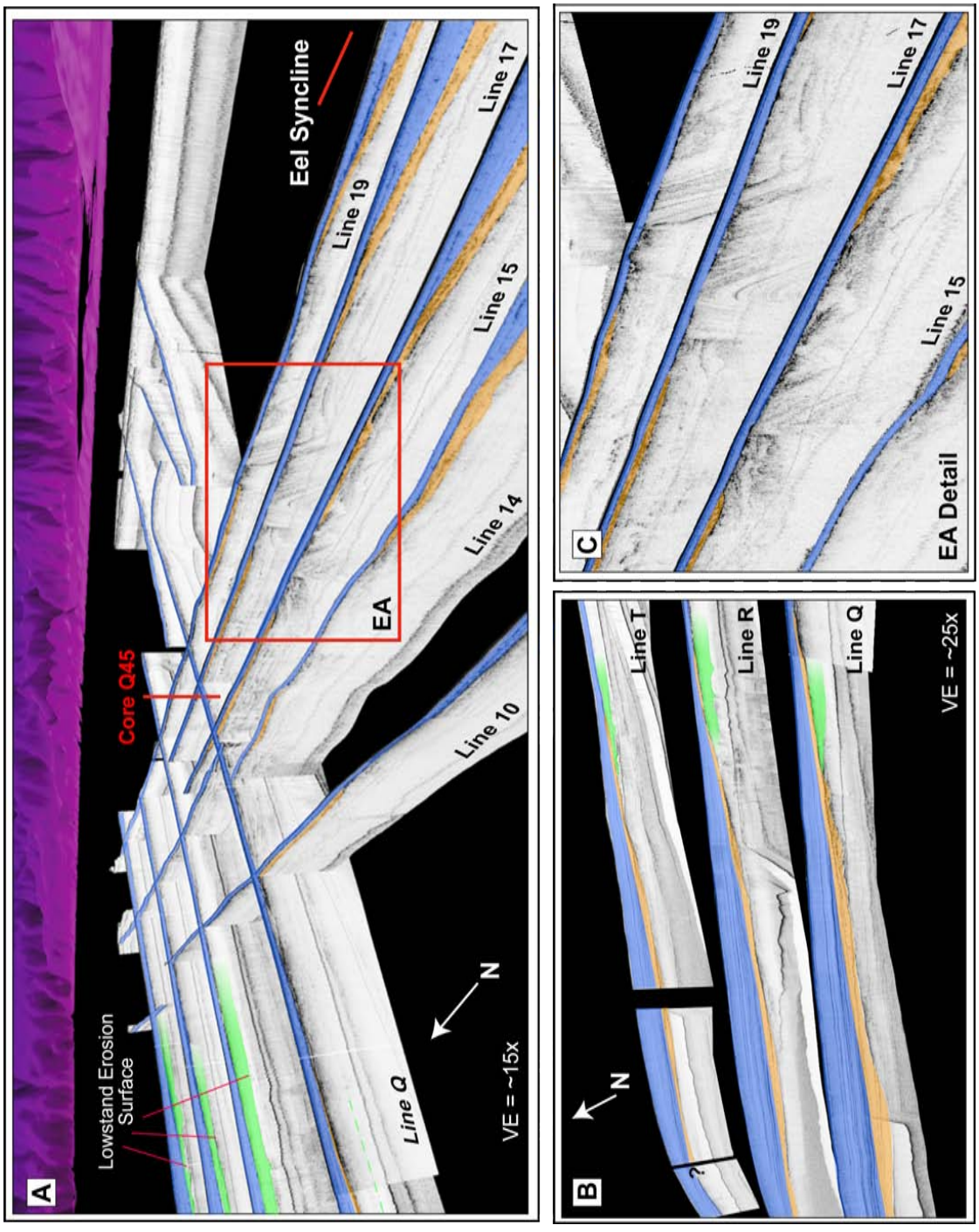


Figure 4-9: Core Q45 recovered the transgressive surface, which separates transgressive marine deposits above from subaerial deposits below. Note the coarse-grained lag deposit associated with the transgressive surface and the marked difference between the upper and lower fine-grained units. See Figures 4 and 10 for core location.

Figure 4-10: A: Perspective view showing strike and dip lines on the edge of the structural high with Sequence I (orange) confined mostly to its flanks and Sequence II (blue) thickening into the Eel River Syncline and offshore. B: Perspective view showing the thickest deposits of Sequence I on the west side of the structural high, the unit thinning both landward and seaward, and the unit truncating the underlying lowstand deposits (green). C: Detailed view from (A) showing the Eureka Anticline.


A
Lowstand Erosion Surface
Core Q45
Eel Syncline
Line 19
Line 17
Line 15
Line 14
Line 10
EA
Line Q
N
VE = ~15x
B
N
Line T
Line R
Line Q
?
VE = ~25x
C
Line 19
Line 17
Line 15
EA Detail

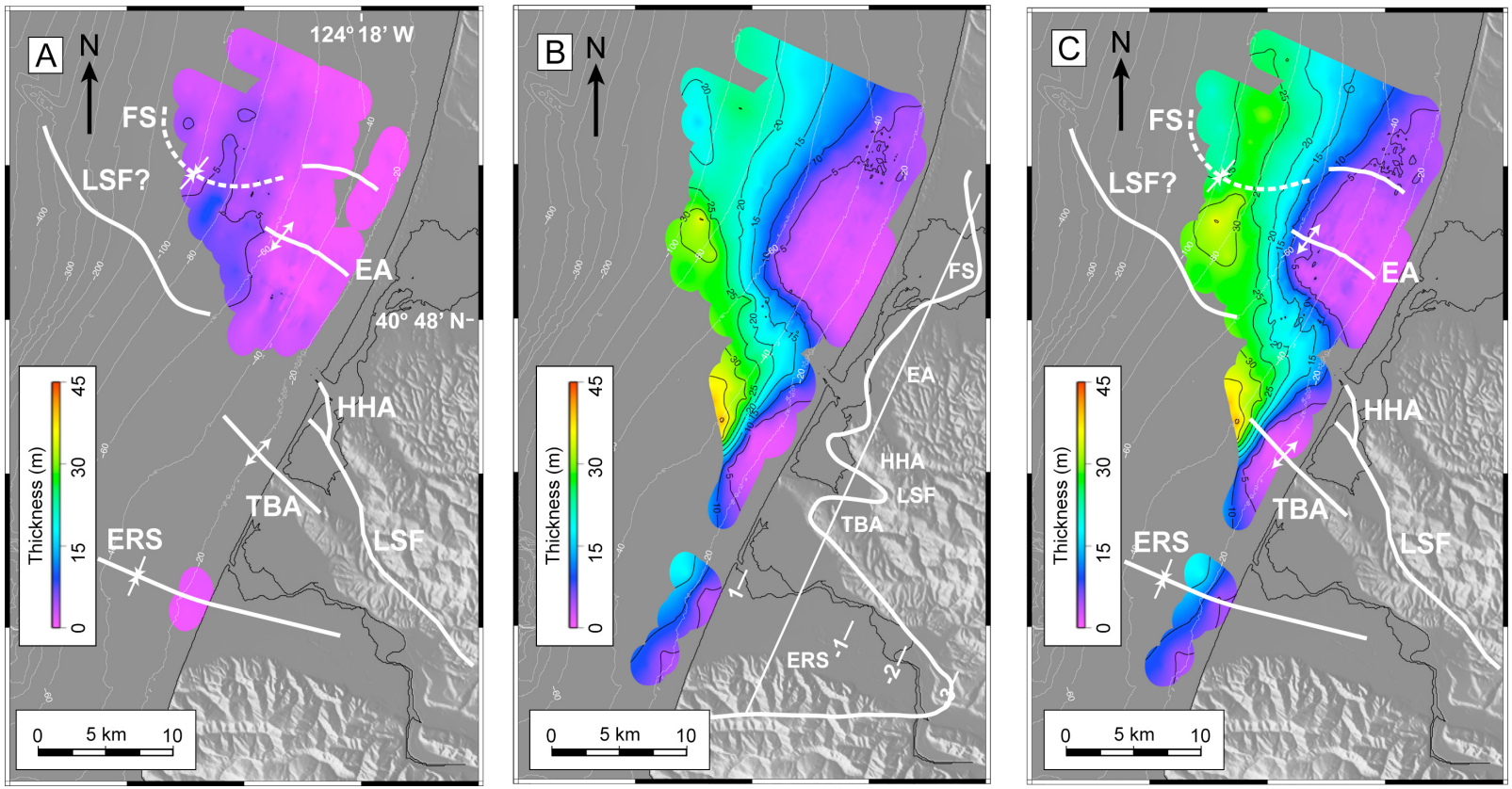


Figure 4-11: Isopach maps. A: Sequence I B: Sequence II C: Sequences I and II. Contour interval is 5 m. In A selected tectonic features are superimposed in white, and in B uplift and subsidence rates onshore are superimposed in white. ERS = Eel River Syncline, LSF = Little Salmon Fault, TBA = Table Bluff Anticline, HHA = Humboldt Hill Anticline, EA = Eureka Anticline, FS = Freshwater Syncline.

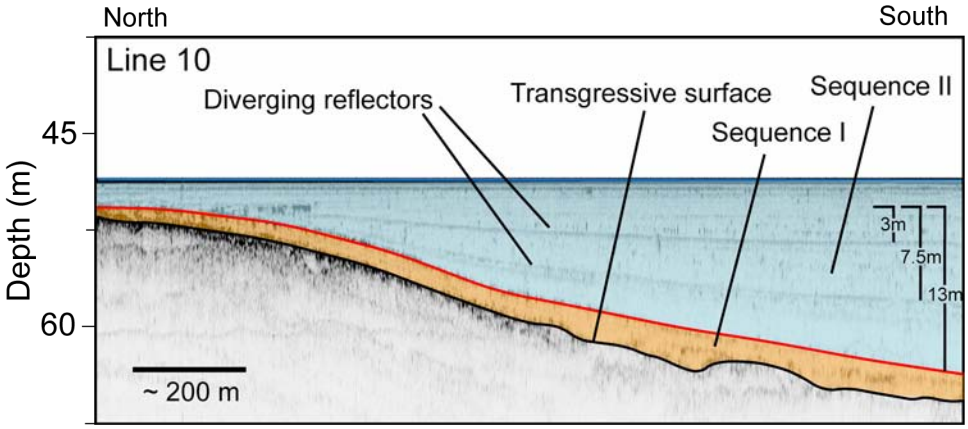


Figure 4-12: Detail of strike line 10 showing divergence of reflectors into the Eel River Syncline. In addition, depths to high-amplitude reflectors within Sequence II are shown for deformation rates derived in text. See Figures 4 and 6 for location.

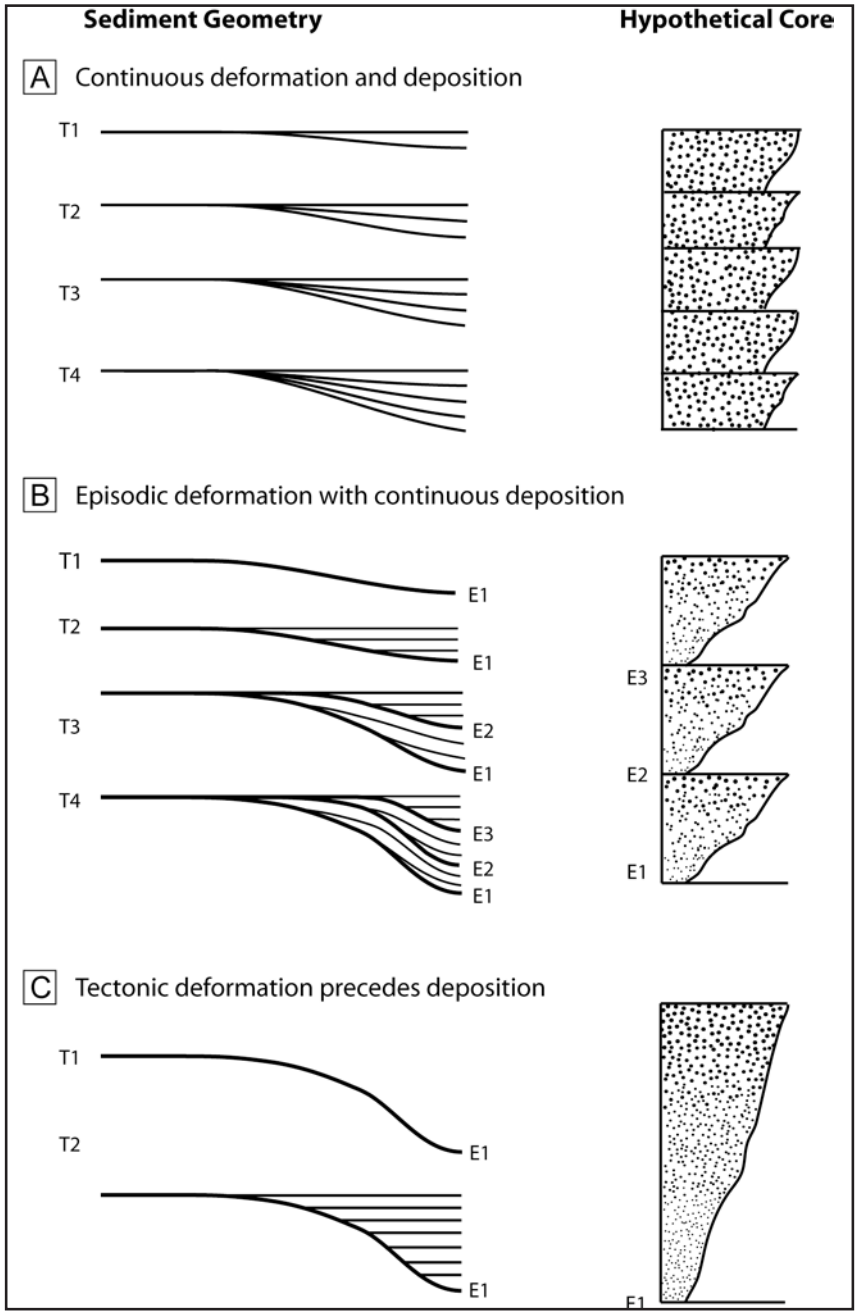


Figure 4-13: Predicted stratigraphic geometry and cores for three possible scenarios of deformation and sedimentation. A: Synchronous and ongoing deformation and sedimentation would result in little change in grain size throughout the core; B: episodic deformation coupled with continuous sedimentation would result in a series of stacked, coarsening upward packages, and C: when all deformation predates sedimentation an expected core would exhibit an overall coarsening upward pattern. T1 = Time 1, E1 = Event 1.

4.1 REFERENCES

Allen, G.P., Posamentier, H.W., 1993. Sequence stratigraphy and facies model of an incised valley fill: the Gironde Estuary, France. Journal of Sedimentary Petrology 63 (3), 378-391.

Brown, L.F. Jr., Fisher, W.L., 1977. Seismic stratigraphic interpretation of depositional systems: examples from the Brazilian rift and pull-apart basins. In: Payton, C.E. (Ed.), Seismic stratigraphy - applications to hydrocarbon exploration: Tulsa, Oklahoma, American Association of Petroleum Geologists Memoir 26, pp. 213-48.

Brown, W. M., Ritter, J., 1971. Sediment transport and turbidity in the Eel river basin, California. U.S. Geol. Surv. Water Supply Paper 1986.

Burger, R.L., Fulthorpe, C.S., Austin, J.A., Gulick, S.P.S., 2002. Lower Pleistocene to present structural deformation and sequence stratigraphy of the continental shelf, offshore Eel River Basin, northern California. Marine Geology 185 (3-4), 249-281.

Cattaneo, A., Steel, R.J., 2003. Transgressive deposits: a review of their variability. Earth-Science Reviews 63, 187-228.

Chappell, J., Omura, A., Esat, T., McCulloch, M., Pandolfi, J., Ota, Y., Pillans, B., 1996. Reconciliation of late Quaternary sea levels derived from coral terraces at Huon Peninsula with deep sea oxygen isotope records: Earth And Planetary Science Letters 141, 227-236.

Christie-Blick, N., 1991. Onlap, offlap, and the origin of unconformity-bounded depositional sequences. Marine Geology 97, 35-56.Christie-Blick, N. and Driscoll, N.W., 1995. Sequence Stratigraphy. Annual Review Of Earth And Planetary Sciences 23, 451-478.

Clarke, S.H., 1992. Geology Of The Eel River Basin And Adjacent Region - Implications For Late Cenozoic Tectonics Of The Southern Cascadia Subduction Zone And Mendocino Triple Junction. AAPG Bulletin 76 (2), 199-224.

Clarke, S.H., Carver, G.A., 1992. Late Holocene Tectonics And Paleoseismicity, Southern Cascadia Subduction Zone. Science 255 (5041), 188-192.

Cohen, J.K., Stockwell Jr., J.W. 1999. CWP/SU: Seismic Unix Release 33: A free package for seismic research and processing, software. Center for Wave Phenomena, Colorado School of Mines, Golden, CO.

Dam, G., Surlyk, F., 1992. Forced regressions in a large wave- and storm-dominated lake, Rhaetian-Sinemurian Kap Stewart Formation, East Greenland. Geology 20, 749-52.

Driscoll, N.W., 1992. Tectonic and depositional processes inferred from stratal relationships. PhD dissertation. Columbia University, New York. 464 pp.

Driscoll, N.W., Hogg, J.R., 1995. Stratigraphic response to basin formation: Jeanne d'Arc Basin, offshore Newfoundland. Geological Society, London, Special Publications: v. 80: pp 145-163.

Driscoll, N.W., Karner, G.D., 1998. Lower crustal extension across the Northern Carnarvon basin, Australia: Evidence for an eastward dipping detachment. Journal of Geophysical Rsearch 103 (B3), 4975-4991.

Driscoll, N.W., Karner, G.D., 1999. Two-dimensional quantitative modeling of Clinoform development. Marine geology 154, 383-398.

Fairbanks, R.G., 1989. A 17,000-year glacio-eustatic sea-level record: influence of glacial melting rates on the Younger Dryas event and deep-ocean circulation. Nature 342, 637-642.

Ferrini, V., Flood, R.D. 2002. Multibeam Sonar on the Inner Shelf of the Eel Margin: Nearshore gravel-floored troughs. Eos Trans. AGU, 83(47), Fall Meeting Supplement, Abstract OS71C-0297.

Goff, J.A., Orange, D.L., Mayer, L.A., Clarke, J.E.H., 1999. Detailed investigation of continental shelf morphology using a high-resolution swath sonar survey: the Eel margin, northern California. Marine Geology 154 (1-4), 255-269.

Gulick, S.P.S., Meltzer, A.S., 2002. Effect of the northward-migrating Mendocino triple junction on the Eel River forearc basin, California: Structural evolution. Geological Society Of America Bulletin 114 (12), 1505-1519.

Gulick, S.P.S., Meltzer, A.S., Clarke, S.H., 2002. Effect of the northward-migrating Mendocino triple junction on the Eel River forearc basin, California: Stratigraphic development. Geological Society Of America Bulletin 114 (2), 178-191.

Harris, C.K., Traykovski, P.A., Geyer, W.R., 2005. Flood dispersal and deposition by near-bed gravitational sediment flows and oceanographic transport: A numerical modeling study of the Eel River shelf, northern California. Journal of Geophysical Research-Oceans, 110: C09025.

Hart, B.S., Plint, A.G., 1993. Tectonic influence on deposition and erosion in a ramp setting: Upper Cretaceous Cardium Formation, Alberta foreland basin. American Association Of Petroleum Geologists Bulletin 77 (12), 2092-2107.

Henkart, P. 2003. SIOSEIS, software. Scripps Institution of Oceanography, La Jolla, CA (available at http://sioseis.ucsd.edu).

Hogarth, L..J., Babcock, J., Driscoll, N.W., Le Dantec, N. Hass, J.K., Inman, D.L., Masters, P.M., 2007. Long-term tectonic control on Holocene shelf sedimentation offshore La Jolla, California. Geology 35 (3), 275-278.

Jervey, M.T., 1988. Quantitative geological modeling of siliciclastic rock sequences and their seismic expression. In: Wilgus, C. K., Hastings, B. S., Kendall, C. G. S. C., Posamentier, H. W., Foss, C. A., Van Wagoner, J. C., (Eds.), Sea-level Changes: an Integrated Approach Society of Economic Paleontologists and Mineralogists Special Publication No. 42, p. 47-69.

Kelsey, H.M., Carver, G.A., 1988. Late Neogene And Quaternary tectonics associated with northward growth of the San-Andreas transform-fault, Northern California. Journal Of Geophysical Research-Solid Earth And Planets 93 (B5), 4797-4819.

Koss, J.E., Ethridge, F.G., Schumm, S.A., 1994. An experimental study of the effects of base-level change on fluvial, coastal plain and shelf systems. Journal of Sedimentary Research B64, 90-08.

Lawton, T.F., Pollock, S.L., Robinson, R.A.J., 2003. Integrating Sandstone Petrology and Nonmarine Sequence Stratigraphy: Application to the Late Cretaceous Fluvial Systems of Southwestern Utah, U.S.A. Journal of Sedimentary Research 73 (3), 389-406.

MacNeil, A.J., Jones, B., 2006. Sequence stratigraphy of a Late Devonian ramp-situated reef system in the Western Canada Sedimentary Basin: dynamic responses to sea-level change and regressive reef development. Sedimentology 53, 321-259.

McCrory, P.A., 1996. Tectonic model explaining divergent contraction directions along the Cascadia subduction margin, Washington. Geology 24 (10), 929-932. McCrory, P.A., 2000. Upper plate contraction north of the migrating Mendocino triple junction, northern California: Implications for partitioning of strain. Tectonics 19 (6), 1144-1160.

McLaughlin, R.J., Ellen, S.D., Blake, Jr., M.C., Jayko, A.S., Irwin, W.P., Aalto, K.R., Carver, G.A., Clarke Jr., S.H., 2000. Geology of the Cape Mendocino, Eureka, Garberville, and Southwestern Part of the Hayfork 30 x 60 Minute Quadrangles and Adjacent Offshore Area, Northern California, USGS Miscellaneous Field Studies MF-2336, Version 1.0

Nittrouer, C.A., 1999. STRATAFORM: overview of its design and synthesis of its results. Marine Geology 154 (1-4), 3-12.

O'Grady, D.B., Syvitski, J.P.M., Pratson, L.F., Sarg, J.F., 2000. Categorizing the morphologic variability of siliciclastic passive continental margins. Geology 28 (3), 207-210.

Orange, D.L., 1999. Tectonics, sedimentation, and erosion in northern California: submarine geomorphology and sediment preservation potential as a result of three competing processes. Marine Geology 154 (1-4), 369-382.

Posamentier, H.W., Allen, G.P. 1999. Siliciclastic Sequence Stratigraphy – Concepts and Applications. Society of Economic Petrologists and Paleontologists. 216 pp.

Posamentier, H.W., James, D.P., 1993. An overview of sequence-stratigraphic concepts: uses and abuses. In: Posamentier, H.W., Summerhayes, C.P., Haq, B.U., Allen, G.P., (Eds.), Sequence Stratigraphy and Facies Associations International Association of Sedimentologists Special Publication 18, pp. 3-18.

Posamentier, H.W., Jervey, M.T., Vail, P.R. 1988. Eustatic controls on clastic deposition I—conceptual frameworks. In: Wilgus, C. K., Hastings, B. S., Kendall, C. G. S. C., Posamentier, H. W., Foss, C. A., Van Wagoner, J. C., (Eds.), Sea-level Changes: an Integrated Approach Society of Economic Paleontologists and

Mineralogists Special Publication No. 42, pp. 39-45.

Posamentier, H.W., Vail, P.R. 1988. Eustatic controls on clastic deposition II—Sequence and systems tract models. In: Wilgus, C. K., Hastings, B. S., Kendall, C. G. S. C., Posamentier, H. W., Foss, C. A., Van Wagoner, J. C., (Eds.), Sea-level Changes: an Integrated Approach Society of Economic Paleontologists and Mineralogists Special Publication No. 42, pp. 39-45.

Ross, W.C., 1990. Modeling base-level dynamics as a control on basin-fill geometries and facies distribution: a conceptual framework. In: Cross, T.A., (Ed.), Quantitative Dynamic Stratigraphy. pp. 387-99. Englewood Cliffs, NJ: Prentice-Hall. 625 pp.

Sarg, J.F. 1988. Carbonate sequence stratigraphy. pp. 155-81. In: Wilgus, C. K., Hastings, B. S., Kendall, C. G. S. C., Posamentier, H. W., Foss, C. A., Van Wagoner, J. C., (Eds.), Sea-level Changes: an Integrated Approach Society of Economic Paleontologists and Mineralogists Special Publication No. 42, p. 39-45.

Schumm, S.A., 1993. River Response To Baselevel Change - Implications For Sequence Stratigraphy. Journal Of Geology 101, 279-294.

Shanley, K.W., McCabe, P.J., 1994. Perspectives on the sequence stratigraphy of continental strata. American Association Of Petroleum Geologists Bulletin 78, 544-568.

Sommerfield, C.K., Nittrouer, C.A., 1999. Modern accumulation rates and a sediment budget for the Eel shelf: a flood-dominated depositional environment. Marine Geology 154 (1-4), 227-241.

Spinelli, G.A., Field, M.E., 2003. Controls of tectonics and sediment source locations on along-strike variations in transgressive deposits on the northern California margin. Marine Geology 197 (1-4), 35-47.

Swenson, J.B., Muto, T., 2007. Response of coastal plain rivers to falling relative sea-level: allogenic controls on the aggradational phase. Sedimentology 54, 207-221.

Swift, D. J. P., Phillips, S., Thorne, J.A., 1991. Sedimentation on continental margins. Part V: Parasequences. In: Swift, D.J. P., Tillman, R.W., Oertel, G.F., Thorne, J.A. (Eds.), Shelf sand and sandstone bodies: Geometry, facies and Sequence

stratigraphy. International Association of Sedimentologists Special Publication 14., pp. 153-187F.

Syvitski, J.P., Morehead, M.D., 1999. Estimating river-sediment discharge to the ocean: application to the Eel margin, northern California. Marine Geology 154, 13-41.

Tornqvist, T.E., Wortman, S.R., Mateo, Z.R.P., Milne, G.A., Swenson, J.B., 2006. Did the last sea level lowstand always lead to cross-shelf valley formation and source-to-sink sediment flux? Journal Of Geophysical Research-Earth Surface 111.

Underhill, J.R., 1991. Controls on late Jurassic seismic sequences, Inner Moray Firth, UK North Sea: a critical test of a key segment of Exxon's original global cycle chart. Basin Research 3, 79-98.

Vail, P.R., Mitchum, R.M., Thompson, S., 1977. Seismic stratigraphy and global changes of sea level, part 3: Relative changes of sea level from coastal onlap, In: Payton, C.E. (Ed.), Seismic stratigraphy - applications to hydrocarbon exploration: Tulsa, Oklahoma, American Association of Petroleum Geologists Memoir 26, pp. 63-81.

Vail, P.R., Audemard, F, Bowman, S.A. Eisner, P.N., Perez-Cruz, C., 1991. The Stratigraphic Signatures of Tectonics, Eustasy and Sedimentology - an Overview. In: Einsele, G., Ricken, W., Seilacher, A., (Eds.), Cycles and Events in Stratigraphy. 955 pp. Springer-Verlag: Berlin. pp. 617-659.

van Heijst, M., Postma, G., 2001. Fluvial response to sea-level changes: a quantitative analogue, experimental approach. Basin Research 13, 269-292.

Van Wagoner, J.C., Posamentier, H.W., Mitchum, R.M., Vail, P.R., Sarg, J.F., Loutit, T.S., Hardenbol, J., 1988. An overview of the fundamentals of sequence stratigraphy and key definitions. In: Wilgus, C. K., Hastings, B. S., Kendall, C. G. S. C., Posamentier, H. W., Foss, C. A., Van Wagoner, J. C., (Eds.), Sea-level Changes: an Integrated Approach Society of Economic Paleontologists and Mineralogists Special Publication No. 42, pp. 39-45.

Van Wagoner, J.C., Mitchum, R.M., Campion, K.M., Rahmanian, V.D., 1990. Siliciclastic sequence stratigraphy in well logs, cores, and outcrops: Tulsa, Oklahoma, American Association of Petroleum Geologists Methods in Exploration Series, No. 7, 55 p.

Vick, G.S. 1988. Late Holocene paleoseismicity and relative sea level changes of the Mad River Slough, Northern Humboldt Bay, California: Masters Thesis, Humboldt State University.

Warrlich, G., Bosence, D., Waltham, D., Wood, C., Boylan, A., Badenas, B., 2008. 3D stratigraphic forward modeling for analysis and prediction of carbonate platform stratigraphies in exploration and production. Marine and Petroleum Geology 25 (1), 35-58.

Wheatcroft, R.A., Sommerfield, C.K., 2005. River sediment flux and shelf sediment accumulation rates on the Pacific Northwest margin. Continental Shelf Research 25 (3), 311-332.

Wheatcroft, R.A., Sommerfield, C.K., Drake, D.E., Borgeld, J.C., Nittrouer, C.A., 1997. Rapid and widespread dispersal of flood sediment on the northern California margin. Geology 25 (2), 163-166.

Wood, L.J., Riley, G.W., Templet, P.L., 1993. The effects of rate of base-level fluctuation on coastal-plain, shelf and slope depositional systems: an experimental approach. In: Posamentier, H.W., Summerhayes, C.P., Haq, B.U., Allen, G.P., (Eds.), Sequence Stratigraphy and Facies Associations International Association of Sedimentologists Special Publication 18, pp. 43-54.

Zhang, Y., Swift, D.J.P., Fan, S.J., Niedoroda, A.W., Reed, C.W., 1999. Two-dimensional numerical modeling of storm deposition on the northern California shelf. Marine Geology 154 (1-4), 155-167.

Chapter 4 is currently being prepared for submission for publication in Marine Geology as: Hogarth, Leah J., Driscoll, Neal W., and Babcock, Jeffrey M. “New Seismic Evidence for Active Deformation and its Control on Long-term Sediment Accumulation on the Eel Margin, Northern California”. The dissertation author was the primary investigator and author of this paper.

5

New Insight into Lowstand Subaerial Accommodation: Implications for Fluvial Processes in a Sequence Stratigraphic Framework

5.1 ABSTRACT

High-resolution CHIRP seismic data collected along the Eel Margin provide evidence for subaerial aggradation and preservation on the shelf during the last sea-level lowstand. Sequence stratigraphic models predict that channel incision and downcutting across the shelf occurs during lowstands, with channel deposits being reworked during the subsequent transgression. In such a scenario, any channel fill would be reworked and truncated by the transgressive surface, and in the adjoining interfluves the transgressive surface should coalesce with the lowstand erosional surface (i.e., the sequence boundary). In the Eel River Basin, however, we observe little evidence of incised channels or shelf edge and slope deposits, but rather a seaward thinning wedge of sediment between the erosional surface and the transgressive surface. Within this package are a number of channels that we interpret as distributary channels based on their morphology. Sediment, up to ~8 m thick, is preserved across the interfluves. Divergence of the sequence boundary and transgressive surface is expected in incised valleys where lowstand sediment has been deposited, but regional divergence of these two surfaces requires the formation of subaerial accommodation during the lowstand. Possible mechanisms to explain the observed aggradation include preexisting morphology of the margin, high rates of tectonic subsidence, and inherent characteristics of fluvial systems. With continued sea-level fall beyond the shelf edge, which would expose a steeper gradient, fluvial incision and retrogressive erosion may have cannibalized some of the deposits sequestered on the shelf during early lowstand. These observations suggest that sediment yield on tectonically active, mountainous margins varies little throughout the sea-level cycle, which has important implications for the global sediment budget and sequence stratigraphic models.

5.2 INTRODUCTION

Conceptual models have considered shelf physiography to be the main factor governing deposition versus incision on the shelf during relative sea-level (RSL) fall (e.g., Posamentier et al., 1992). The widely held view is that sea-level fall leads to a decrease in accommodation, cross-shelf valley incision, and transport of fluvial sediment to the slope or deep ocean (Fig. 1; Vail et al., 1977; Posamentier et al., 1988). Some researchers attribute this to the fact that as RSL falls, rivers extend across the shelf, are closer to the shelf edge, and can more easily distribute their sediments over the shelf edge (Covault et al., 2007; Mulder and Syvitski, 1996). Other models predict that the rivers will respond according to the change in slope of the system as RSL falls (Fig. 2; Posamentier et al., 1992; Shanley and McCabe, 1994; Posamentier and Allen, 1999). In these models, the most common scenario is that with a RSL fall, a steeper gradient is exposed and thus, fluvial incision is initiated at the river mouth, upstream knickpoint migration ensues, and the river incises a channel on the newly exposed shelf (Fig. 2A). When there is no change in slope, no aggradation or degradation occurs (Fig. 2B). At the other extreme, if the newly exposed shelf has a slope less than that of the original fluvial profile, the rate of river flow will diminish and sediments will accumulate on the inner shelf (Fig. 2C). Evidence in the stratigraphic record of the latter appears to be either rare or at least interpreted incorrectly (Ainsworth and Pattison, 1994). The geometry of the shelf is often more complex and the presence of a relatively steep shoreface due to a highstand delta or coastal prism can lead to incision of the coastal highstand deposits (Fig. 3A; Posamentier et al., 1992; Talling, 1998; Posamentier and Allen, 1999). The shallower slope of the coastal prism compared to that of the shelf results in an increase in slope and consequent incision of the coastal plain (Posamentier et al., 1992). Furthermore, the importance of RSL dropping below the shelf edge has been realized; if sea level does not fall below the shelf edge, incision across the entire shelf can be

limited (Fig. 3; Talling, 1998; Tornqvist et al., 2006). For example, Tornqvist et al. (2006) showed that the Gulf of Mexico shelf, with a relatively shallow shelf/slope break (~30-50 m shallower than LGM sea level), developed deep, cross-shelf incised valleys and lowstand slope deltas during the last sea-level fall. Conversely, the Bay of Biscay shelf, with a shelf/slope break > 20 m deeper than the LGM sea level exhibited little channel incision.

Results from recent numerical models and experiments challenge the classic conceptual model by implying that during initial RSL fall, many settings will experience a period of sediment aggradation. For example, the one-dimensional numerical model and flume experiments of Swenson and Muto (2007) examine fluviodeltaic response to RSL fall, with a focus on the timing of transition from aggradation to degradation. In their model, the magnitude and duration of aggradation depend largely on the response time of the fluvial system relative to the duration of RSL fall. The fluvial response time depends on sediment supply, water supply, and the rate of RSL fall. The model indicates that for a fluvial system with an uniform slope gradient (e.g., similar to Fig. 2B), there is likely a period of aggradation during RSL fall. In addition, the three-dimensional experimental models of Van Heijst and Postma (2001), with sea level as the only independent variable, indicate that there is a delay between exposure of the shelf and fluvial erosion during the sea-level fall. In their experiments, when sea level reaches the shelf edge, headward erosion begins to erode the shelf edge, eventually propagating updip and cannibalizing older distributary channel deposits. The connection rate, that is how quickly the cross shelf erosion commences, depends on the degree of headward erosion at the shelf edge and shelf width, and it controls much of the dynamics of the ultimate degree of erosion and deposition on the shelf. These models imply that widespread sediment accumulation on the shelf is possible during sea-level fall and that the influence of preexisting morphology on aggradation versus incision is more complex than previously thought.

Here we present new evidence of subaerial accommodation during sea-level lowstand on the Eel Margin. Lowstand deposits observed in CHIRP seismic data and sampled by cores give insight into their environment of formation, and we discuss several factors that could have led to their deposition and preservation. Furthermore, these observations allow us to hypothesize about the role of steep mountain rivers, their contribution to global sediment supply throughout the sea-level cycle, and implications for fluvial processes in a sequence stratigraphic context.

5.3 REGIONAL SETTING

The Eel River forearc basin formed between the accretionary prism overlying the Cascadia subduction zone (CSZ) to the west and the Cascade magmatic arc to the east (Fig. 4; Clarke, 1992). Encroachment of the Pacific Plate and the northward migration of the San Andreas Fault have imparted a north-northeast compression across the basin causing major folding and high-angle reverse and thrust faulting along north-northwest trends and reactivation of older north-trending fabrics. This has resulted in a varying pattern of uplift and subsidence along the margin of up to 3 mm/yr (Vick, 1988; Orange, 1999). The most prominent sediment sources to the region are the Eel and Mad rivers, which occupy subsiding synclines; the Eel and Freshwater synclines, respectively (Fig. 4). The Eel River, with a drainage basin area of 8640 km^2, yields ~2232x10^3 kg/km^2/yr of suspended sediment to the margin, the largest sediment yield to the California margin (Nittrouer, 1999; Wheatcroft and Sommerfield, 2005). Sediment supply is episodic largely in the form of large winter storms, and large amounts of sediment are derived from easily eroded sedimentary and metamorphic rocks. The margin is currently accumulating a thick transgressive sequence and may be transitioning into a highstand geometry offshore of the sediment sources (Hogarth et al., in prep).

5.4 METHODS

In 1998, 1999, and 2000 over 1000 km of CHRIP seismic data were acquired offshore from the Eel River in northern California as part of the Office of Naval Research (ONR) STRATAFORM project (Fig. 5). Nearshore strike lines were collected in 1998 onboard the R/V Coral Sea and regional dip lines were acquired in 1999 and 2000 onboard the R/V Thompson. The regional dip lines coincided with coring transects and vibracore numbers indicate their locations on survey lines and their water depths. For example, core Q45 was collected coincident with dip line Q at 45 m water depth. For the regional dip and strike lines a 1-5.5 kHz chirp signal with a 50 ms sweep was used, while for the nearshore surveys a 1-15 kHz chirp signal with a 10 ms sweep gave better vertical resolution and minimized time between shots. These signals yielded submeter vertical resolution to subsurface depths of 50-100 m. Data were corrected for ship heave using SIOSEIS (P. Henkart, SIO http://sioseis.ucsd.edu) and further processed using Seismic Unix (Cohen and Stockwell, 1999). To correct for layback, one set of survey lines collected at one azimuth were held constant and the navigation for other lines was shifted to match the fixed lines. Isopach and depth to formation maps were created with Kingdom Software (Seismic Micro Technology http://www.seismicmicro.com). An average of 1500 m/s was used to convert two way travel time to depth.

5.5 RESULTS

The transgressive surface is imaged throughout most of the study area and its structure reflects deformation associated with the Little Salmon Fault and Eureka Anticline (see Hogarth et al., in prep). To the north of the Eureka Anticline, a second surface is imaged below the transgressive surface. This surface may also be present to the south of the anticline, but widespread gas wipe-out in that area limits acoustic penetration. The surface is generally characterized by high reflectivity (e.g., Line 8;

Fig. 7), but the reflector in some areas fades and becomes indistinct (e.g., Line T; Fig. 6). The high-amplitude reflector is characterized by several wide (100s of meters), shallow (meters) erosional features (Figs. L7 and 6). In dip lines, the surface is observed between ~45 and 60 m water depth. The surface slopes gently and is truncated by the transgressive surface in ~65 m water depth (Figs. 6 and 10). Shoreward of the ~45 m isobath the acoustic amplitude of the surface systematically decreases shoreward (Fig. 6). In strike lines, however, the surface is imaged both at the depths imaged in dip lines and at shallower depths in the northern part of the study area, offshore of the Mad River. In strike, the surface is absent over the Eureka Anticline, but its northern extent is not imaged and likely continues to the north. A structure map of this surface shows that it a lower slope than the bathymetry (Fig. 11A).

The sediment unit between this surface and the transgressive surface ranges between ~5-15 m thick and is generally acoustically transparent. Locally there are areas with parallel, low-amplitude reflectors (Fig. 7) and other areas characterized by dipping, concave, and nested reflectors (Fig. 8). The southern extent of the unit is unclear, as several high-amplitude reflectors at variable depths are present, likely indicating gas. It is clear, however, that the unit is absent over the Eureka Anticline (Fig. 10). The sediments of this unit are observed both in the channels formed in the lower surface and the adjacent interfluve regions (Figs. 7, 8, and 9). At shallower depths, a distinctly nested channel appears to have sediment preserved in the interfluves as well (Fig. 9). An isopach map of these sediments shows that they are absent on top of the structural highs, have an along-shore extent of at least 15 km, appear thickest to the north of Eureka Anticline, and thin seaward (Fig. 11B). A number of cores were acquired as part of the STRATAFORM initiative (Nittrouer, 1999), however, only one core collected along line Q penetrated the transgressive surface and sampled ~50 cm of sediment from the unit described here (see Fig. 5 for location). This sediment was bluish gray fine silt and clay with a sulfide odor

and rhizome root structures.

5.6 DISCUSSION

5.6.1 Fluvial Accommodation During Sea-level Lowstand

CHIRP seismic data from the Eel River Margin show little evidence of incised channels formed during the last sea-level lowstand. We do, however, map a surface that we interpret as an erosional surface formed during the last sea-level fall. As such, this surface might be the sequence boundary, but the absence of significant acoustic penetration beneath this surface leaves the possibility that a deeper erosional surface exist (i.e., the sequence boundary). The timing of this deposition must have been during the last sea-level fall (~120ka–20ka), during the LGM (~20 ka), or during early sea-level rise (Fig. 12). Although the sediment deposited above the presumed sequence boundary is located offshore of the Mad River, onshore it is not distinctly confined to the river mouth, but has a large along-shore extent. Furthermore, the geometries of this lowstand erosive surface and the overlying sediments suggest that the channels are distributary in nature associated with widespread deposition at this time. The seaward-thinning geometry of the unit is unexpected, if we assume a model of lowstand shoreline incision (e.g., Fig. 3B). According to Posamentier et al. (1992) during a forced regression (due to RSL fall), one would expect that the sequence boundary and transgressive surface would coalesce landward of the lowstand shoreline pinch-out and divergence seaward of this point (Fig. 3B). On the Eel Margin we see the opposite geometry; the two surfaces coalesce seaward and diverge landward (Figs. 6 and 10). These observations suggest a different mechanism than simple lowstand shoreline deposition on the shelf. The grain size, sulfide odor, and root structures present in the core collected in the unit indicate a subaerial depositional environment. This could indicate estuarine deposition during early sea-level rise. Unfortunately, whether or not they were deposited during sea-level fall or

during the early sea-level rise is unclear without a better chronostraphic framework from cores. The presence of this seaward-thinning wedge of sediment, however, implies there was accommodation on the shelf during sea-level lowstand, a time often characterized by bypass or channel incision and downcutting.

It is clear from observations across a variety of fluvial and marine settings that the response of a system to base-level fall varies depending on numerous factors (e.g., Schumm, 1993). Several mechanisms could explain the unexpected observation of lowstand accommodation offshore of the Mad River:

1) the physiography of the margin is such that as sea level falls, the newly exposed shelf has a slope less than the updip fluvial system;
2) the last sea-level lowstand did not descend below the shelf edge or only for a short duration that was insufficient to induce erosion at the shelf edge and subsequent retrogressive channel incision;
3) the high subsidence rate of the river valley creates accommodation despite sea-level fall; and/or
4) the response time of the fluvial system, which has a markedly high sediment load, allows a large amount of aggradation on the shelf.

It is not apparent, however, from the sequence architecture or initial considerations of the shelf physiography what factor(s) led to aggradation on the shelf. Preliminary measurements of the slopes of the coastal fluvial system and the sequence boundary (both ~0.2˚) show little difference in slope between the two surfaces. Depending on the characteristics of the fluvial system, a small change could lead to a simple reduction in channel sinuosity to increase the channel slope to that of the original channel, rather than aggradation to a new equilibrium (Schumm, 1993). Furthermore, offshore of the Mad River, the depth of modern shelf edge (estimated at the point of maximum curvature) is below that of sea level during the LGM (-130 to -120 m; Fig.

12). It would follow from the work of Tornqvist and others (2006) that this setting would be less likely to experience channel incision across the shelf that transports sediment to the shelf edge. Although the effects of isostatic rebound and regional tectonic forces have not been taken into account, the proximity of the shelf edge depth to the LGM sea level indicates that if sea level did fall below the shelf edge, it is unlikely that it stayed there for period long enough to induce cross-shelf incision. In a model based on sequence stratigraphic concepts (e.g., Figs. 1 and 3A), a RSL fall could lead to distributary channels and deposition on the shelf until sea level falls below the shelf edge (Fig. 13A and B). Headward erosion of the shelf edge could create limited incision, oceanic conditions could rework the small amount of sediment deposited on the slope, and subsequent transgression might rework those sediments deposited on the shelf (Fig. 13C and D). However, the geometry of such a deposit would likely thin landward and seaward if exposed to sufficient reworking during transgression (Fig. 13E). This does not fully explain our observations that the lowstand deposit on the Eel Margin thins markedly seaward, requiring another mechanism.

The highly active tectonic nature of the Eel Margin may create accommodation on the shelf during sea-level lowstand; the Mad River occupies the Freshwater Syncline, which is subsiding up to 1 mm/yr onshore (Vick, 1988). This rate is very close to the rate expected for sea-level fall averaged over the last glaciation (120 m / 100 kyr = 1.2 mm/yr), which implies little to no creation of new accommodation due to subsidence as sea level fell. However, sea level fell in a nonlinear manner, with occasional meltwater pulses (Fig. 12), which could have led to periods of time where accommodation was created to allow sediment aggradation. CHIRP data, however, show little evidence that the offshore section of the Freshwater Syncline has undergone deformation during the Holocene transgression (Hogarth et al., in prep). Furthermore, based on multi-channel seismic data, Burger et al. (2002) reported that deformation and differential subsidence across the

offshore Freshwater Syncline ceased at ~600 ka. The large sediment supply to the region could also explain lowstand aggradation on the shelf. The sediment supply could increase the fluvial system's response time to perturbations and result in widespread aggradation, as suggested by the model of Swenson and Muto (2007). Ultimately, the presence of the lowstand sediment could be explained by a combination of several of the above factors. Additional data to constrain the northern extent of the lowstand sediment unit and long cores to establish age constraints are needed.

It is likely that structural features confined the river drainages during sea-level lowstand, which explains the localization of sediments offshore of the Mad River. It is possible that similar deposits are present offshore of the Eel River to the south. However, the acoustic wipeout due to gas in seismic images prevents our imaging to that depth. We expect that the lowstand sediment deposition in this area would be limited by the morphology of the margin as the shelf-slope break is at a shallower depth than offshore of the Mad River, the shelf edge is closer to shore, and the Eel Canyon dissects the shelf. The Eel River Syncline, however, has been subsiding at a much more rapid rate (~3 mm/yr) than the Freshwater Syncline (~1-0 mm/yr), which may create accommodation during the sea-level fall.

5.6.2 Implications for Fluvial Morphodynamics and Global Sediment Budget

In recent years, researchers have recognized the importance of small, mountainous rivers in the supply of sediment to the global ocean (e.g., Milliman and Syvitski, 1992). This focus, however, has been based on modern sediment discharge. Evidence from this study implies that fluvial sediment was sequestered on the inner shelf rather than transported offshore to the slope or basin during the last sea-level lowstand on the Eel Margin. This observation suggests that similar small, high-gradient rivers may behave differently than low gradient rivers during RSL fall and lowstand. We propose a revised

model of global sediment supply that takes into account changes in sediment discharge throughout a sea-level cycle. Although they can have large sediment discharges, low gradient, passive margin river systems (Type 1) often sequester large amounts of sediment in their coastal plains during highstand. Conversely, high gradient, active margin rivers (Type 2) rivers generally have little onshore storage capacity during highstand. These small, mountainous catchments may dominate during highstand (Milliman, 1992), but may be subordinate to Type 1 rivers during lowstand conditions (Fig. 14). Massive submarine fans are associated with many Type 1 rivers (Fig. 14) and are, in large part, deposited during RSL fall when incised channels reactivate onshore distributary networks with large storage capacities. We predict that sediment yield to the margin from Type 2 rivers will exhibit much less variability than that from Type 1 rivers throughout a sea-level cycle as any channel incision will mobilize little sediment from onshore (Fig. 12). The reactivation of distributary channel networks onshore by channel incision on the shelf near Type 1 rivers can potentially deliver huge amounts of stored sediment during short time spans during the lowstand. This may explain the difference in Gulf of Mexico Rivers (e.g., Anderson et al., 2005; Vail-type sequence stratigraphic model; Vail et al., 1977) with large lowstand deposits due to incised channels reactivating large volumes of sediment in distributary channels versus Northern California Rivers (e.g., Eel River) that have less lowstand deposition offshore because minimal onshore storage (steep, narrow rivers with minimal coastal plain) provides little sediment to the slope.

Previous researchers have explored the importance of factors other than sea-level fall and rate of fall in governing sediment discharge to the oceans, but have not differentiated between river storage capacities. In their discussion of the evolution of world rivers with sea-level fall, Mulder and Syvitski (1996) imply that, in terms of deposition and erosion, on a worldwide scale, Type 2 rivers would yield more sediment

than during today's highstand, but they limit their insight to change in basin area and slope with sea-level fall. Therefore, they conclude that narrow shelves seaward of Type 2 rivers would cause more incision and downcutting than would be experienced by Type 1 rivers adjacent to broad continental shelves. Recent work by Covault et al. (2007) demonstrated that shelf width was indeed a primary control on sediment transport to the deep ocean in the California borderlands where rivers are Type 2 in nature. Comparing sediment volume fluctuations from submarine canyon systems during sea-level changes of the late Quaternary (~58 ka-present), they found that channels and submarine canyons on a wide shelf were connected during lowstand, but disconnected during highstand. Conversely, on the narrow shelf near La Jolla the proximity of the La Jolla submarine canyon to shore results in its capture and offshore transport of a majority of the sediment in the system during sea-level highstands. The estimates of highstand deposition rates on the La Jolla submarine fan by Inman (historical; 2008) and Covault et al. (13 ka-present; 2007), however, are nearly equal to the combined lowstand deposition rates of the Oceanside and Carlsbad fans, which were active during lowstand. Thus, in southern California the shelf width appears to have played little role in the total amount of sediment liberated to the deep sea throughout the sea-level cycle.

We propose that the most important factor leading to a contrast in sediment discharge during lowstand may be the different highstand storage capacities of basins. Studies in Lake Powell have shown that periods of lowstand, even though marked by decreased water discharge, exhibited increased occurrence of hyperpycnal flows (Pratson et al., 2009). Although they expected water discharge and the frequency of hyperpycnal flows to be proportional, researchers observed that sediment was easily eroded from unconsolidated delta topsets exposed by lake-level fall (Pratson et al., 2009). Presumably, the same phenomenon would occur in a marine setting: sea-level fall would result in rapid incision into unconsolidated delta and river sediment. On a margin with little

onshore sediment storage, incision and re-excavating of filled channels during sea-level fall would be limited.

An example where we would expect to see markedly different behavior throughout the sea-level cycle is the rivers of Papua New Guinea. Milliman (1995) observed that high mountain (> 3000 m headwater elevation) rivers, such as the Fly and Purari of Papua New Guinea, had significantly higher sediment discharges than coastal plain rivers of the island. However, although both the Fly and Purari Rivers have headwaters in the high mountains, the Fly River crosses a large coastal plain before reaching the ocean (Fig. 15). Observations on the shelf indicate there is little modern sediment yield from the Fly River (Slingerland et al., 2008). We expect, however, that the ample sediment stored in its coastal plain can be remobilized during sea-level fall. Furthermore, Milliman (1995) noted that the nearby oceanic trench is filled and buried by sediment likely sourced from these rivers. We predict that sediment filling the trench is largely sourced from the Fly River during sea-level lowstand. These two rivers, with similar climate, headwater elevation, and sea-level history, would provide an ideal setting to test the hypothesis put forth here.

If correct, this modifies the hypothesis that Type 2 rivers provide more sediment to the ocean when normalized for drainage area (Milliman, 1995; Milliman, 1997). During highstands this is correct because they have little to no onshore storage (Fig. 12; Milliman, 1995). During sea-level falls, however, where the shelf edge is exposed and retrogressive erosion (upstream nick point migration) reactivates the onshore storage, Type 1 rivers supply a disproportionate amount of sediment to the ocean (Fig. 12). Type 2 rivers supply roughly the same amount to the ocean during lowstands and vary little throughout the sea-level cycle.

How, when, and where do incised valleys form during RSL fall has important implications for connectivity of the incised channels offshore (at the shelf edge) and

the distributary channels onshore. As the incised channels retrogressively backstep they reactivate the distributary channels on the margin and can liberate large volumes of sediment to the basin in potentially a short period of time. Furthermore, the rates of incision and reactivation, as well as the upstream extent of reactivation are important factors to consider. It is clear that further comparison of observations and model predictions are required to understand the response of fluviodeltaic systems during sea-level falls.

5.7 CONCLUSIONS

A seaward thinning wedge beneath the transgressive surface is imaged in the CHIRP data. The geometry of this wedge and core data suggest it is fluvial and estuarine deposition recording accommodation on the shelf during the last sea-level fall or lowstand. Several researchers have suggested that high fluvial gradients relative to the shelf slope may lead to deposition on the shelf during lowstand (Fig. 2C). However, in the actively uplifting area onshore of the Eel River Basin, it is not clear that this criteria is met. Although the mountainous terrain has a much steeper gradient than that of the shelf, modern river gradients are nearly equal to slope of the shelf. Creation of accommodation due to rapid subsidence of synclines may play a role offshore of the Eel River, but it is not clear that this mechanism works for the Mad River, where we observe the most lowstand deposition. New stratigraphic modeling purports that there is a link between fluviodeltaic response time and sediment accumulation on the shelf during early lowstand, which might explain the observations in the Eel River Basin. It is more likely that lowstand sea level did not descend below the shelf edge for a sufficient period of time to create erosion and connect to onshore distributary channels. However, it is also likely that several of these factors contributed to sediment deposition and subsequent preservation on the shelf during the last sea-level fall.

These results have generated insight into the connection between marine stratigraphic and sedimentological observations and fluvial morphodynamics throughout a sea-level cycle. The absence of incised channels on the Eel Margin suggests that small, high-gradient river systems vary little in their sediment yield throughout the sea-level cycle, whereas larger, low-gradient rivers with large onshore storage capacities during highstand yield comparatively large amounts of sediment during lowstand.

The research on the Eel Margin helps connect marine stratigraphic and sedimentological observations and fluvial morphodynamics throughout a sea-level cycle. Based on our observations, we predict the following: Type 1 rivers will have large lowstand deposits as the incised valleys reactivate onshore distributary networks with large storage capacity. Type 2 rivers will have small lowstand deposits as the onshore storage capacity is small and furthermore sediment yield to the margin from Type 2 rivers will exhibit much less variability throughout a sea-level cycle. This concept evolves from the fact that we have two very different types of rivers. As such, we would expect that much/most of the present-day fluvial sediment supplied to the oceans is from small mountainous rivers (Type 2), but during a period of regressive sea level – perhaps a short period – sediment discharge may be dominated by Type 1 rivers in response to the erosion of subaerially accommodated sediment. Thus, while the small mountainous rivers are more responsive to short-term events (e.g. floods, storms), large low-gradient river systems might be more responsive to sea-level change.

5.8 ACKNOWLEDGEMENTS

This project was funded by ONR as part of the STRATAFORM initiative. Special thanks to Joe Kravitz. We greatly appreciate support provided by the ARCS Foundation.

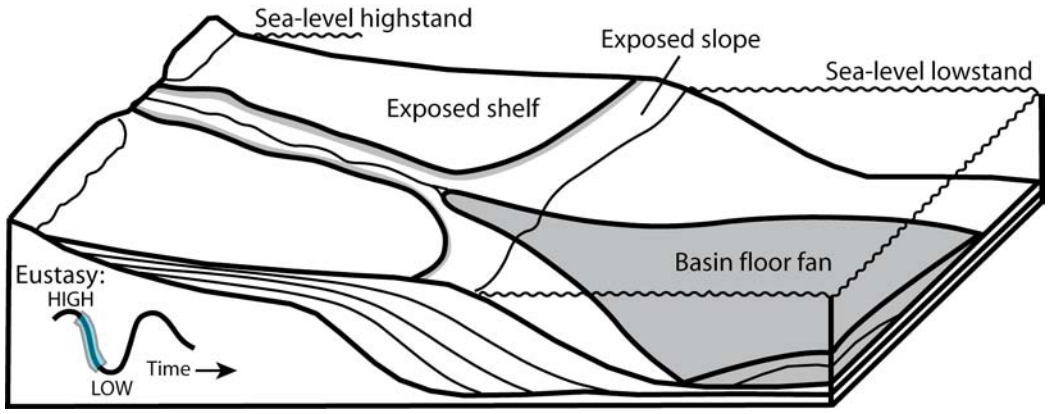


Figure 5-1: Classic sequence stratigraphic model block diagram of Posamentier et al. (1988) predicting cross-shelf valley incision with sea-level fall.

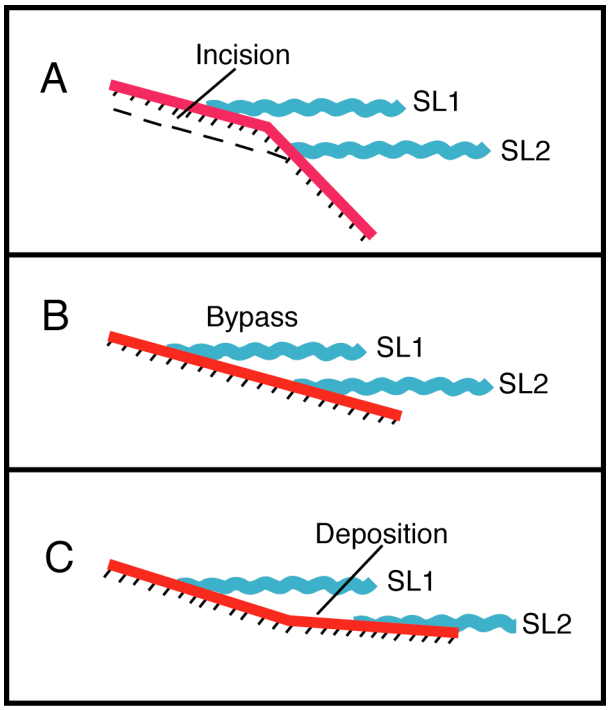


Figure 5-2: Physiographic model for fluvial response to baselevel fall based on Allen and Posamentier (1992). The physiography of the slope during a regression can dictate whether A: rivers incised, B: sediments bypass, or C: sediments accumulate on the shelf. Modified from Posamentier et al. (1992).

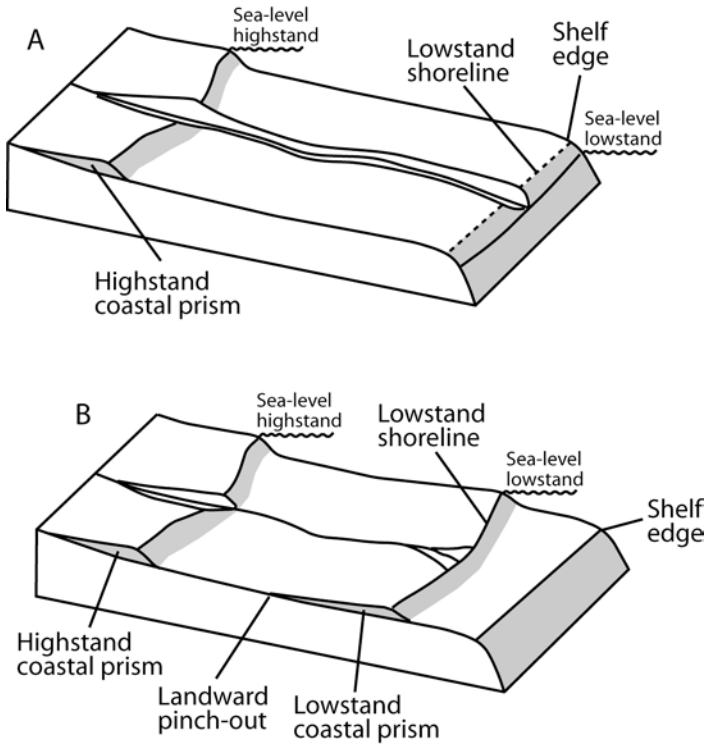
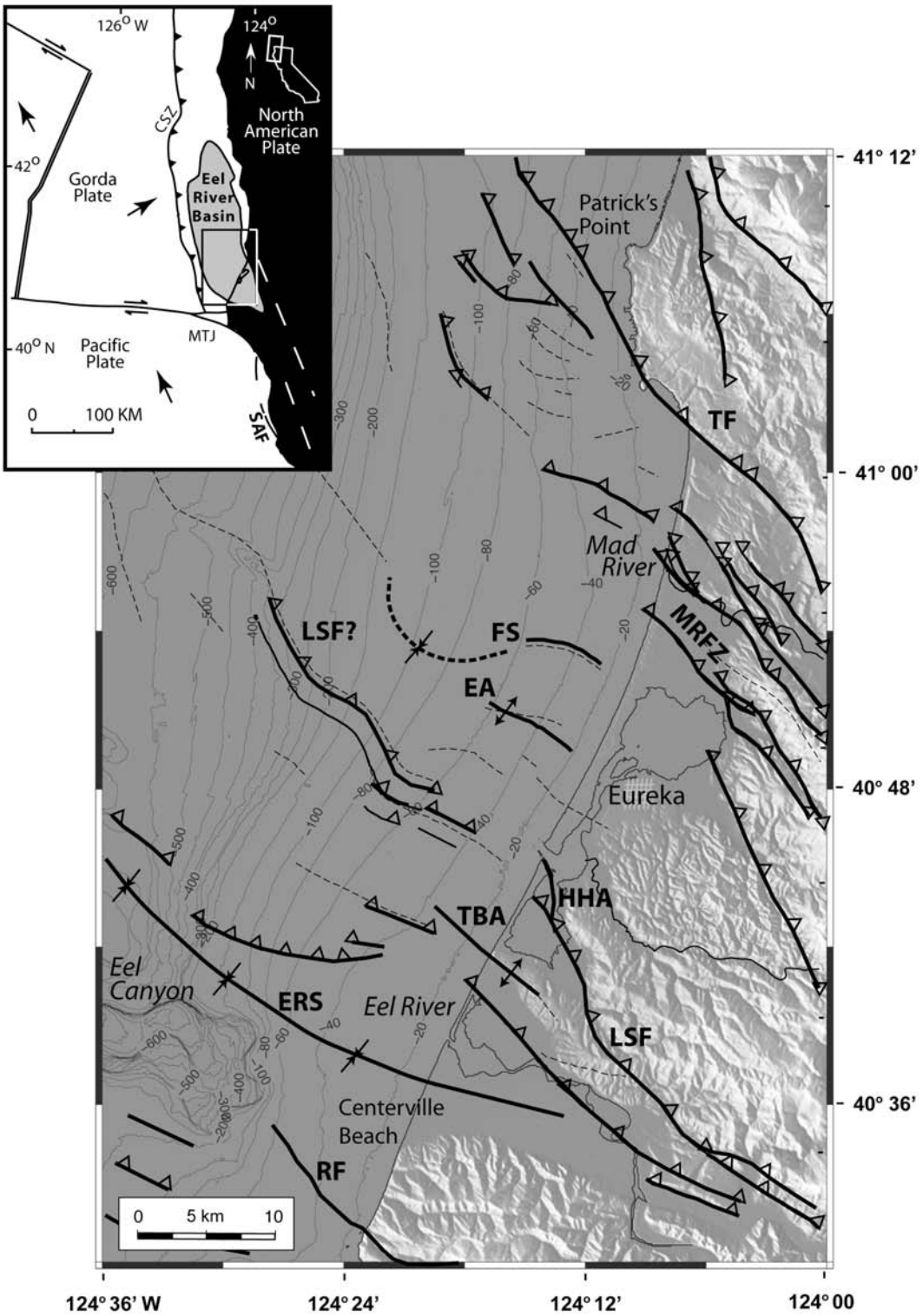


Figure 5-3: Predicted morphology of the shoreline on the shelf and slope depending on the depth of the shelf-slope break compared to lowstand sea level. A: When sea level falls below the shelf edge cross-shelf valley incision occurs. B: When sea level does not fall below the shelf edge valley incision will be limited to the coastal prism. Coastal prism erosion Modified from Posamentier and Allen (1999) and Tournqvist (2006).

Figure 5-4: Location map with local structural features and inset showing plate boundaries offshore northern California (after Clarke, 1992). Note that major local structures (black lines) are oriented at a higher angle to the coastline than the regional structures (e.g., San Andreas Fault (SAF), inset). CSZ = Cascadia Subduction Zone, MTJ = Mendocino Triple Junction, RF = Russ Fault, ERS = Eel River Syncline, LSF = Little Salmon Fault, TBA = Table Bluff Anticline, HHA = Humboldt Hill Anticline, EA = Eureka Anticline, FS = Freshwater Syncline, MRFZ = Mad River Fault Zone, TF = Trinidad Fault. Structures from Clarke (1992) and McLaughlin et al. (2000).


126° W
124°
N
CSZ
North American Plate
42°
Gorda Plate
Eel River Basin
40° N
Pacific Plate
MTJ
0 100 KM
SAF
Patrick's Point
TF
Mad River
MRFZ
LSF?
FS
EA
Eureka
HHA
TBA
Eel Canyon
ERS
Eel River
LSF
Centerville Beach
RF
0 5 km 10
41° 12'
41° 00'
40° 48'
40° 36'
124° 36' W
124° 24'
124° 12'
124° 00

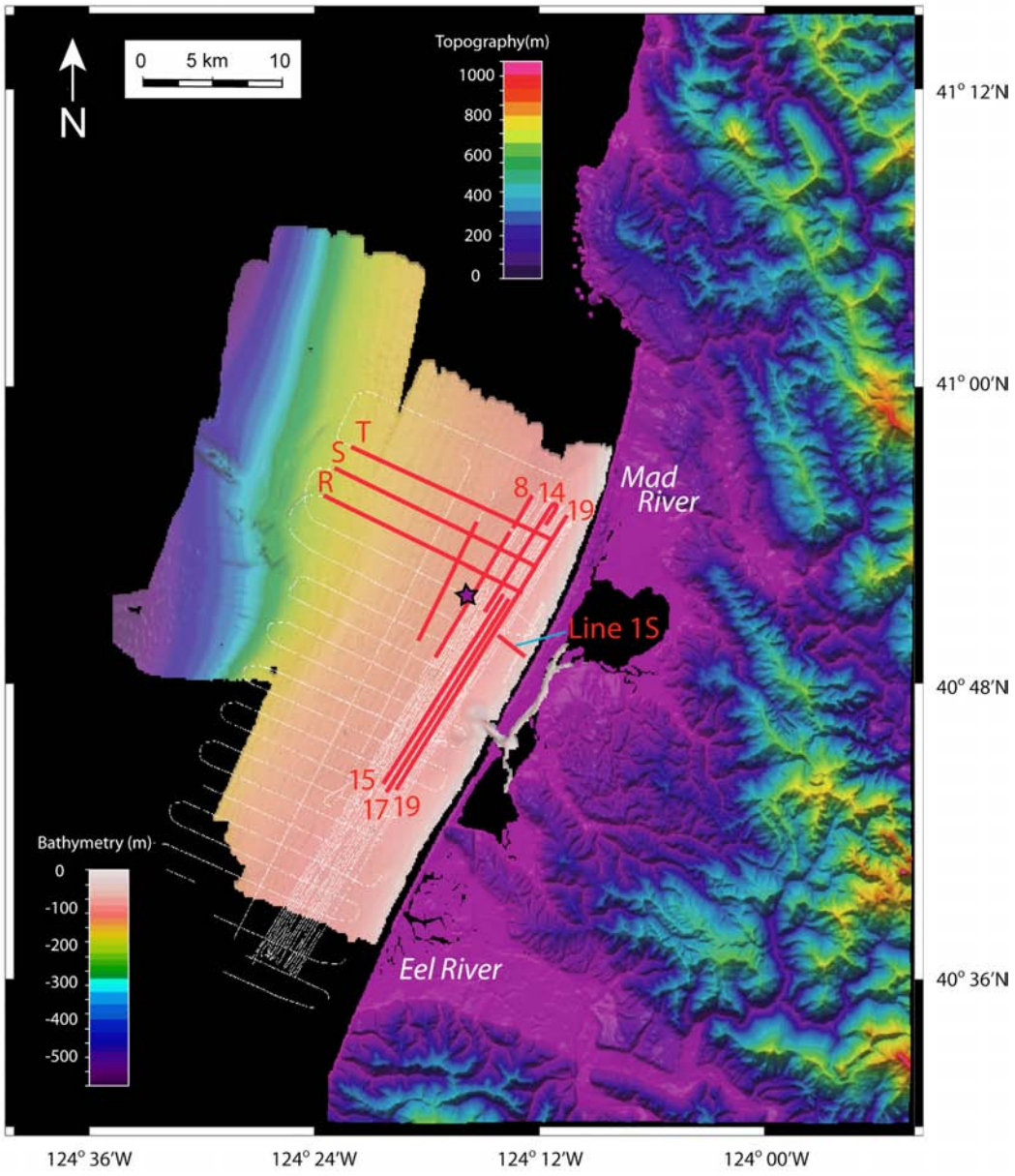


Figure 5-5: Ship tracks superimposed on bathymetry collected as a part of the STRATAFORM initiative (Goff et al., 1999; Ferrini and Flood, 2002). Red lines indicate locations of seismic profiles in other figures, and purple star indicates location of core Q45 described in text.

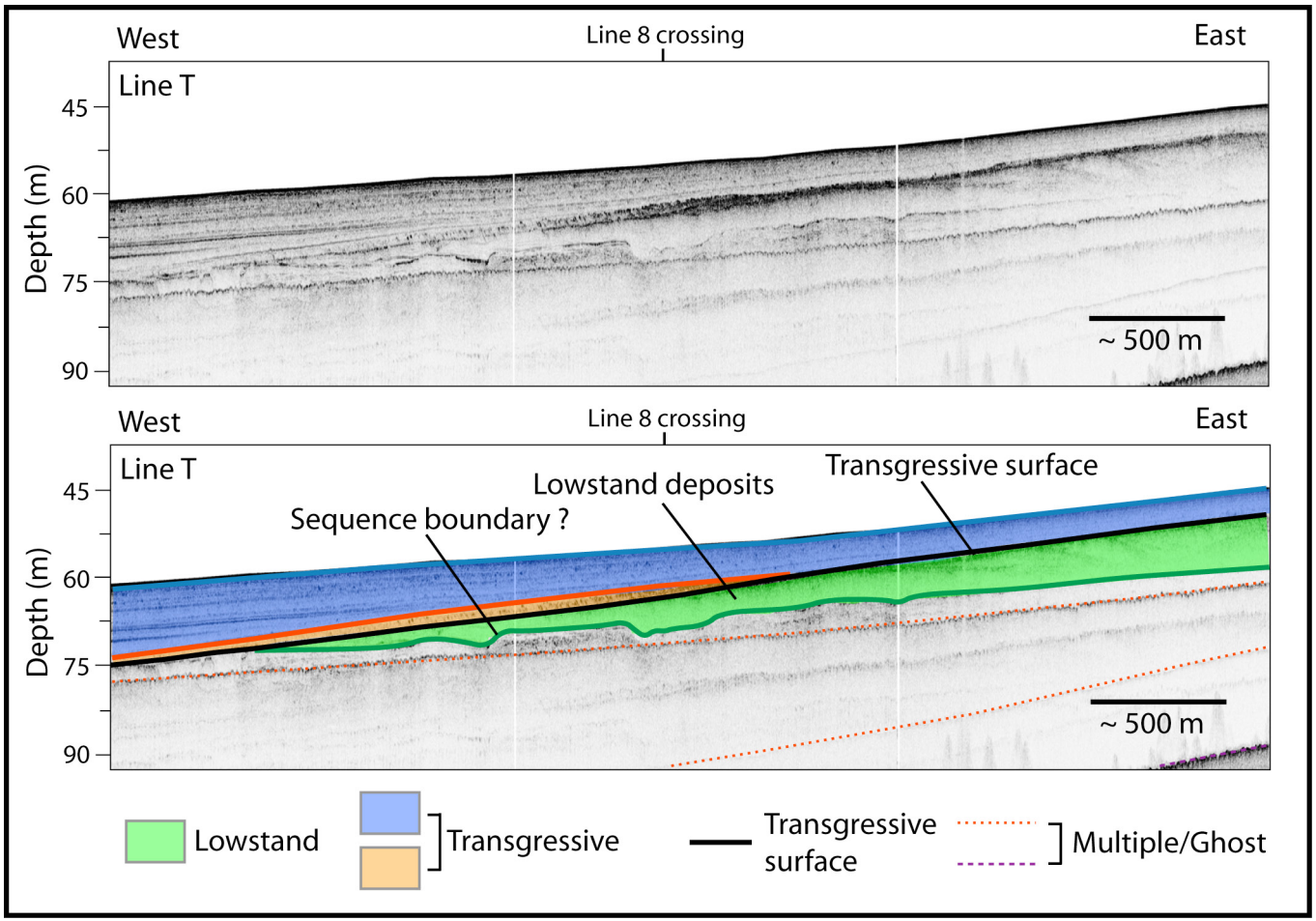


Figure 5-6: Strike line T shows the lowstand deposit (green fill) pinching out towards the west and channel-like erosion of the sequence boundary (green line). Note that the sequence boundary and the transgressive surface (black) are separated by several meters of sediment in the interfluve regions. Sediments above are the healing-phase (orange) and marine transgressive (blue) units.

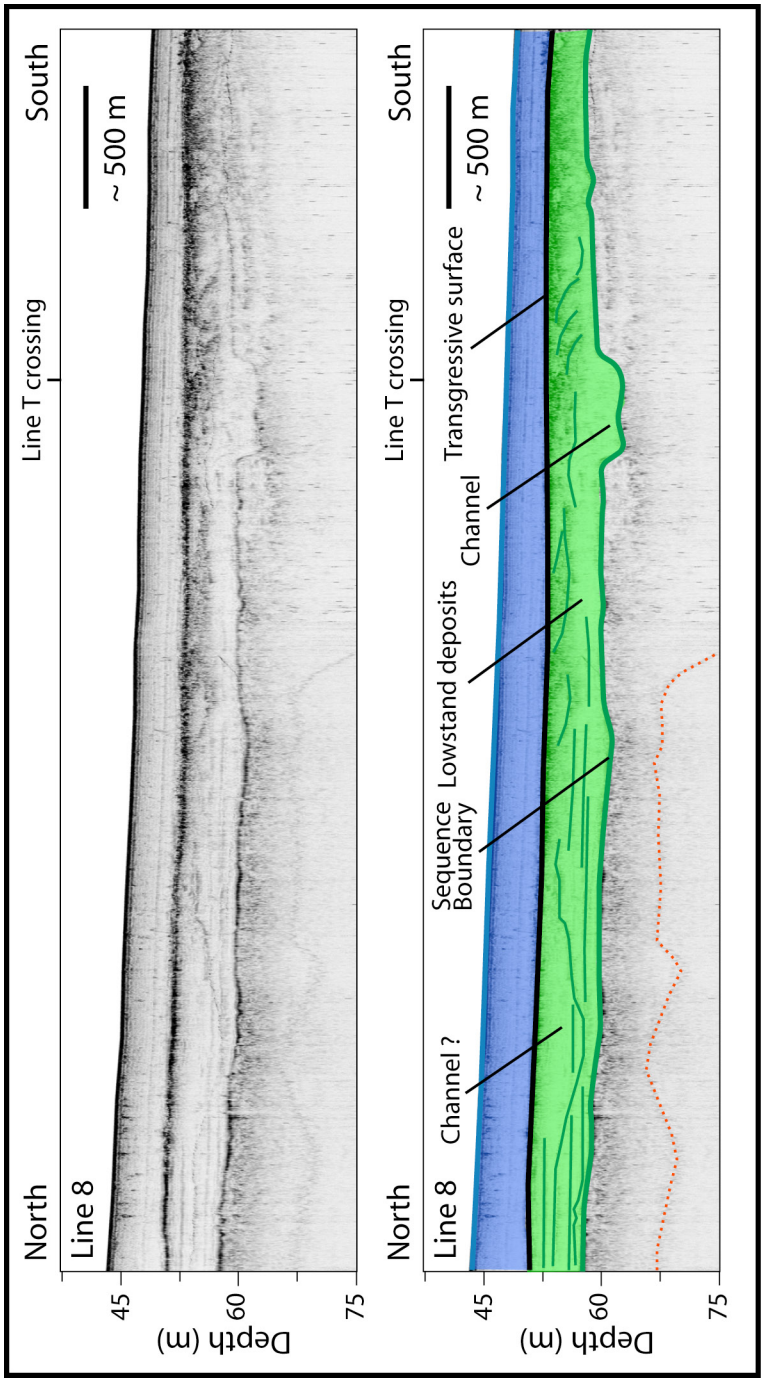


Figure 5-7: Dip line 8 shows the sequence boundary and associated channel shapes. Color scheme as in Fig. 6.

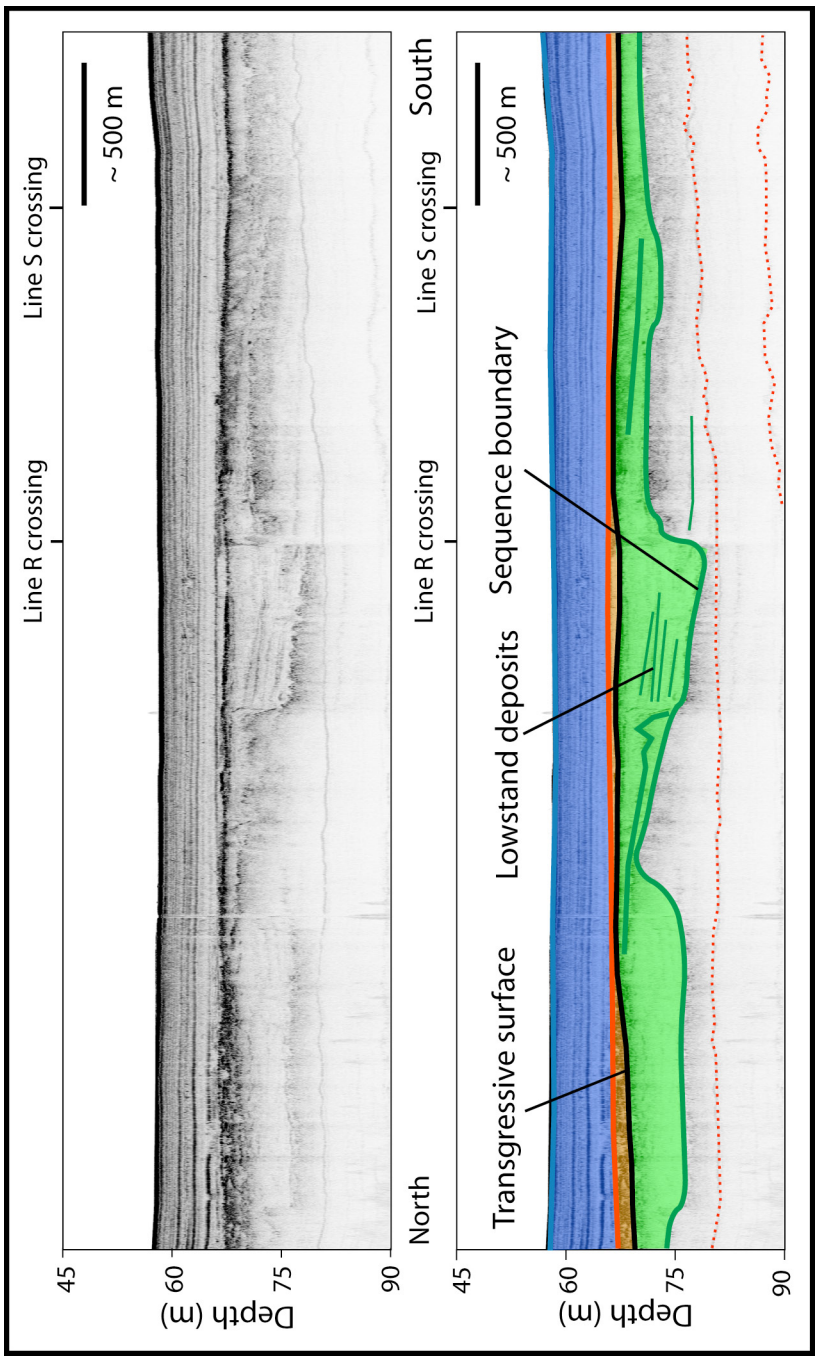


Figure 5-8: Strike line from offshore shows a wide, flat channel within the sequence boundary surface, the overlying sediments, and the transgressive surface. Color scheme as in Fig. 6.

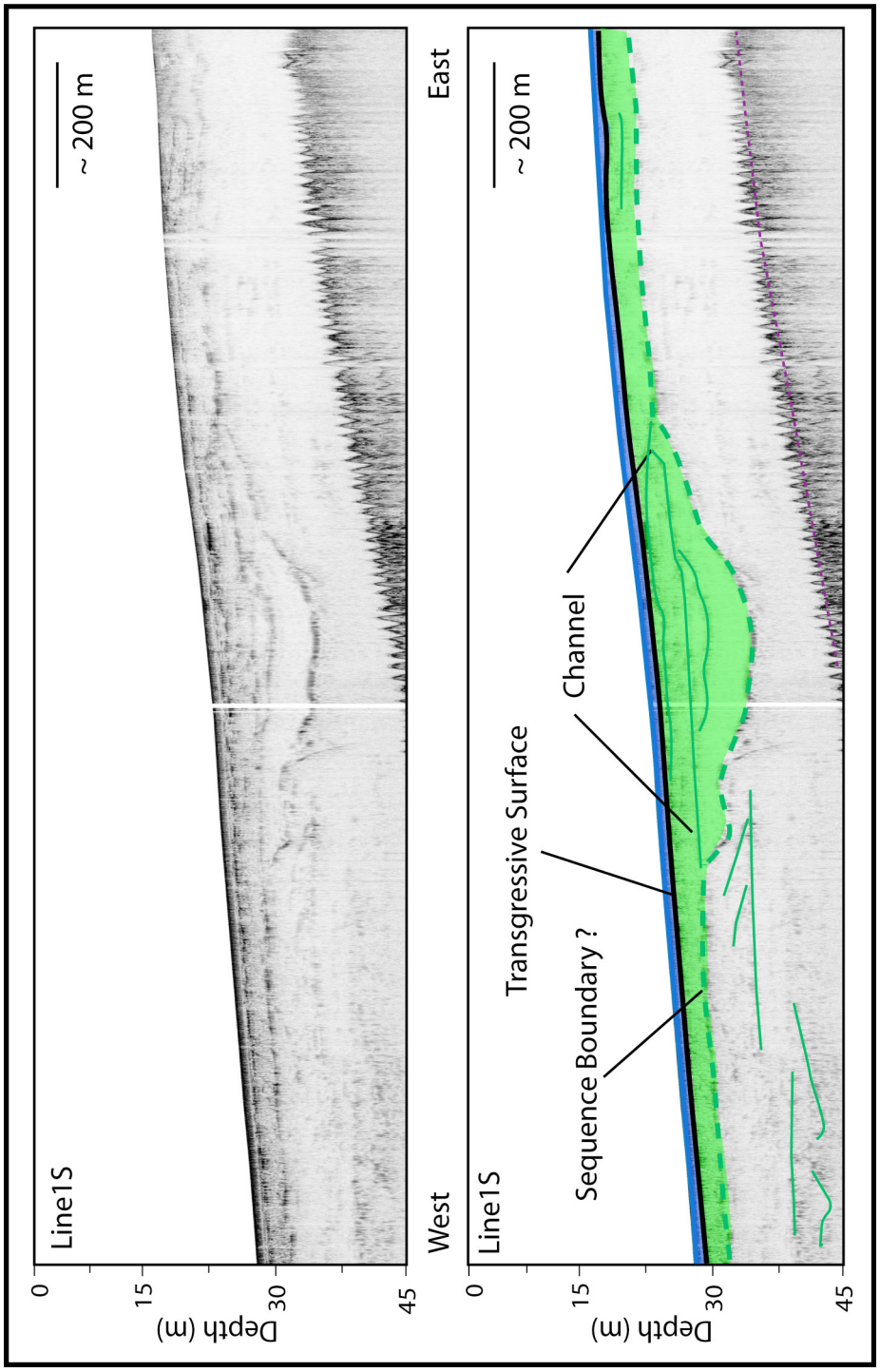


Figure 5-9: Dip line 1S shows a nested channel at ~25-30 m water depth. Color scheme as in Fig. 6.

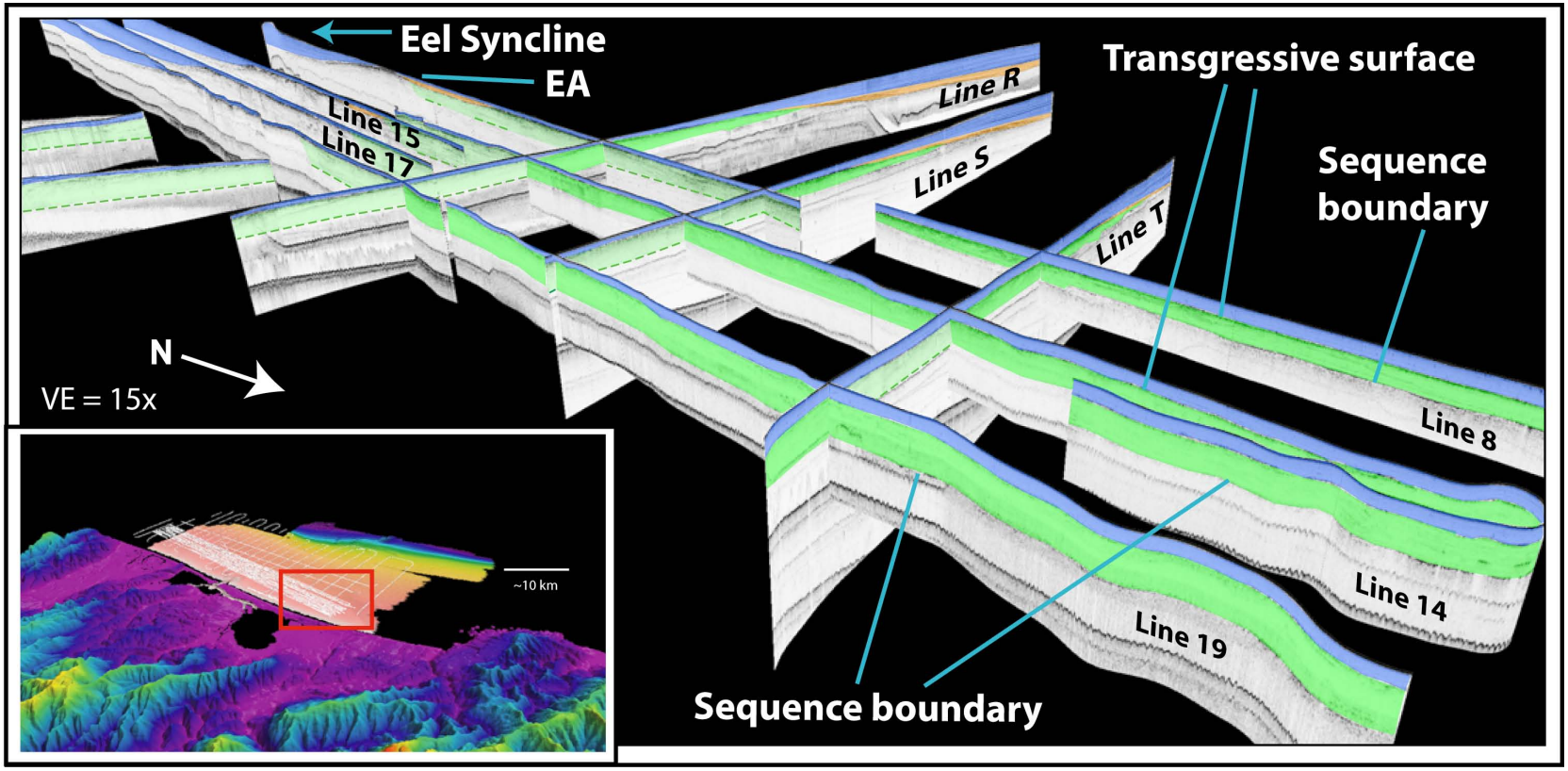


Figure 5-10: Perspective view of lowstand wedge. Looking offshore to the west, the lowstand wedge is thick adjacent to the Mad River and thins over the Eureka, Humboldt Hill, and Little Salmon anticlines. Red lines designate the lateral extent of the profiles seen in Figures 6 and 7 as well as the location of core Q45 described in the text. Color scheme as in Fig. 6.

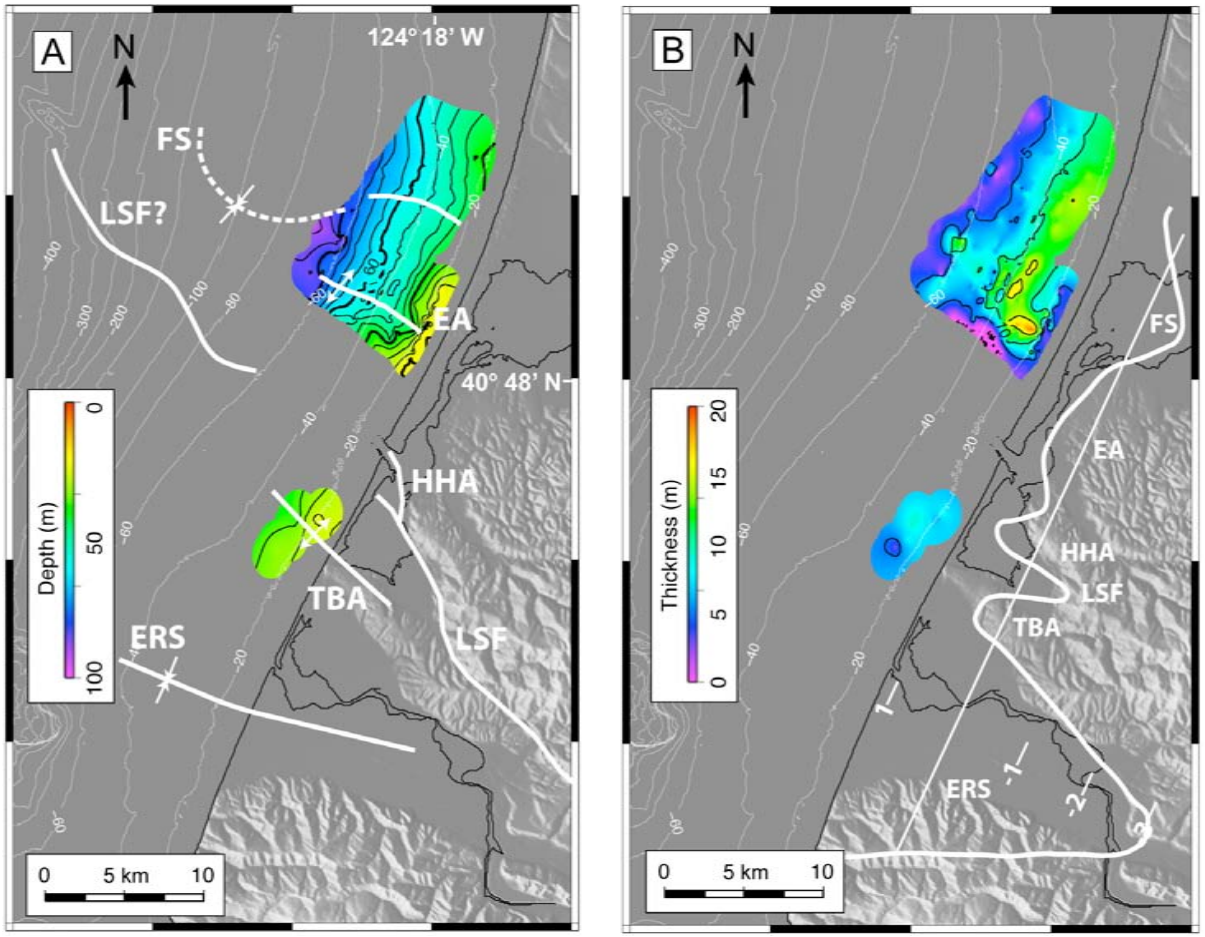


Figure 5-11: A: Structure map of sequence boundary, which becomes shallow over Eureka Anticline. B: Isopach map of lowstand deposits shows maximum thickness nearshore with offshore thinning. Lowstand sediments are absent over the anticlines and are thickest adjacent to the Mad River. In A selected tectonic features are superimposed in white, and in B uplift and subsidence rates onshore are superimposed in white. ERS = Eel River Syncline, LSF = Little Salmon Fault, TBA = Table Bluff Anticline, HHA = Humboldt Hill Anticline, EA = Eureka Anticline, FS = Freshwater Syncline.

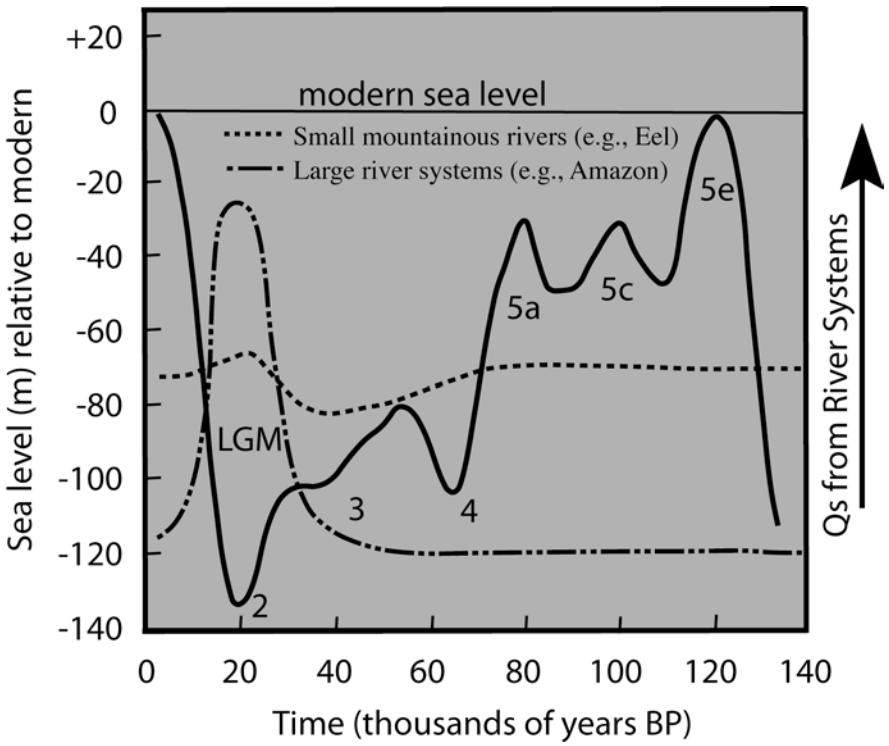
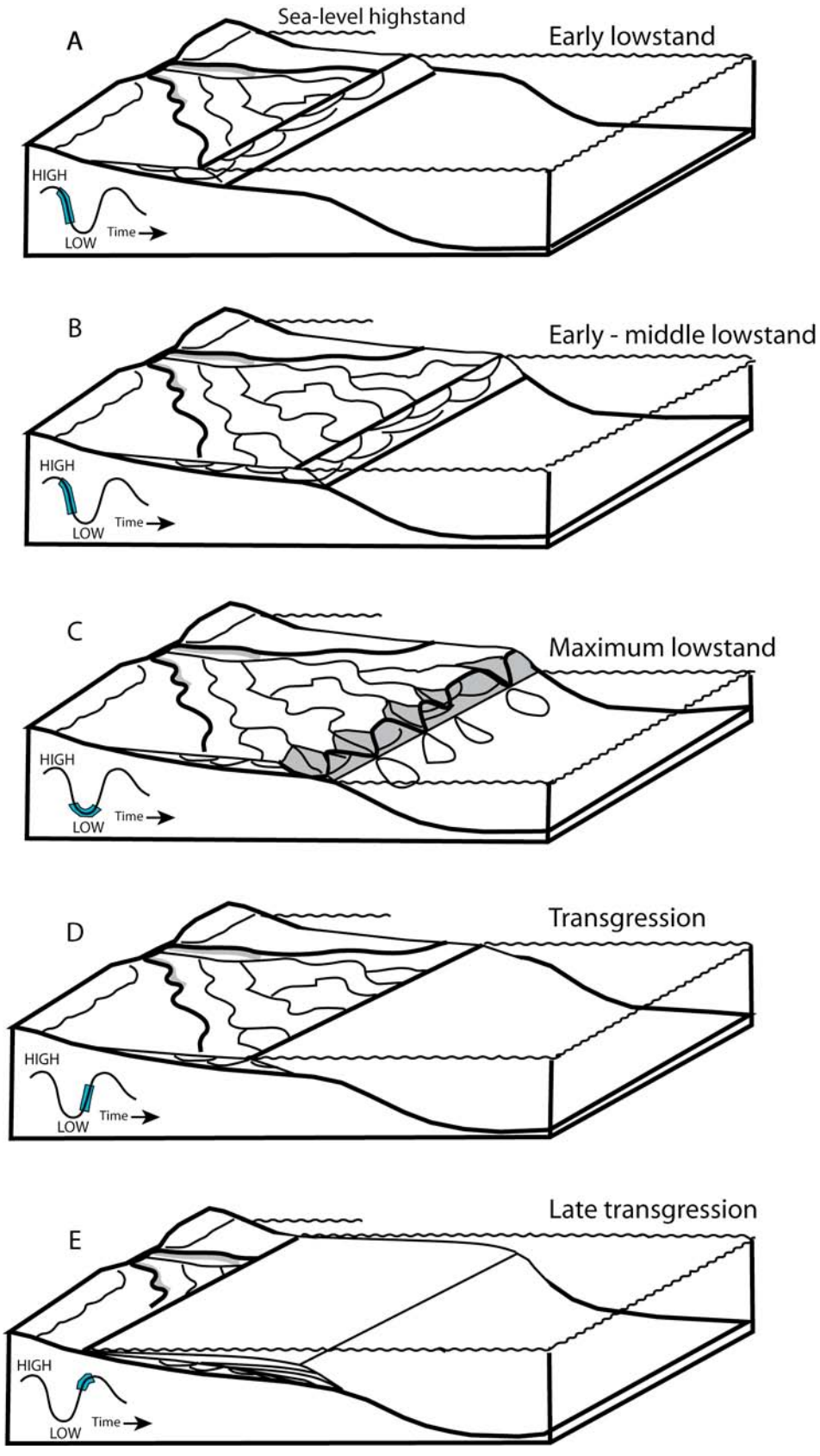


Figure 5-12: Simplified sea-level curve for the last glacial cycle (140 ka-present) and proposed discharge (Qs) for small mountainous rivers and large rivers. Note the prediction of relatively consistent discharge associated with small mountainous rivers and the large pulse of sediment discharge associated with sea-level lowstand on large rivers. Sea-level curve based on Shackleton and Pisias (1985), Fairbanks (1989), and Chappell (1996). LGM = Last Glacial Maximum.

Figure 5-13: Model for lowstand aggradation based on Posamentier and Allen (1999) and Van Heijst and Postma (2001). In a simple model with sea-level fall below the shelf edge being limited, the early lowstand shoreline would remain on the shelf and aggrade, with minor incision as sea-level falls below the shelf edge. Slope deposits will be minor or removed by reworking. In this case, sediments thicken seaward contrary to observations offshore of the Mad River.


A
Sea-level highstand
Early lowstand
HIGH
LOW
Time
B
Early - middle lowstand
HIGH
LOW
Time
C
Maximum lowstand
HIGH
LOW
Time
D
Transgression
HIGH
LOW
Time
E
Late transgression
HIGH
LOW
Time

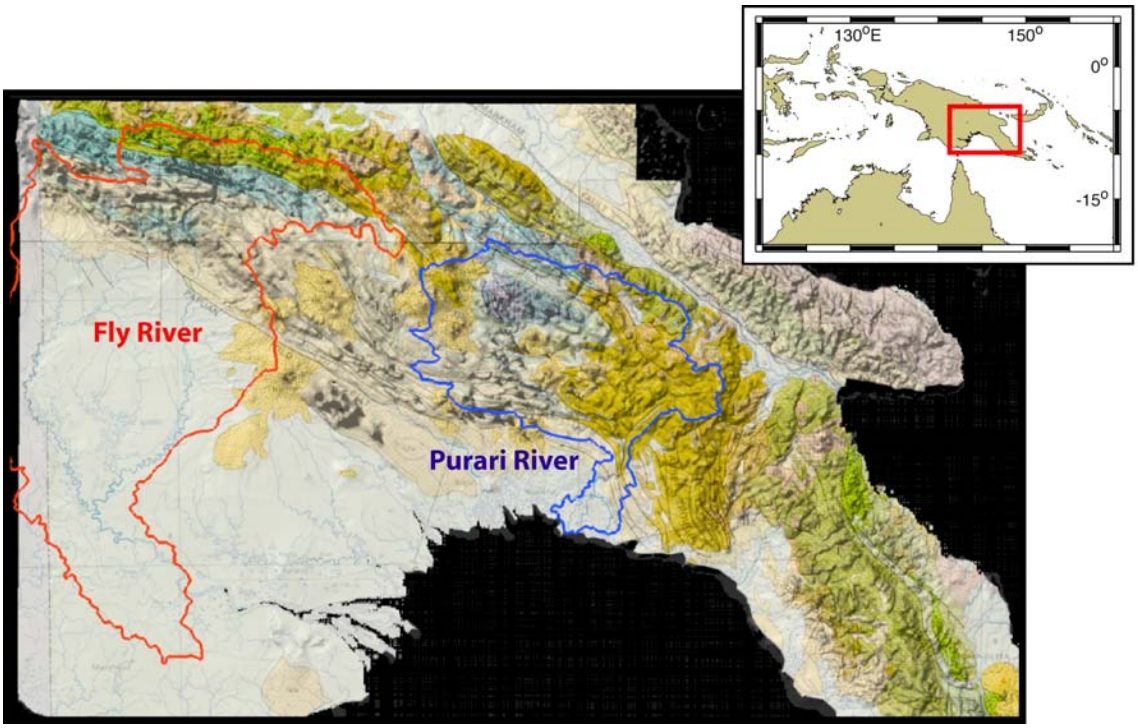


Figure 5-14: Southern Papua New Guinea showing the Fly and Purari Rivers. Note the large coastal plain of the Fly River and the steep, rugged catchment of the Purari River.

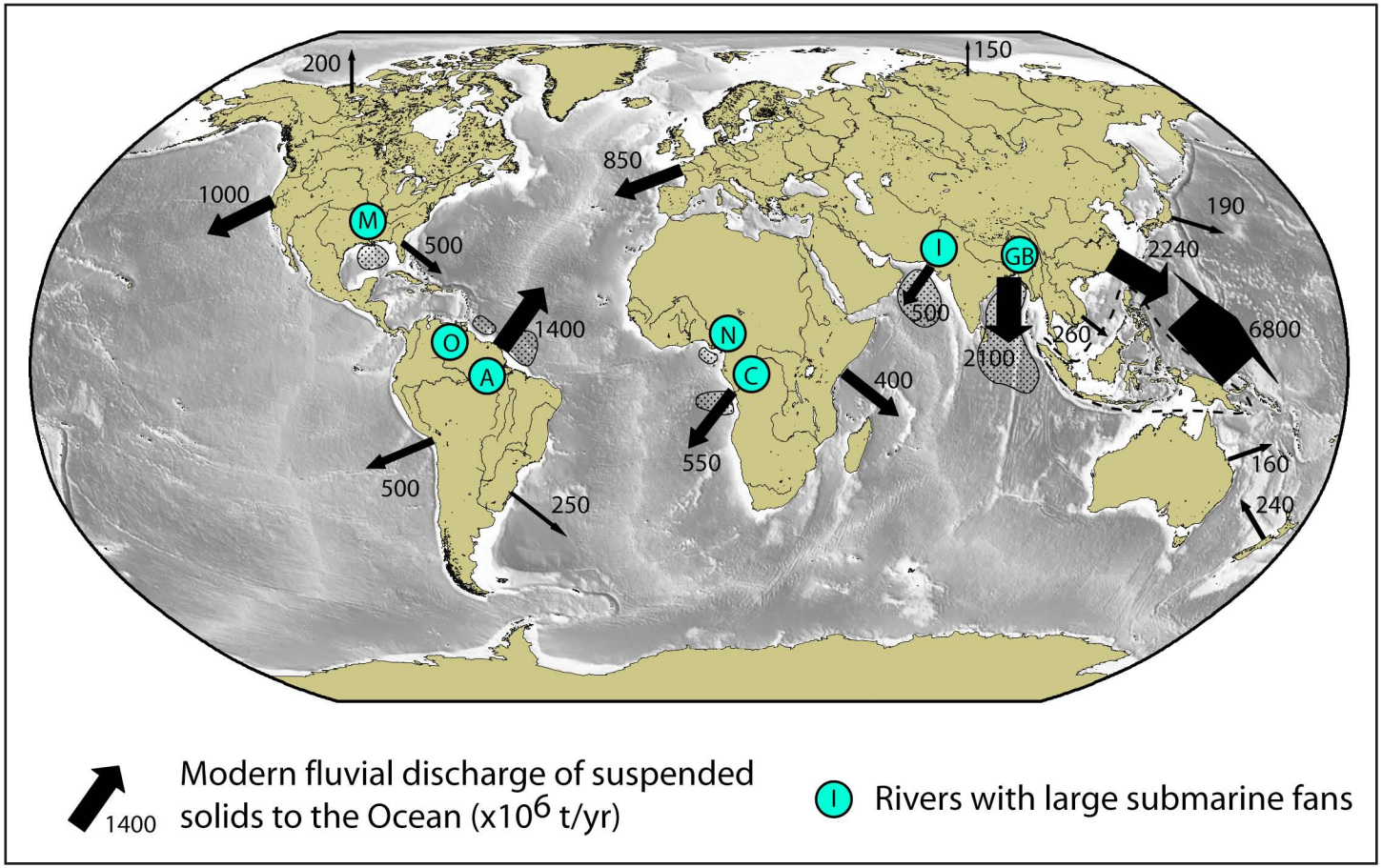


Figure 5-15: Global sediment flux to the oceans in black arrows and major submarine fans in black dots and green labels. GB=Ganges-Brahmaputra, I=Indus, N=Niger, C=Congo, O=Orinoco, A=Amazon, M=Mississippi.

5.9 REFERENCES

Ainsworth, R.B., and Pattison, S.A.J., 1994. Where have all the lowstands gone? Evidence for attached lowstand systems tracts in the Western Interior of North America: Geology, v. 22, p. 415-418.

Anderson, J.B., Rodriguez, A.B., Abdulah, K.C., Fillon, R.H., Banfield, L.A., McKeown, H.A., and Wellner, J.S., 2004. Late Quaternary Stratigraphic evolution of the northern Gulf of Mexico margin: A synthesis, *in* Anderson, J.B., and Fillon, R.H., eds., Late Quaternary Stratigraphic Evolution of the Northern Gulf of Mexico Margin: SEPM Special Publication 79, p. 237-269.

Burger, R.L., Fulthorpe, C.S., Austin, J.A. and Gulick, S.P.S., 2002. Lower Pleistocene to present structural deformation and sequence stratigraphy of the continental shelf, offshore Eel River Basin, northern California. Marine Geology 185(3-4), 249-281.

Chappell, J., Omura, A., Esat, T., McCulloch, M., Pandolfi, J., Ota, Y., and Pillans, B., 1996. Reconciliation of late Quaternary sea levels derived from coral terraces at Huon Peninsula with deep sea oxygen isotope records: Earth And Planetary Science Letters141, 227-236.

Clarke, S.H., 1992. Geology Of The Eel River Basin And Adjacent Region - Implications For Late Cenozoic Tectonics Of The Southern Cascadia Subduction Zone And Mendocino Triple Junction. AAPG Bulletin 76 (2), 199-224.

Cohen, J.K., and Stockwell Jr., J.W. 1999. CWP/SU: Seismic Unix Release 33: A free package for seismic research and processing, software. Center for Wave Phenomena, Colorado School of Mines, Golden, CO.

Covault, J.A., Normark, W.R., Romans, B.W., and Graham, S.A., 2007. Highstand fans in the California borderland: The overlooked deep-water depositional systems: Geology 35, 783-786.

Fairbanks, R.G., 1989. A 17,000-year glacio-eustatic sea-level record: influence of glacial melting rates on the Younger Dryas event and deep-ocean circulation. Nature 342, 637-642.

Ferrini, V., Flood, R.D. 2002. Multibeam Sonar on the Inner Shelf of the Eel Margin:

Nearshore gravel-floored troughs. Eos Trans. AGU, 83(47), Fall Meeting Supplement, Abstract S71C-0297.

Hogarth, L.J., Babcock, J., Driscoll, N.W., Le Dantec, N., Haas, J.K., Inman, D.L., and Masters, P.M., 2007. Long-term tectonic control on Holocene shelf sedimentation offshore La Jolla, California: Geology 35, 275-278.

Hogarth, L.J., Driscoll, N.W., Babcock, J.M., *in prep.,* New seismic evidence for active deformation and its control on long-term sediment accumulation on the Eel Margin, Northern California.

Inman, D.L., 2008. Highstand fans in the California borderland: Comment: Geology 36, 166.

McLaughlin, R.J., Ellen, S.D., Blake, Jr., M.C., Jayko, A.S., Irwin, W.P., Aalto, K.R., Carver, G.A., Clarke Jr., S.H., 2000. Geology of the Cape Mendocino, Eureka, Garberville, and Southwestern Part of the Hayfork 30 x 60 Minute Quadrangles and Adjacent Offshore Area, Northern California, USGS Miscellaneous Field Studies MF-2336, Version 1.0

Merritts, D., and Vincent, K.R., 1989. Geomorphic Response Of Coastal Streams To Low, Intermediate, And High-Rates Of Uplift, Mendocino Triple Junction Region, Northern California: Geological Society Of America Bulletin 101, 1373-1388.

Milliman, J.D., and Syvitski, J.P.M., 1992. Geomorphic/tectonic control of sediment discharge to the ocean: the importance of small mountainous rivers: Journal Of Geology 100, 525-544.

Milliman, J.D., 1995. Sediment discharge to the ocean from small mountainous rivers: The New Guinea example: Geo-Marine Letters 15(3-4), 127-133.

Milliman, J.D., 1997. Fluvial sediment discharge to the sea and the importance of regional tectonics. *in:* Ruddiman, W.F., Editor, Tectonic Uplift and Climate Change, Plenum Press, New York, pp. 240–257.

Mulder, T., and Syvitski, J.P.M., 1996. Climatic and morphologic relationships of rivers: Implications of sea-level fluctuations on river loads: Journal Of Geology 104, 509-523.

Nittrouer, C.A., 1999. STRATAFORM: overview of its design and synthesis of its results: Marine Geology 154, 3-12.

Orange, D.L., 1999. Tectonics, sedimentation, and erosion in northern California: submarine geomorphology and sediment preservation potential as a result of three competing processes. Marine Geology 154 (1-4), 369-382.

Paine, J.G., 1993. Subsidence of the Texas coast: inferences from historical and late Pleistocene sea levels: Tectonophysics 222, 445-458.

Posamentier, H.W., Allen, G.P., James, D.P., and Tesson, M., 1992. Forced regressions in a sequence stratigraphic framework; concepts, examples, and exploration significance: American Association of Petroleum Geologists Bulletin, v. 76, p. 1687-1709.

Posamentier, H.W. and Allen, G.P. 1999. Siliciclastic Sequence Stratigraphy – Concepts and Applications. Society of Economic Petrologists and Paleontologists. 216 pp.

Posamentier, H.W., Jervey, M.T. and Vail, P.R. 1988. Eustatic controls on clastic deposition I—conceptual frameworks. *in* Wilus, C.K., Hastings, B.S., Kendall, C.G.S.C., Posamentier, H.W., Foss, C.A., and Van Wagoner, J.C., eds., Sea-level Changes: an Integrated Approach: Society of Economic Paleontologists and Mineralogists Special Publication 42, p. 39-45..

Pratson, L., Hughes-Clarke, J., Anderson, M., Gerber, T., Twichell, D., Ferrari, R., Nittrouer, C., Beaudoin, J., Granet, J., Crockett, J., 2009. Timing and patterns of basin infilling as documented in Lake Powell during a drought: Geology 36(11), 843-846.

Schumm, S.A., 1993. River response to baselevel change: implications for sequence stratigraphy: Journal Of Geology 101, 279-294.

Shackleton, N.J., Pisias, N.G., 1985. Atmospheric carbon dioxide, orbital forcing, and climate. In: Sunquist, E.T., Broecker, W.S. (Eds.), The Carbon Cycle and Atmospheric CO2: Natural Variations Archean to Present. American Geophysical Union, Washington, D.C., pp. 303–317.

Shanley, K.W., and McCabe, P.J., 1994. Perspectives on the sequence stratigraphy of

continental strata: American Association Of Petroleum Geologists Bulletin 78, 544-568.

Slingerland, R., Driscoll, N.W., Milliman, J.D., Miller, S.R., and Johnstone, E.A., 2008. Anatomy and growth of a Holocene clinothem in the Gulf of Papua, Journal of Geophysical Research 113, F01S13, doi:10.1029/2006JF000628.

Swenson, J.B., and Muto, T., 2007. Response of coastal plain rivers to falling relative sea-level: allogenic controls on the aggradational phase: Sedimentology 54, 207-221.

Talling, P.J., 1998. How and where do incised valleys form if sea level remains above the shelf edge? Geology 26, 87-90.

Tornqvist, T.E., Wortman, S.R., Mateo, Z.R.P., Milne, G.A., and Swenson, J.B., 2006. Did the last sea level lowstand always lead to cross-shelf valley formation and source-to-sink sediment flux? Journal Of Geophysical Research-Earth Surface, v. 111.

Vail, P.R., R.M. Mitchum, and S. Thompson, 1977. Seismic stratigraphy and global changes of sea level, part 3: Relative changes of sea level from coastal onlap, in C.E. Clayton, ed., Seismic stratigraphy - applications to hydrocarbon exploration: Tulsa, Oklahoma, American Association of Petroleum Geologists Memoir 26, p. 63-81.

van Heijst, M., and Postma, G., 2001. Fluvial response to sea-level changes: a quantitative analogue, experimental approach: Basin Research 13, 269-292.

Wheatcroft, R.A., and Sommerfield, C.K., 2005. River sediment flux and shelf sediment accumulation rates on the Pacific Northwest margin: Continental Shelf Research 25, 311-332.

Vick, G.S. 1988. Late Holocene paleoseismicity and relative sea level changes of the Mad River Slough, Northern Humboldt Bay, California: Masters Thesis, Humboldt State University. 87 p.

Chapter 5 is currently being prepared for submission for publication in Marine Geology as: Hogarth, Leah J., Driscoll, Neal W., and Babcock, Jeffrey M. “New Insight into Lowstand Subaerial Accommodation: Implications for Fluvial Processes in a Sequence Stratigraphic Framework”. The dissertation author was the primary investigator and author of this paper.

Appendix

Correcting Seismic Profiles for Ship Heave and Fish Depth

A.1 INTRODUCTION

Heave artifacts result when the ship position is influence by waves. This often results in a high-frequency sawtooth or lower frequency wavy appearance in the seafloor reflector in seismic data. Changes in fish depth due to wire in or wire out result in abrupt changes in depth. This appendix includes a sioseis script and detailed explanation to correct for these two issues. Sections A.2 and A.3 detail the relevant processes, and Section A.4 includes the whole sioseis code.

A.2 HEAVE CORRECTION

Heave is largely corrected for by applying a “mix” process to the indexed values for the apparent seafloor depth (recorded in two way travel time, TWTT):

```
mix
   type 4  lhdr 59 weight
   1 1 1 1 1 1 1 1 1 1
   1 1 1 1 1 1 1 1 1 1
   1 1 1 1 1 1 1 1 1 1 end
end
```

Type 4 indicates a header mix (located in index 59) rather than a data trace mix. The integers represent thirty header values given equal weight. This mix will smooth the sawtooth heave.

A.3 FISH DEPTH CORRECTION

As the fish is pulled in and out, it’s depth below the sea surface changes, and this is recorded in the seismic profiles (Figures 1A and 2). In addition, unless the fish is

floated on the surface, the apparent two way travel time (TWTT) is less than the actual water depth. This part of the script adjusts for this, adding the depth to the fish to the apparent depth (in TWTT). Processes wbt, wbt2, header2, and shift accomplish this step as follows.

The input files are 1) a segy file (filename.sgy) and 2) a text file with shot number and twtt pairs designating the depth to the ghost (filename.ghst; “b” in Figures 1A and 2). The following commands adjust the apparent depth (“a” in Figures 1A and 2) to the true depth by accounting for the depth at which the fish is towed.

```
wbt
`cat filename.ghst`
end
```

Process wbt calls for the list of shot number/ twtt values, and fills index r50 with the values for the ghost (“b” in Figures 1A and 2).

```
wbt2
  index 60
  thres .2e-8 track .1 end
end
```

Process wbt2 automatically picks the water bottom (using a threshold approach) and places these values in r60.

```
header2
  fno $FNO lnO $LNO ftr 1 ltr 99
  r59 = r50 - r60
end
```

Process header2 finds the depth to the fish (r59, “d” in Figures 1 and 2) by subtracting the apparent water bottom (r60, “a”) from the picked ghost (r50, “b”).

```
mute
  fno 1 ttp 1 0 addwb yes end
end
```

Process mute masks out noise in the water column.

```
shift
  indices r59 end
end
```

Process shift shifts the twtt of the first arrival (“a”) down by the depth to fish in twtt (r59, “d”) to result in the true water depth in twtt (“b”).

* see sioseis.ucsd.edu for further information on the processes and their parameters

A.4 FULL SIOSEIS CODE

```
#!/usr/bin/env bash

declare -r FNO=$2
declare -r LNO=$3
declare -r BASENAME=$1

sioseis << eof
procs diskin header mix wbt wbt2 header2 prout shift mute diskoa end
diskin
  set 0 .8
  ipath ../segy/$1.sgy end
end
diskoa
  ofmt 1 opath .../segy/$1h-m.sgy end
end
header
   fno $FNO lnO $LNO ftr 1 ltr 99 l6 = l3 end
end
mix
```

```
    type 4  lhdr 59 weight
    1 1 1 1 1 1 1 1 1 1
    1 1 1 1 1 1 1 1 1 1
    1 1 1 1 1 1 1 1 1 1 end
end
wbt                                     ! shot-time pairs for ghost
`cat $1.ghst`
end
wbt2                                    ! pick the water bottom
  index 60   ! put this pick in real word 60
  thres .2e-8 track .1 end
end
header2
  fno $FNO lnO $LNO ftr 1 ltr 99
  r59 = r50 - r60                       ! find the depth to the fish by subtracting the
                                        apparent water bottom from the picked ghost
end
end
prout
  indices r50 r59 r60
  fno $FNO lno $LNO noinc 100 end
end
mute
  fno 1 ttp 1 0 addwb yes end           ! apply mute to water column
end
shift
  indices r59 end                       ! shift the first arrival (seafloor) down by fish depth
end
end
eof
```

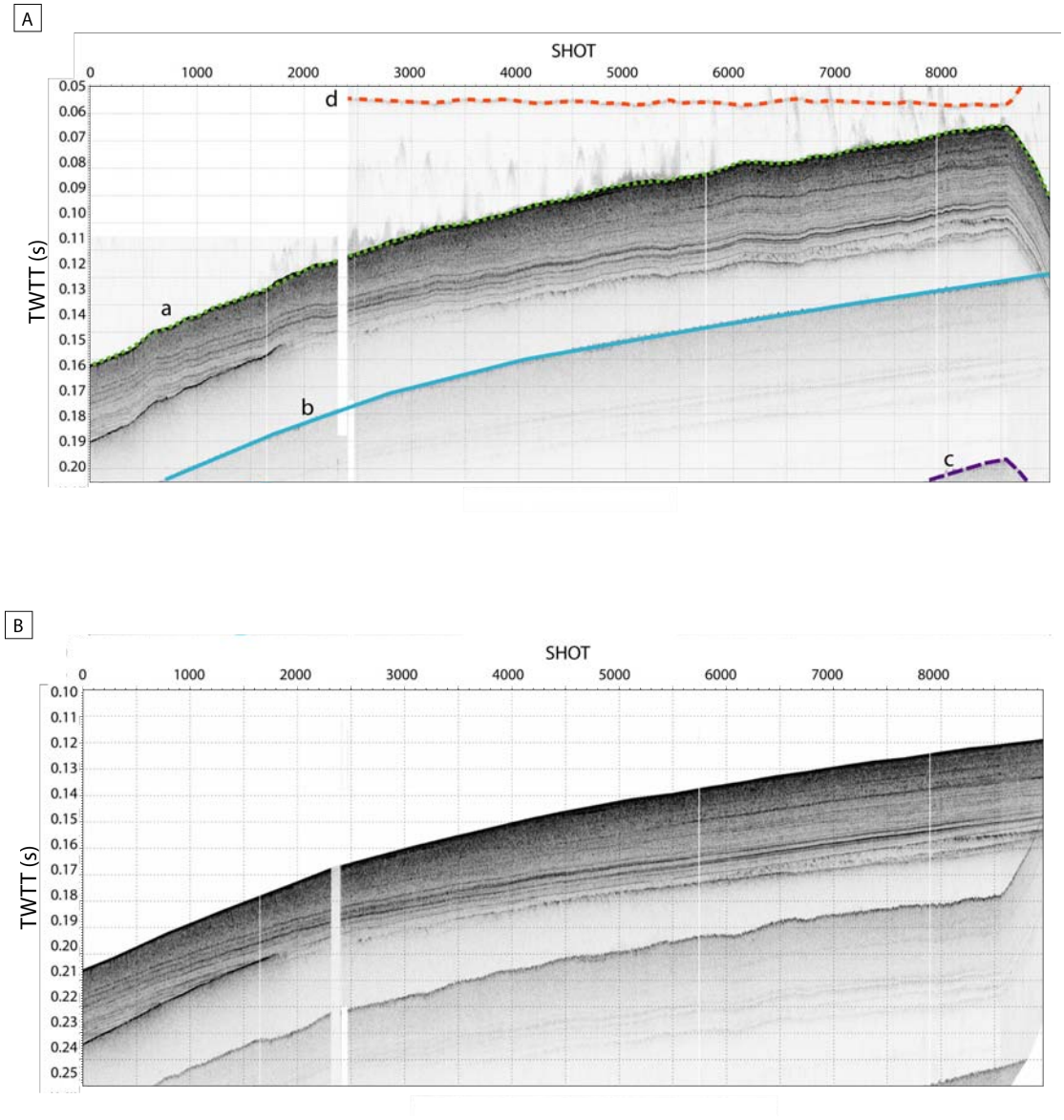


Figure A-1: A: seismic profile prior to correction for heave and fish depth, showing the apparent depth of the water bottom (a), ghost 1 (b), multiple (c), and ghost 2 (d), note the short and long wavelength variations in the seafloor reflector and the noise in the water column; B: same profile after correction for ship heave and fish depth.

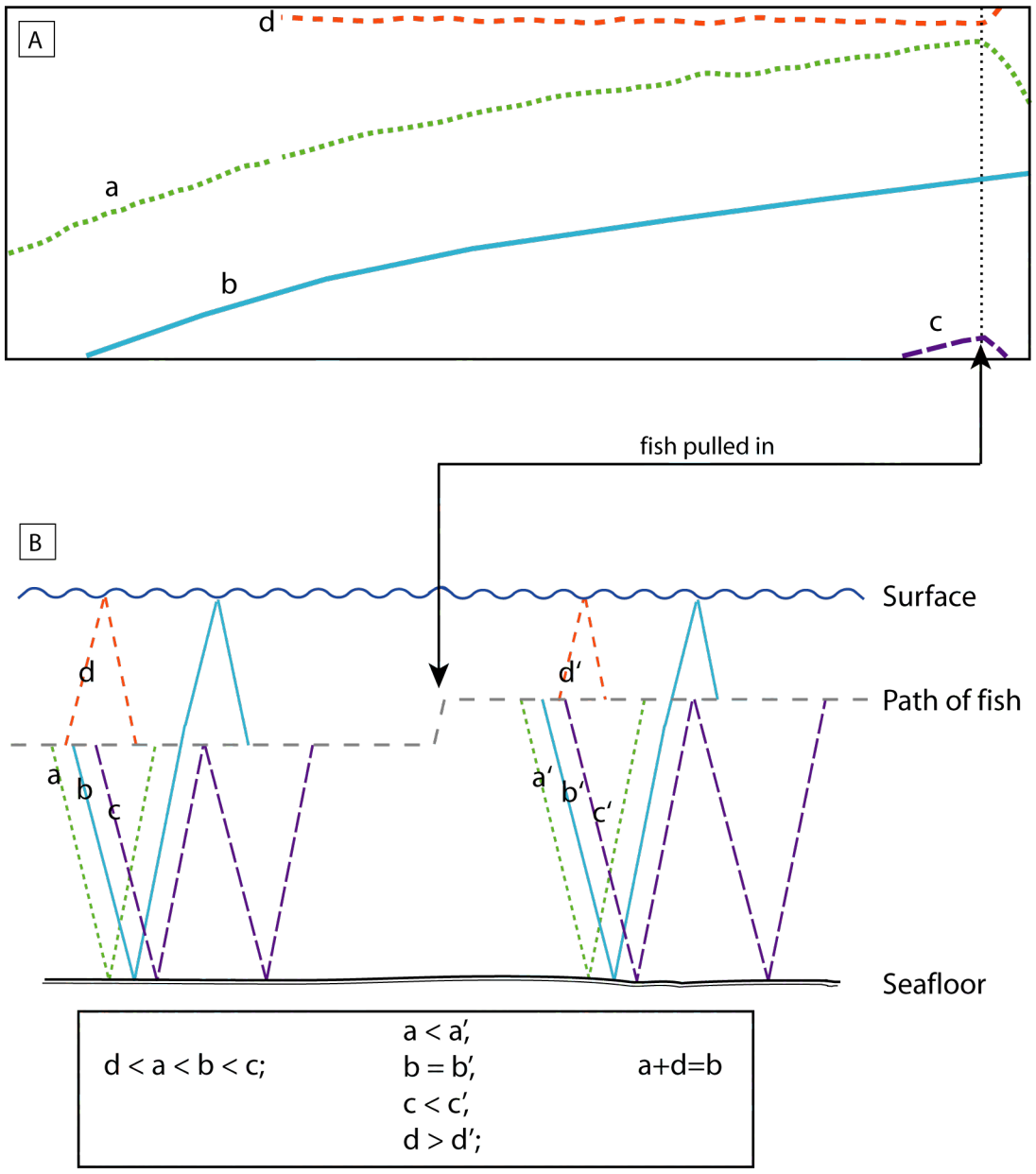


Figure A-2: A: uncorrected horizons color coded as in Figure 1A; B: schematic of ray paths representing each horizon before (a-d) and after (a'-d') fish depth change. Scale is not equivalent to scale in seismic profile. Note that, as the fish is pulled in, a and c increase, d decreases, and b remains constant.